

**UNIVERSITY OF BRASILIA
FACULTY OF TECHNOLOGY
DEPARTMENT OF CIVIL AND ENVIRONMENTAL ENGINEERING**

**DYNAMIC PARAMETERS FOR CAPWAP ANALYSES IN
CONTINUOUS FLIGHT AUGER PILES**

CLAYTON HENRIQUE DALLA CORT NASCIMENTO

SUPERVISOR: RENATO PINTO DA CUNHA, Ph.D.

MASTER'S DISSERTATION IN GEOTECHNICAL ENGINEERING

PUBLICATION: G.DM-412/2024

BRASÍLIA / DF: JULY / 2024

**UNIVERSITY OF BRASILIA
FACULTY OF TECHNOLOGY
DEPARTMENT OF CIVIL AND ENVIRONMENTAL ENGINEERING**

**DYNAMIC PARAMETERS FOR CAPWAP ANALYSES IN
CONTINUOUS FLIGHT AUGER PILES**

CLAYTON HENRIQUE DALLA CORT NASCIMENTO

**MASTER'S DISSERTATION SUBMITTED TO THE DEPARTMENT OF CIVIL AND
ENVIRONMENTAL ENGINEERING AT THE UNIVERSITY OF BRASÍLIA AS
PART OF THE REQUIREMENTS FOR THE MASTER'S DEGREE.**

APROVED BY:

**RENATO PINTO DA CUNHA, Ph.D. (UnB)
(SUPERVISOR)**

**SILVANA BLUMEN FOA, DSc.
(EXTERNAL EXAMINER)**

**RAFAEL CERQUEIRA DA SILVA, DSc. (UnB)
(INTERNAL EXAMINER)**

BRASÍLIA, DF, JULY 5, 2024.

CATALOGUING DATA

DALLA CORT NASCIMENTO, CLAYTON HENRIQUE

Dynamic Parameters for CAPWAP Analyses in Continuous Flight Auger Piles. Brazil, 2024.

xi, 141p., 210x297 mm (ENC/FT/UnB, Master, Geotechnics, 2024)

Master's Dissertation – University of Brasilia. Faculty of Technology.

Department of Civil and Environmental Engineering.

1. Deep foundation

2. Dynamic load testing

I. ENC/FT/UnB

3. Performance analysis

4. Cast-in-situ pile

II. MASTER

BIBLIOGRAPHIC REFERENCE

Dalla Cort, C. H. N. (2024). Dynamic Parameters for CAPWAP Analyses in Continuous Flight Auger Piles. Master's dissertation. Publication PPG. G.DM-412/2024, Department of Civil and Environmental Engineering, University of Brasilia, Brasilia/DF, 141p.

ASSIGNMENT OF RIGHTS

Author: Clayton Henrique Dalla Cort do Nascimento.

Title: Dynamic Parameters for CAPWAP Analyses in Continuous Flight Auger Piles.

Degree: Master of Science Year: 2024.

Permission is granted to University of Brasilia to reproduce copies of this Master's dissertation and to loan or sell such copies for academic and scientific purposes only. The author reserves other publication rights, and no part of this Master's dissertation may be reproduced without the author's written permission.

Clayton H. N. Dalla Cort.

University of Brasilia (UnB)

Brasilia – DF CEP 70919-970

DEDICATION

To my family, a source of love and affection. I dedicate this to my mother for always motivating and believing in me. To my father for being my role model of an honest and persevering man.

ACKNOWLEDGEMENTS

I would like to express my heartfelt gratitude to my family for their unwavering support and encouragement throughout my academic journey, from preschool to completing my master's dissertation. Almira, Rosimar, and Polyana, your support has been invaluable to me, and I am deeply thankful for your presence in every step of this endeavor. I am also grateful to Gabrielly for her constant support, encouragement, and companionship during the challenging moments of this journey.

My sincere appreciation goes to the entire faculty of the Postgraduate Department of Geotechnical Engineering at the University of Brasilia, particularly to my advisor Renato Pinto da Cunha, for their guidance, mentorship, and knowledge shared both inside and outside the classroom. I would also like to thank all the professionals at UnB for their contributions to maintaining the cleanliness, safety, and functionality of its facilities. I extend my thanks to my friends from the Postgraduate Program for the enriching experiences, shared insights, and moments of relaxation during my time in Brasília.

Special thanks to EPF Geotecnia for generously sponsoring this research project. Its support has been instrumental in making this work possible.

ABSTRACT

Dalla Cort, C. H. N. (2024). **Dynamic Parameters for CAPWAP Analyses in Continuous Flight Auger Piles**. Master's Dissertation. University of Brasilia, Faculty of Technology, Department of Civil and Environmental Engineering, Brasilia DF, 141p.

Load testing is the primary means of mitigating uncertainties in deep foundation geotechnical projects. In this regard, dynamic load testing (DLT) is a highly attractive solution as it allows for rapid results with lower financial costs compared to static load testing. DLT is interpreted through CAPWAP analyses, which utilize signal-matching techniques between field readings and those obtained from a pile-soil model. This technique involves trial-and-error, and interpreting the results requires good judgment from the engineer conducting the analyses and inputting the soil and pile parameters into the model. The most important parameters in the analysis are the shaft quake (q_s) and damping factor (J_s), which are commonly assumed to be constant along the pile shaft, regardless of soil stratigraphy (variation in soil type and mechanical properties). In other words, CAPWAP analyses in this approach become highly dependent on experience and subjectivity.

The aim was to establish correlations between the undrained shear strength (S_u) and the q_s and J_s of the soil along the shaft of continuous flight auger (CFA) piles. It also aimed to correlate q_s and J_s with the penetration resistance index (N). To achieve this, Vane Shear Tests (VST) and Standard Penetration Tests (SPT) were conducted, along with a static load test and two dynamic load tests on piles at a construction site in Sinop, Mato Grosso, Brazil. The soil in the city has an alluvial origin and consists of poorly consolidated sediments. The terrain at the site comprises cohesive soil up to a depth of 15 meters (inorganic clay), transitioning to cohesionless soil (silty gravel, sandy silt and sand) down to a depth of 32 meters (limit of the boreholes). The groundwater table was observed at a depth of 2 meters.

The results of the tests were analyzed, and some correlations between soil properties and the q_s and J_s parameters obtained from the CAPWAP analyses were observed. Within the limitations of the analyses conducted, it was concluded that the CAPWAP model parameters are indeed not constant throughout the depth and vary according to the type and mechanical properties of the soil. It was found that most of the results diverged from those expected in the literature, possibly due to the different soil properties in Sinop, Mato Grosso, and the type of pile analyzed (CFA).

RESUMO

Dalla Cort, C. H. N. (2024). **Parâmetros Dinâmicos para Análises CAPWAP em Estacas Hélice Contínua**. Dissertação de Mestrado. Universidade de Brasília, Faculdade de Tecnologia, Departamento de Engenharia Civil e Ambiental, Brasília DF, 141p.

Prova de carga é a principal forma de atenuar as incertezas de um projeto geotécnico de fundação profunda. Nesse sentido, o ensaio de carregamento dinâmico (ECD) é uma solução bastante atrativa, uma vez que permite uma rápida obtenção de resultados com um menor custo financeiro, se comparado às provas de carga estática. O ECD é interpretado por meio de análises CAPWAP que utiliza a técnica de ajuste entre os sinais lidos em campo e os obtidos por meio de um modelo estaca-solo. Essa técnica é conduzida por meio de tentativa e erro e a interpretação dos resultados requer um bom julgamento do engenheiro que realiza as análises e insere os parâmetros do solo e da estaca no modelo. Os parâmetros mais importantes da análise são o quake (q_s) e o damping factor (J_s) que corriqueiramente são considerados constantes ao longo do fuste da estaca, independentemente da estratigrafia do solo (variação no tipo de solo e de suas propriedades mecânicas). Ou seja, as análises CAPWAP nessa abordagem se tornam muito dependentes da experiência e da subjetividade.

Buscou-se estabelecer correlações entre a resistência ao cisalhamento não drenada (S_u) com o q_s e J_s do solo ao longo do fuste de estacas hélice contínua (HCM). Também objetivou-se correlacionar q_s e J_s com o índice de resistência à penetração (N). Para isso, foram realizados ensaios de palheta e ensaios do tipo SPT, além de uma prova de carga estática e dois ensaios de carregamento dinâmico em estacas de uma obra localizada na cidade de Sinop, Mato Grosso, Brasil. O solo da cidade tem origem aluvial e é composto por sedimentos pouco consolidados. O terreno da obra é composto solo coesivo até 15 metros de profundidade (argila inorgânica), passando para solo não-coesivo (silte pedregulhoso, silte arenoso e areia) até os 32 metros de profundidade (limite das sondagens). Foi observado nível d'água a 2 metros de profundidade.

Os resultados dos ensaios foram confrontados e observou-se algumas correlações entre as propriedades do solo e os parâmetros q_s e J_s obtidos nas análises CAPWAP. Dentro das limitações das análises realizadas, concluiu-se que os parâmetros do modelo CAPWAP de fato não são constantes ao longo da profundidade e variam conforme o tipo e as propriedades mecânicas do solo. Constatou-se que a maioria dos resultados divergiu daqueles esperados na literatura possivelmente devido às diferentes propriedades do solo de Sinop – MT e também ao tipo de estaca analisada (HCM).

CONTENTS

- 1. INTRODUCTION..... 1
 - 1.1 MOTIVATION..... 2
 - 1.2 OBJECTIVES..... 3
 - 1.3 METHODOLOGY 4
 - 1.4 DISSERTATION OUTLINE 4
- 2. LITERATURE REVIEW..... 6
 - 2.1 DYNAMIC LOAD TESTING (DLT)..... 14
 - 2.2 CAPWAP METHOD 18
 - 2.2.1 PILE MODEL 19
 - 2.2.2 SOIL MODEL..... 20
 - 2.2.3 CAPWAP PROCEDURE 24
 - 2.3 QUAKE AND DAMPING FACTOR VALUES 27
 - 2.4 FOUNDATION ENGINEERING PRACTICE IN SINOP..... 30
 - 2.5 LITERATURE REVIEW COMMENTS 31
- 3. METHODOLOGY..... 33
 - 3.1 SINOP CITY: LOCATION AND CLIMATE 33
 - 3.1.1 GEOLOGICAL ASPECTS 33
 - 3.2 TEST SITES..... 35
 - 3.3 GEOTECHNICAL INVESTIGATION 36
 - 3.4 STATIC LOADING TEST (SLT)..... 43
 - 3.4.1 STIFFNESS METHOD (DÉCOURT, 1998)..... 46
 - 3.5 DYNAMIC LOADING TESTS (DLT)..... 48
 - 3.5.1 CAPWAP ANALYSES 49
 - 3.6 METHODOLOGY SUMMARY 54
- 4. RESULTS 55
 - 4.1 SITE A..... 55

4.1.1	SOIL PROPERTIES	55
4.1.2	SLT ANALYSIS	59
4.1.3	CAPWAP ANALYSIS	64
4.2	VALIDATION: SITE B	71
4.2.1	SOIL PROPERTIES	71
4.2.2	STATIC ANALYSIS	74
4.2.3	CAPWAP ANALYSES	75
5.	RECOMMENDATIONS FOR DESIGN PURPOSES	79
6.	CONCLUSIONS	81
6.1	RECOMENDATIONS	83
	REFERENCES	84
	Appendix A	91
	Appendix B	94
	Appendix C	102
	Appendix D	104

LIST OF TABLES

Table 2.1: Typical shaft quake and damping according to different authors. 30

Table 3.1: Stratigraphic chart of Sinop (Cutrim et al., 2021)..... 34

Table 3.2: Summary of tests carried out at each site..... 38

Table 3.3: Characteristics of the CFA piles according to monitoring..... 42

Table 3.4: Summary of blows selected for CAPWAP analyses. 52

Table 3.5: C-parameter for tip resistance (Décourt & Quaresma, 1978). 53

Table 4.1: Summary of the four failure criteria. 60

Table 4.2: Resistance components obtained by the Stiffness Method. 62

Table 4.3: Summary of the obtained correlations at Site A. 70

Table 4.4: Resistance components according to adjusted α and β - Site B. 74

LIST OF FIGURES

Figure 1.1: Methodology of the dissertation.	4
Figure 2.1: Descending compression stress wave (PDI, 2014).	6
Figure 2.2: Displacement as stress wave propagates (PDI, 2014).	9
Figure 2.3: Ascending and descending components (PDI, 2014).	9
Figure 2.4: Shaft resistance waves. (PDI, 2014).	11
Figure 2.5: Wave reflection process. (PDI, 2014).	12
Figure 2.6: Force and velocity times impedance over time.	12
Figure 2.7: Pile's discrete model (Flynn & McCabe, 2021).	13
Figure 2.8: Static and dynamic resistances according to Smith. (Velloso & Lopes, 2011).	14
Figure 2.9: Accelerometer (on the left) and strain transducer (on the right).	16
Figure 2.10: Pile Driving Analyzer (PDA).	17
Figure 2.11: Typical signals recorded by the PDA® in dynamic testing.	17
Figure 2.12: Pile model (PDI, 2014).	19
Figure 2.13: Static resistance as a function of shaft displacement (left) and toe displacement (right) (PDI, 2014).	21
Figure 2.14: Smith's soil model considered fixed.	24
Figure 2.15: The complete CAPWAP's soil model with radiation damping.	24
Figure 2.16: <i>MQ</i> time periods (PDI, 2014).	25
Figure 3.1: Location of Sinop (Martim et al., 2020).	33
Figure 3.2: Location of testing sites.	35
Figure 3.3: Areas of sites A and B	36
Figure 3.4: Experimental field at Site A (see Appendix A).	37
Figure 3.5: Experimental field at Site B (see Appendix A).	37
Figure 3.6: The vane design.	39
Figure 3.7: The vane used in the tests.	39
Figure 3.8: The torque wrench used in the VSTs.	39
Figure 3.9: Torque application in the VST.	40
Figure 3.10: Vane with tested soil.	40
Figure 3.11: Application of vacuum for determination of grain specific gravity.	41
Figure 3.12: Samples used in sieving for determination of Atterberg's limits	41
Figure 3.13: Pile monitoring record for DLT - 1A pile (see Appendix A).	43
Figure 3.14: SLT setup.	45

Figure 3.15: External view of the load test covering.	45
Figure 3.16: Internal view of the load test setup.	45
Figure 3.17: Foundation stiffness graph with physical failure.	46
Figure 3.18: Foundation stiffness graph without physical failure.	46
Figure 3.19: Drop weight hammer used.	49
Figure 3.20: Force and particle velocity - DLT 1A.	50
Figure 3.21: Force and particle velocity - DLT 2A.	50
Figure 3.22: Force and particle velocity - DLT 1B.	50
Figure 3.23: Force and particle velocity - DLT 2B.	51
Figure 3.24: Force and particle velocity - DLT 3B.	51
Figure 3.25: Force and particle velocity - DLT 4B.	51
Figure 3.26: Flowchart summarizing the methodology used in this dissertation.	54
Figure 4.1: Grain size distribution at Site A.	56
Figure 4.2: Geotechnical profile of Site A with the results of SPTs and VSTs (no scale).	57
Figure 4.3: Average geotechnical profile of Site A.	58
Figure 4.4: Load-displacement curve from the SLT.	59
Figure 4.5: Four failure criteria applied to the SLT curve.	60
Figure 4.6: Application of the Stiffness Method for the SLT.	62
Figure 4.7: Shaft resistance – Site A.	63
Figure 4.8: Load transfer - Site A.	63
Figure 4.9: DLT – 1A - Measured and computed <i>WU</i> signals.	64
Figure 4.10: DLT – 2A - Measured and computed <i>WU</i> signals.	64
Figure 4.11: Variation of q_s and J_s as a function of depth - Site A.	65
Figure 4.12: Variation of q_s , J_s , SPT N -value and S_u as a function of depth - Site A.	67
Figure 4.13: Shaft quake as a function of undrained shear strength.	68
Figure 4.14: Shaft quake as a function of SPT N -value.	68
Figure 4.15: Damping factor as a function of undrained shear strength.	68
Figure 4.16: Damping factor as a function of SPT N -value.	68
Figure 4.17: Geotechnical profile of Site B with the results of SPTs and VSTs (no scale).	72
Figure 4.18: Average geotechnical profile of Site B.	73
Figure 4.19: Shaft resistance - Site B.	75
Figure 4.20: Load transfer - Site B.	75
Figure 4.21: Variation of q_s , J_s , SPT N -value and S_u as a function of depth - Site B.	76
Figure 4.22: DLT 1B - Measured and computed <i>WU</i> signals.	77

Figure 4.23: DLT 2B - Measured and computed <i>WU</i> signals.	77
Figure 4.24: DLT 3B - Measured and computed <i>WU</i> signals.	77
Figure 4.25: DLT 4B - Measured and computed <i>WU</i> signals.	77
Figure 4.26: Match qualities for CFA piles at Site B.....	78
Figure 4.27: <i>MQ</i> Log Normal Distribution - Site B.....	78
Figure 5.1: Suggested methodology for pile foundation design and quality control.	80
Figure B.0.1: Pile monitoring record for SLT pile – Site A.....	95
Figure B.0.2: Pile monitoring record for DLT 1A.	96
Figure B.0.3: Pile monitoring record for DLT 2A.	97
Figure B.0.4: Pile monitoring record for DLT 1B.	98
Figure B.0.5: Pile monitoring record for DLT 2B.	99
Figure B.0.6: Pile monitoring record for DLT 3B.	100
Figure B.0.7: Pile monitoring record for DLT 4B.	101
Figure C.0.1: SLT field report - Site A.	103

LIST OF SYMBOLS

Δ_Z : average displacement in a reading of SLT
 Δ_{ZCR} : average displacement of the current reading of SLT
 Δ_{ZPR} : average displacement of the previous reading of SLT
 Δ_{ZPS} : final average displacement of the previous stage of SLT
 A_p : area of the pile toe
 C_c : Coefficient of gradation
 C_u : uniformity coefficient
 F_d : downward wave in terms of force
 F_u : upward wave in terms of force
 J_{CG} : Coyle & Gibson (1970) damping factor
 J_{RD} : radiation damping factor
 J_s : shaft damping factor
 J_t : toe damping factor
 MQ_B : CAPWAP blow count penalty
 N_b : average value of the SPT index at the pile base
 N_s : average value of the SPT index at the shaft
 R^2 : coefficient of determination
 R_b : total base resistance
 R_d : dynamic resistance
 R_n : lower limit of shaft resistance
 R_s : mobilized static resistance
 R_{su} : ultimate static resistance
 S_u : undrained shear resistance of soil
 S_{ur} : undrained shear strength of the soil under disturbed condition
 T_{max} : maximum torque of the vane shear test
 T_r : torque of the vane shear test under disturbed condition
 U_n : unloading ultimate static resistance multiplier
 a_u : unloading quake multiplier
 d_{vane} : vane's width
 k_{SM} : stiffness of the pile measured at the top (Décourt, 1998)
 m_s : soil mass at the pile shaft
 m_t : soil mass at the pile toe
 n_p : number of pile elements in the CAPWAP model
 q_s : shaft quake
 q_t : toe quake
 q_u : unloading quake
 r_0 : radius of the cross-section of the pile;
 r_m : radius at which the shear stress becomes negligible
 t_g : toe gap
 v_d : downward particle velocity
 v_u : upward particle velocity
 σ_{ubr} : unit pile base resistance
 τ_u : yield shear stress at pile interface;
LI: Liquidity index
LL: Liquid limit
PI: Plasticity index
PL: Plastic limit

A: cross-sectional area
C: characteristic coefficient of the soil
D: cross-sectional diameter
E: longitudinal dynamic modulus
F: force
G: shear modulus of soil.
J: damping factor
L: pile length
MQ: CAPWAP match quality
N: uncorrected SPT index
Q: load applied in the SLT
T: torque of the vane shear test
U: perimeter of the cross-sectional area of the pile
WD: wave down
WU: wave up
Z: impedance
a: particle acceleration
c: longitudinal wave velocity
m: mass
n: Coyle & Gibson (1970) particle velocity coefficient
q: quake
s: permanent displacement
t: time
u: displacement
v: particle velocity
 α : factor depending on the pile type and the soil type at the pile tip
 β : factor depending on the pile type and the soil type along the shaft of the pile
 ε : axial strain of the pile
 ρ : specific mass of the pile material
 σ : normal stress on the cross-sectional area of the pile

1. INTRODUCTION

Pile testing is one of the most effective means of dealing with inherent uncertainties of geotechnical deep foundation design and its construction. Pile testing provides critical information, including the ultimate load capacity, load-settlement behavior, acceptability of installation methods, and structural integrity. This information is important for quality control, confirming the design assumptions and collecting data for the design, which ultimately leads to more reliable results. (Poulos, 2017).

An advantage to the quality control of piled foundations is that pile testing increases the reliability. Standards and building codes allow for lower safety factors in well-controlled foundations, which can save on the total foundation cost when pile testing is performed at the design stage. In this sense, several tests can be used for the quality control of foundations, such as Static Load Testing (SLT) and Dynamic Load Testing (DLT) (Likins, 2015).

SLT is performed by applying static and increasing loads to the top of the pile, using hydraulic jacks and a reaction system (beams, piles and anchors). These loads cause displacements that are recorded over time, forming a load-displacement curve at the top of the pile. Depending on the testing methodology employed, it is not uncommon for each STL to take about two days (or more) from preparation to completion. However, DLT is characterized by the application of one or more impacts of a falling hammer on the pile head that generate downward longitudinal stress waves that are reflected upwards due to soil strength, variations in cross-sectional properties and pile material. The signals of these waves are captured near the top of the piles by means of accelerometers and strain transducers, through which the values of velocity and force of the particles in the instrumented section are determined. The main objective of DLT is to determine the geotechnical pile capacity, also making it possible to obtain information about its structural integrity, efficiency of the impact system, stresses along the pile, as well as mechanical properties of the soil. (Pereira et al., 2009).

Although the STL is the most reliable method for determining the long-term behavior of a single pile, the cost of the reaction system and the duration of the test make the DLT widely used. This is because it can be performed on a larger number of piles, enabling the qualitative assessment of local variability, adapting to short work schedules (Rausche, 2018). According to Fellenius (2023), the main advantage of DLT is that a large number of piles can be tested quickly, compared to SLT, in which a small number of piles are tested in longer times. Furthermore, in addition to determining the pile load capacity, the DLT associated with the

CASE Pile Wave Analysis Program (CAPWAP) can provide valuable information about its load-transfer.

CAPWAP is based on the one-dimensional stress-wave propagation theory and the soil model, calculations complexity and experience dependence on the selection of soil parameters affect the reliability of pile capacity prediction (Tu et al., 2022). CAPWAP models both the pile and the soil as a series of masses, springs, and dashpots, with passive soil resistance. The unknowns are obtained through trial-and-error, determining the pile movement, using the measured signals in the instrumented section as boundary conditions in the field (Gonçalves et al., 2000).

In this process, the field sensors capture the signals, and in the office, a new signal is calculated to achieve the maximum possible matching between the measured and calculated signals (signal-matching). Consequently, the pile-soil model will be established, along with the distribution of mobilized resistances along the shaft and toe, as the displacements and velocities of each pile element are determined due to the propagation of the stress wave. Its procedure is iterative and requires judgment from the engineer performing the analysis. In this approach, several researchers discuss the uniqueness of the CAPWAP solution, as Danziger et al. (1996) and Alvarez et al. (2006).

Two of the most significant unknowns within the pile-soil model employed are quake (q) and damping factor (J). Quake refers to the displacement at which the mobilized static resistance is maximum, associated with elastic strains, while damping factor represents the soil's damping coefficient. In practice, q and J are considered constant along the pile, neglecting the soil type and the ground stratigraphy (Aghayarzadeh et al., 2020). In this context, the work by Ng & Sritharan (2013) introduced a significant advancement in the signal-matching technique. While conventional practice often involves employing constant values for the entire length of the pile shaft, the authors assigned a specific set of q and J values to individual soil layers, resulting in optimal signal-matchings. Subsequently, they established correlations between these variables and the outcomes of field tests (SPT and CPTu), yielding noteworthy relationships and trends. This approach enables results to be less influenced by the subjectivity of the CAPWAP analysis performer and also facilitates a more rational consideration of subsurface stratigraphic characteristics.

1.1 MOTIVATION

Initially developed for driven piles, the DLT along with the CAPWAP method has also been used in cast-in-place piles through improvements in the pile-soil model. In Brazil, there is

a predominance of this type of pile, especially the CFA pile, which has a good volume-load ratio and can reach significant depths without vibrations or noise, making it excellent for urban centers.

In this regard, it is important to conduct a more detailed study of the CAPWAP methodology for DLT applied to CFA piles, as it is a relatively new subject in Brazil (since the 1990s and early 2000s). The experience gained has been primarily in the major urban centers of the Southeast region of the country. Therefore, given that the Central-West region, especially the northern part of the state of Mato Grosso, has gained economic prominence with agribusiness and real estate investments, it was decided to conduct this research on CFA piles in the alluvial soil of the city of Sinop.

Therefore, this research will conduct CAPWAP analyses on CFA piles using the methodology proposed by Ng & Sritharan (2013), in which the model parameters (quake and damping) are determined based on the soil type and its properties at different depths. Hence, these parameters will not be considered constant along the length of the pile, as mistakenly assumed in analysis practice. For this reason, this dissertation will systematically address the CAPWAP methodology, with the aim of establishing meaningful relationships between field tests and the parameters adopted in the analysis model.

1.2 OBJECTIVES

The main objective of this dissertation is to propose a rational method for CAPWAP analysis in CFA piles in the region of the city of Sinop, Brazilian state of Mato Grosso. In this rational method, the results will depend less on the subjectivity of the professional performing the analyses. To achieve this, the parameters shaft quake (q_s) and shaft damping factor (J_s) will be investigated as a function of soil type and its resistance properties. Therefore, the specific objectives of this dissertation are:

- Correlate the shaft quake (q_s) and shaft damping factor (J_s) parameters with the type of soil (cohesion and cohesionless soils);
- Establish relationships between q_s and J_s with the SPT N -value. It also aimed to correlate q_s and J_s with the undrained shear strength of the soil (S_u);
- Propose a rational methodology for the use of DLT and CAPWAP analyses for defining deep foundation designs in practice.

1.3 METHODOLOGY

The primary focus of this research is determining shaft quake and damping for CAPWAP analyses in CFA piles as a function of soil type, SPT N -value and S_u . The dissertation is divided into five main parts: i) Introduction, ii) Literature Review, iii) Methodology, iv) Results, and v) Conclusions.

Figure 1.1 summarizes the methodology employed for the development of this research:

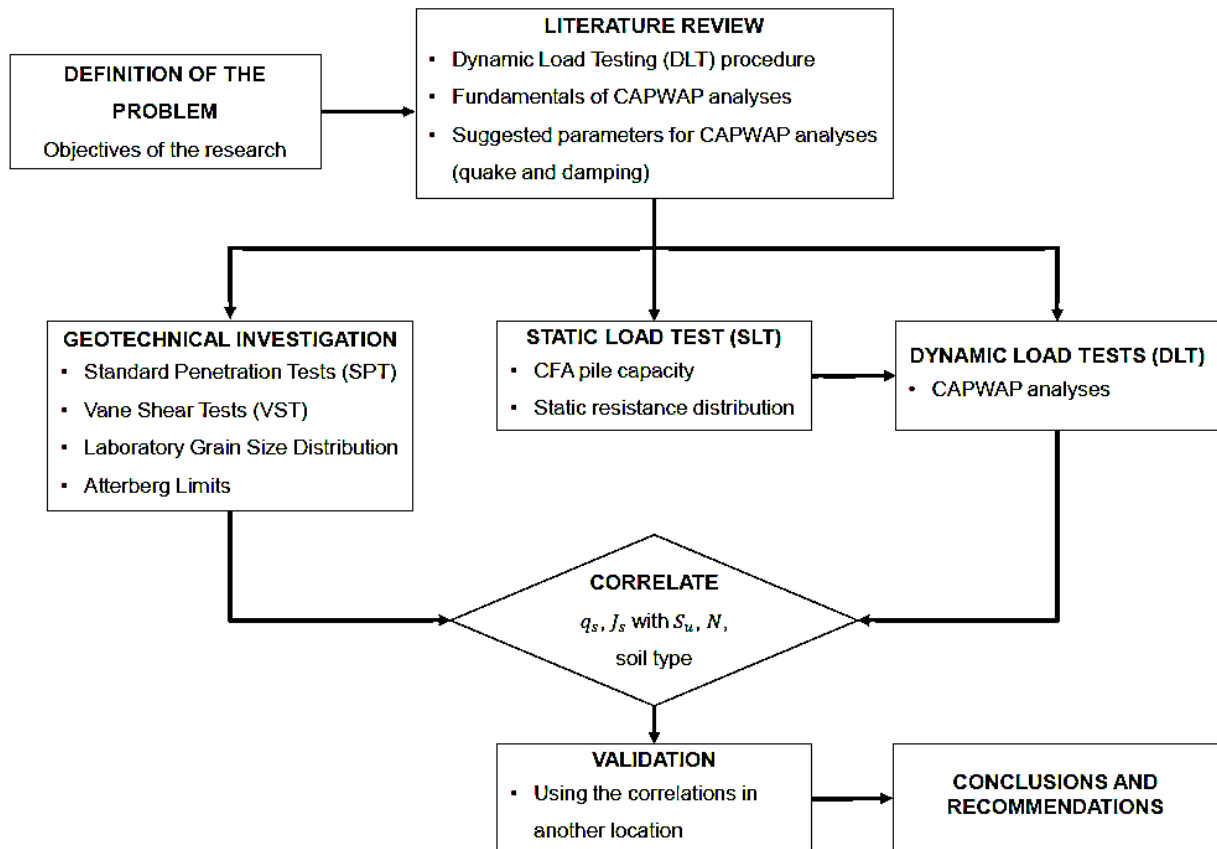


Figure 1.1: Methodology of the dissertation.

1.4 DISSERTATION OUTLINE

This Master's dissertation is divided into five chapters. The first chapter is this introduction.

Chapter 2 will present the theoretical fundamentals regarding the phenomenon of longitudinal stress wave propagation in piles and the resulting effects due to the mobilization of geotechnical resistance. Additionally, a concise overview of the DLT on cast-in-place piles will be provided. Towards the end of Chapter 2, the CAPWAP method will be extensively

discussed, including the presentation of the pile-soil model, along with defining the parameters used in the analysis and their suggested values by various researchers.

Chapter 3 will present the methodology used in this dissertation. It will outline the geotechnical characterization of the study areas, including the positions of the standard penetration tests (SPT) boreholes and vane shear tests (VST) concerning the tested piles. Furthermore, within this chapter, the methodology employed in the CAPWAP analyses will be detailed, consistently relating them to the results of a static load testing and the geotechnical investigations conducted.

In Chapter 4, the results of the geotechnical investigation of the site are presented, along with the load-displacement curve of the SLT and its interpretation. The values of q_s and J_s determined at depth in the CAPWAP analyses are also presented. Subsequently, correlations between the dynamic parameters and the S_u and the uncorrected SPT N -value are proposed. Finally, the results are validated and discussed to better justify the use of the established correlations.

In Chapter 5, a brief conclusion of the achieved results is provided along with some observations on the limitations of the methodology employed. Subsequently, several procedures are recommended with the aim of future research mitigating or even eliminating the limitations in the adopted analyses.

2. LITERATURE REVIEW

Upon the application of an impact from a hammer with a given energy at the top of the pile, the upper zone undergoes compression, transmitting stress to lower regions. This compression process is continuous, resulting in the generation of a stress wave that propagates along the pile. The product of the stress at the top and the cross-sectional area of the pile represents the impact force caused by the hammer (Bernardes, 1989).

Therefore, considering that a uniform, linearly elastic and slender rod is suddenly loaded by a force F due to an impact at its top, a stress wave propagates downward at a velocity c . At the instant t immediately before the impact, all particles are at rest; thus, immediately after the impact, after a time interval Δt , the impact force compresses a portion of the rod's top, propagating over a length ΔL (Figure 2.1).

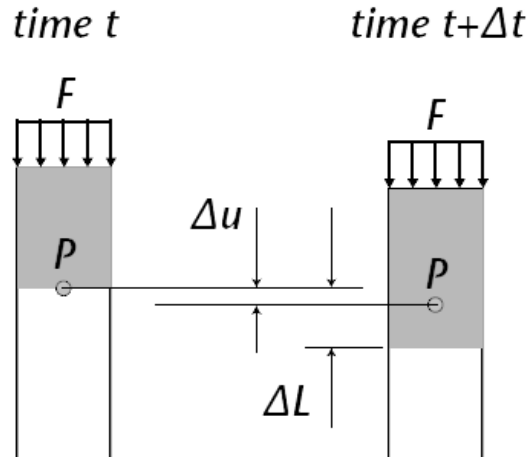


Figure 2.1: Descending compression stress wave (PDI, 2014).

Hence, the wave speed (c) is given by:

$$c = \frac{\Delta L}{\Delta t} \quad (2.1)$$

As observed in the Figure 2.1, the stress wave induces a deformation Δu of the particle represented by point P . Assuming the validity of Hooke's Law, the deformation of the particle can be calculated as follows:

$$\Delta u = \frac{F\Delta L}{EA} \quad (2.2)$$

Where:

E : Longitudinal dynamic modulus of the rod;

A : Cross-sectional area of the rod.

Just as the stress wave has its propagation velocity (c), the particle also has its velocity. This is due to the deformation of Δu over the time interval Δt ; thus, the particle's velocity (v) can be calculated as follows:

$$v = \frac{\Delta u}{\Delta t} \quad (2.3)$$

Combining Eqs. (2.1) and (2.2) in Eq. (2.3) results in

$$v = \frac{Fc}{EA} \quad (2.4)$$

Thus, the c represents the velocity at which a wave travels along the pile, and the v indicates the speed at which a particle moves along the pile as a wave passes by.

Also, the particle's acceleration (a) can be determined by

$$a = \frac{Fc}{EA\Delta t} \quad (2.5)$$

According to Newton's Second Law

$$F = ma \quad (2.6)$$

With the specific mass of the pile material (ρ) known, the mass (m) of the compressed length can be determined by calculating $m = \rho A\Delta L$. Therefore, by applying this value to Eq. (2.6) and using Eqs. (2.4) and (2.5), the following expression for c is obtained:

$$c = \sqrt{\frac{E}{\rho}} \quad (2.7)$$

Thus, c depends solely on the properties of the medium through which it propagates. In contrast, as indicated by Eq. (2.4), v is a function of impact force magnitude, geometry and also the properties of the pile material.

Furthermore, Eq. (2.4) can be rewritten as follows:

$$v = \frac{\sigma c}{E} = \varepsilon c \quad (2.8)$$

σ : is the normal stress on the cross-sectional area of the pile;

ε : is the axial strain of the pile.

In other words, the preceding expression reveals a proportionality between particle velocity and the propagation velocity of the stress wave. Additionally, based on Eq. (2.4), the impedance of the pile (Z) can be defined as the proportionality constant between v and F :

$$Z = \frac{EA}{c} \quad (2.9)$$

$$F = Zv \quad (2.10)$$

According to Querelli (2019), pile impedance can be interpreted as a "resistance" that the pile presents to changes in particle velocity. This proportionality only holds if there are no other waves traveling on the pile (PDI, 2014).

Combining the Newton's Second Law (Eq. 2.6), Hooke's law, and Eq. 2.7, the equilibrium of forces results in the equation of the one-dimensional wave, known as the Wave Equation (Eq. 2.11). The derivation of this equation can be found in Velloso & Lopes (2011).

$$\frac{\partial^2 u}{\partial t^2} = c^2 \cdot \frac{\partial^2 u}{\partial x^2} \quad (2.11)$$

Where u represents the displacement of the particle in time t and at position x . In the subsequent Figure 2.2, it is conventionally established that the x -axis is oriented in the positive downward direction, with particle displacement also considered positive in this direction.

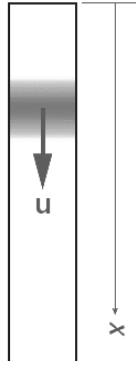


Figure 2.2: Displacement as stress wave propagates (PDI, 2014).

The solution of the Wave Equation takes the following form:

$$u = f(x - ct) + g(x + ct) \quad (2.12)$$

Therefore, the displacement of the particle at position x can be obtained by the sum of two functions, f and g , representing two independent waves, one propagating downward and the other upward along the rod (Figure 2.3). These two functions, can also be interpreted as displacements that, when combined, result in the total particle displacement (u) at position x .

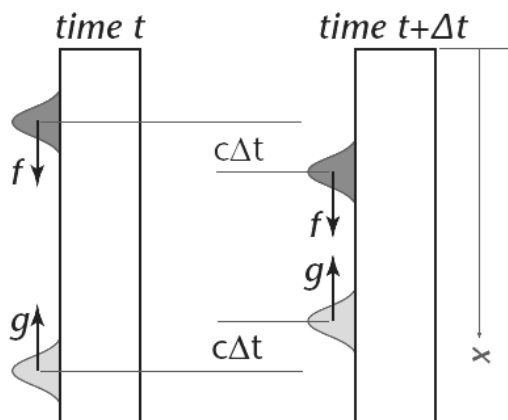


Figure 2.3: Ascending and descending components (PDI, 2014).

Given an impact at the top of the pile, the generated wave will reach the bottom and be reflected upward after a time L/c , where L is the length of the pile. The properties of the reflected impact wave will depend on the boundary conditions at the pile's bottom. Therefore, the following sign conventions are defined:

- Forces, stresses and compressive strains are positive;
- Forces, stresses and tensile strains are negative;
- Downward displacements, velocities, and accelerations are positive;
- Upward displacements, velocities, and accelerations are negative.

While the downward compression wave propagates along the pile, the particles move in the same direction, following the positive convention of the x -axis. Therefore, both force and particle velocity are positive. Thus, the following relationship is valid:

$$F_d = Zv_d \quad (2.13)$$

Where

F_d : is the downward wave in terms of force;

v_d : is the downward particle velocity as the stress wave moves along the pile.

However, if the wave reflected at the pile toe is compressive (positive force), the particles will move upwards (negative particle velocity). In the case of a tensile reflected wave (negative force), the particles will move downwards (positive particle velocity), in the positive direction of the x -axis. Therefore, the sign of the upward force (F_u) will always be opposite to that of the particle velocity (v_u):

$$F_u = -Zv_u \quad (2.14)$$

Recalling that

$$F = F_d + F_u \quad (2.15)$$

$$v = v_d + v_u \quad (2.16)$$

By multiplication with the rod impedance (Z), Eq. (2.16) becomes

$$Zv = F_d - F_u \quad (2.17)$$

Solving for F_d and F_u in Eq. (2.17) and substituting both expressions into Eq. (2.15) the two equations below are obtained

$$F_d = WD = \frac{F + Zv}{2} \quad (2.18)$$

$$F_u = WU = \frac{F - Zv}{2} \quad (2.19)$$

Therefore, if the total force (F) and particle velocity (v) at a given cross-section of the rod are known, the magnitudes of the downward and upward forces can be easily calculated

using the two aforementioned equations. In addition, F_d and F_u are also known as Wave Down (WD) and Wave Up (WU), respectively.

Imagining a pile embedded in the soil, the WD causes a downward movement in the pile, resulting in the mobilization of a resisting force (R_i) at the pile-soil interface. This force is the product of the unit mobilized resistance, the perimeter of the pile and a certain pile length Δx . Thus, the resisting force is of passive nature, meaning it is mobilized only after relative movement between the pile and the soil occurs (neglecting the effect of residual stresses). The mobilized resisting force (R_i) generates two waves of resistance, one upward and one downward, with intensities equal to $R_i/2$ (Figure 2.4). The upward wave compresses the pile shaft, causing particle movement in the same direction as the wave. To maintain continuity in the pile shaft, lower particles also move upward. As a result, the downward wave is a tension wave (propagating in the opposite direction to the particle movement) (PDI, 2014).

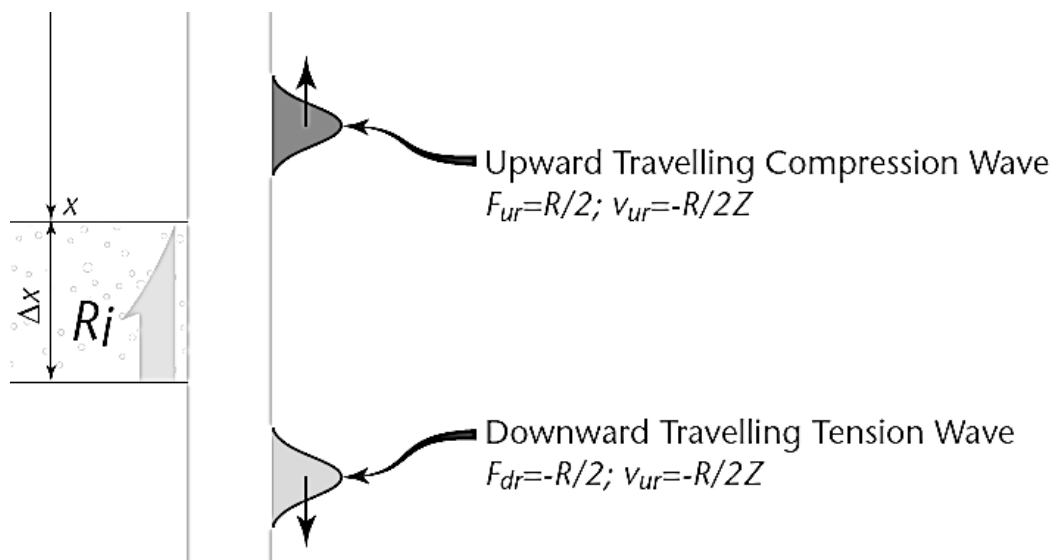


Figure 2.4: Shaft resistance waves. (PDI, 2014).

Analogously, the pile toe resistance (R_b) is an applied force that generates only a single upward compression wave, displacing the particles upward. Since the pile toe resistance is mobilized only after the arrival of the impact wave at the pile toe at a time of L/c , its effect is observed at the top after a time of $2L/c$. The upward compression wave due to frictional resistance ($R_i/2$) reaches the top of the pile at a time of $2x/c$, while the descending wave ($-R_i/2$) reflects from the base as compression ($R_i/2$) and arrives at the top of the pile at a time of $2L/c$, along with the impact wave in tension ($-F_{d,1}$) and the toe resistance in compression (R_b). In this way, the wave reflection process is depicted in the following Figure 2.5:

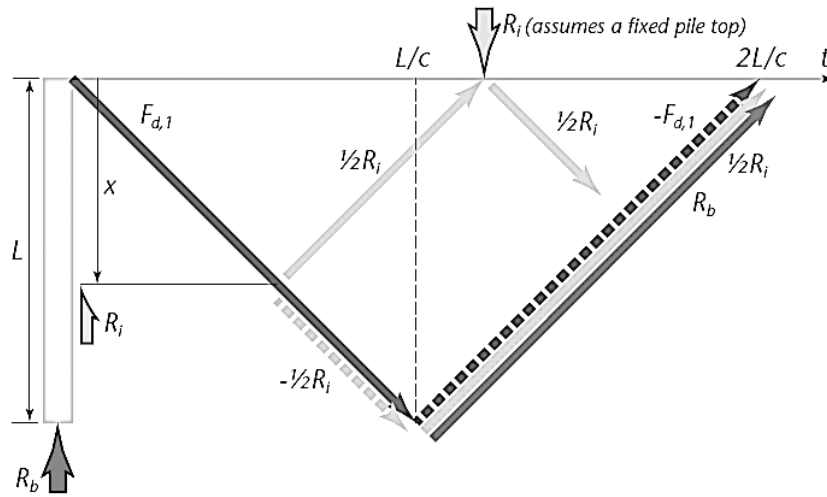


Figure 2.5: Wave reflection process. (PDI, 2014).

Figure 2.6 illustrates the signals of total force and total particle velocity times impedance that can be continuously measured in a section near the top of the pile. It can be observed that the force signals (solid line) and velocity times impedance signals (dashed line) diverge as the resistance waves reach the top. The distance between the two curves is equal to the total mobilized frictional resistance (ΣR_i). The R_i forces presented in Figure 2.6 are the frictional resistances mobilized during the dynamic event, and R_b is the mobilized tip resistance.

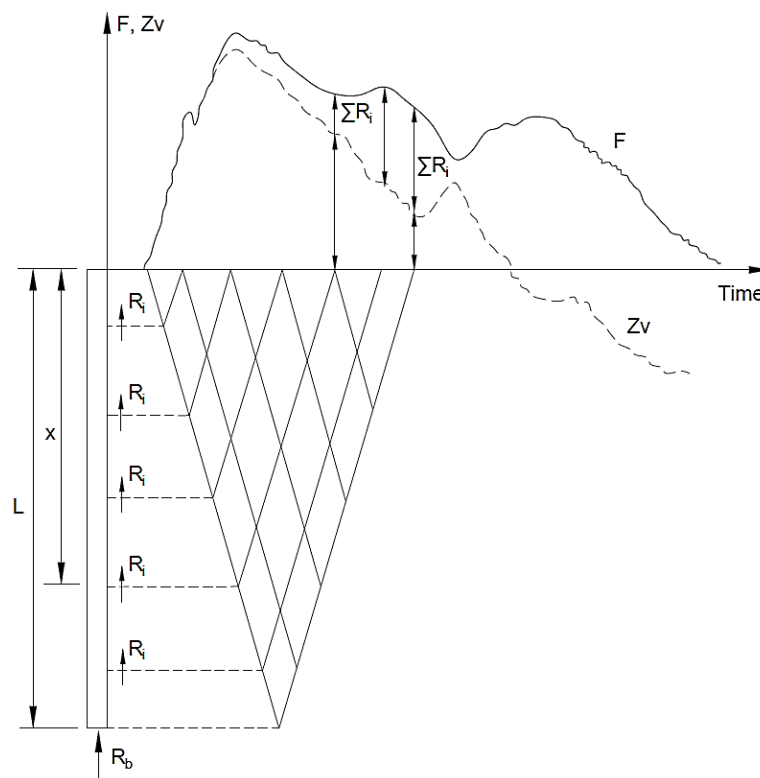


Figure 2.6: Force and velocity times impedance over time.

Therefore, considering the soil resistance, the relationship $F = Zv$ is no longer valid. This is because the curves of F and Zv diverge over time due to the mobilization of skin friction. Thus, the wave equation becomes:

$$\frac{\partial^2 u}{\partial x^2} = \frac{1}{c^2} \frac{\partial^2 u}{\partial t^2} - \frac{R}{EA} \tag{2.20}$$

Where R is the resistance mobilized per unit length. As a result, the wave equation must be solved for the boundary conditions of the problem, which makes its solution quite challenging (Velloso & Lopes, 2011).

A numerical solution for the problem was proposed by Smith (1960), in which the pile, impact system, and damping were modeled using a series of masses and springs (Figure 2.7). In this approach, each mass-spring pair corresponds to a pile segment, with the hammer and helmet considered rigid and represented solely by their respective weights. The cushion is represented solely by a spring (negligible weight). The mobilized shaft and end-bearing resistances are represented by concentrated forces.

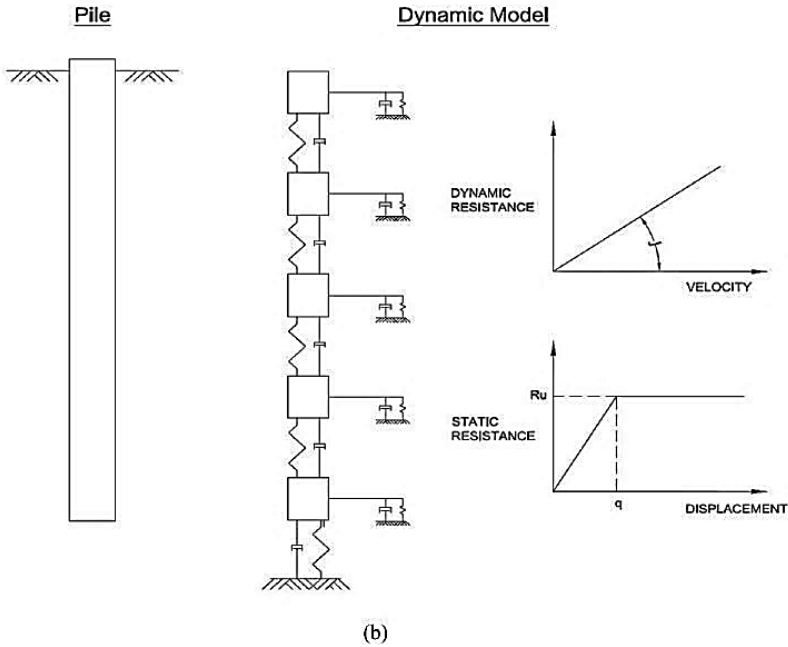


Figure 2.7: Pile’s discrete model (Flynn & McCabe, 2021).

In this model, the shaft and end-bearing resistances can be divided into two components: static and dynamic. The static component exhibits perfectly plastic elastic behavior, where the

static resistance is fully mobilized when the pile element displaces a distance q (quake) due to elastic strain of the soil. Beyond this value, the pile element displaces a permanent amount (s) due to plastic strains under the maximum mobilized static resistance (R_u) (Figure 2.8d). On the other hand, the damping resistance is attributed to the viscous effects of the soil, considering the penetration velocities of the pile elements. This resistance is instantaneous and therefore does not contribute to the actual load-carrying capacity of the pile. Thus, the damping coefficient (J) represents the constant proportionality between damping resistance and the displacement velocity of the pile element (Figure 2.8b).

Hence, the total mobilized resistance is determined by considering the maximum displacements due to elastic strain (quake), the maximum static resistances (R_u) and the damping coefficients (J). Therefore, the behaviors of static and dynamic resistances of each pile element can be represented as those of a spring and a dashpot, respectively (Figure 2.8a).

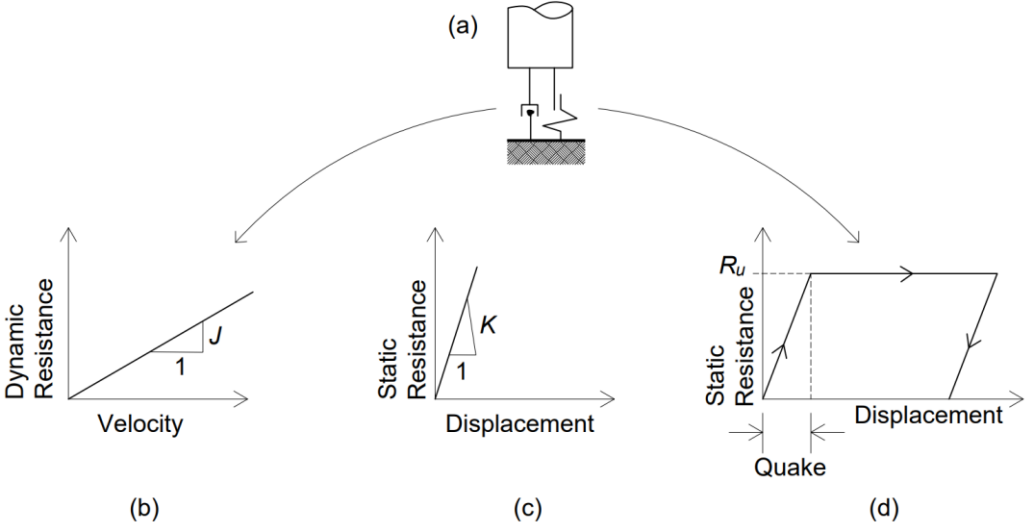


Figure 2.8: Static and dynamic resistances according to Smith. (Velloso & Lopes, 2011).

2.1 DYNAMIC LOAD TESTING (DLT)

The DLT (also known as high-strain dynamic test – HSDT) involves the application of one or more impacts from a hammer with sufficient energy at the top of the pile to induce significant strains. As mentioned by Rausche et al. (2008), it is a common practice to apply 2 to 10 impacts with progressively increasing energy at the top of the pile (by increasing drop heights). Tests with increasing energy impacts enable the creation of a mobilized resistance-maximum displacement curve, where each point corresponds to an applied blow. This approach was introduced in Brazil by Bernardes (1989) and Aoki (1989, 1997), offering a significant

advantage in understanding the load-displacement behavior evolution as hammer blows are applied. This can be related to determining the static load capacity of the pile.

In the case of driven piles, the impacts are delivered through the pile driving accessories (cushions, helmet and hammer). However, for cast-in-place piles, an appropriate impact-damping system must be used, involving the use of cushions and a reinforced concrete cap at the top of the pile to receive the hammer impacts. The concrete used for the cap should have a strength greater than or equal to that of the concrete used in the pile and preferably the same cross-sectional dimensions as the tested pile. In this aspect, the hammer, drop heights and damping accessories have a significant influence on the energy transferred to the tested pile (Rausche & Seidel, 1984).

Hussein et al. (1996) conducted a study analyzing impact and damping systems in the behavior of cast-in-place piles. They concluded that the hammer weight should be approximately 1.5% of the predicted static load capacity of the pile; the hammer drop height should reach approximately 8.5% of the pile length, with a minimum value of 2m; the thickness of the plywood cushion should be approximately $L^2/2D$, minimum value of 100mm, where L and D are the length and diameter of the pile, respectively.

Rausche (1997) presents the design of two drop hammers. According to the author's experience, the weight should range between 1% and 1.5% of the resistance to be mobilized in the test, with the higher value being appropriate for piles with significant tip resistance in cohesionless soils. In such soils, substantial permanent displacements of the tip are necessary to mobilize the entire lateral friction resistance. Especially for CFA piles in cohesive soils or those supported on rock, the hammer weight can be minimized since smaller tip displacements are required to mobilize the total resistance.

Briaud et al. (2000) analyzed three drilled shafts using the DLT with increasing energy. They observed that heavy drop hammers result in larger permanent displacements and require fewer blows, leading to higher mobilized resistances. In the case of a lightweight hammer, the permanent displacements are smaller, requiring a greater number of blows and the mobilized resistances are lower. Thus, larger hammers are more suited for piles with larger displacement (set in sand), while smaller hammers are better suited for piles with smaller displacement (supported on rock).

Rausche et al. (2008) studied the effect of hammer mass on stresses developed in the pile, as well as its permanent displacements in the soil. They employed a WEAP (Wave Equation Analysis of Pile Driving) program to simulate the relationships between the impact and damping systems. In conclusion, they found that:

- Compression stresses increase with the weight of the hammer and the stiffness of the cushion.

- For impacts at the same velocity, tension stresses increase with the stiffness of the cushion. Conversely, increasing the weight of the hammer reduces tension stresses.

- If the ratio between the weight of the hammer and that of the pile is reduced, it is necessary to increase the drop height, which may cause damage to the top of the pile due to high tension stresses.

- If the ratio between the weight of the hammer and that of the pile is high, damage to the shaft of the pile may occur due to high compression stresses.

- Stresses in the pile during impact are a function of the weight of the hammer, impact velocity, drop height, and stiffness of the impact damping system.

Murakami et al. (2022) reaffirmed that a proper selection of the impact system should consider equipment that provides sufficient energy to mobilize pile resistance with an appropriate safety factor and the testing procedures should ensure its structural integrity (acceptable stresses).

The signals of the waves can be recorded over time through reusable strain and accelerometers sensors often bolted two diameters below the pile top (Figure 2.9). In order to compensate for eccentricities and obtain only the axial response of the impact, it is common practice to use at least two strain transducers positioned diametrically opposite to each other relative to the pile axis. This configuration allows for the calculation of a strain average at the instrumented section. Similarly, accelerometers are also positioned diametrically opposite, but they are less sensitive to eccentricities, resulting in nearly identical acceleration signals. The sensors should be axially positioned and securely bolted to the pile body, making contact with a smooth surface (Likins & Rausche, 2008).



Figure 2.9: Accelerometer (on the left) and strain transducer (on the right).



Figure 2.10: Pile Driving Analyzer (PDA).

These sensors remain connected to a data acquisition system that records the signals of acceleration and axial strain, converting them into particle velocity and force signals, respectively (as seen earlier). The most commonly used data acquisition system is the PDA® (Pile Driving Analyzer), developed by the American company Pile Dynamics Inc. (Figure 2.10). Figure 2.11 illustrates an example of force and velocity times impedance signals as functions of time, resulting from a blow applied to the top of a pile:

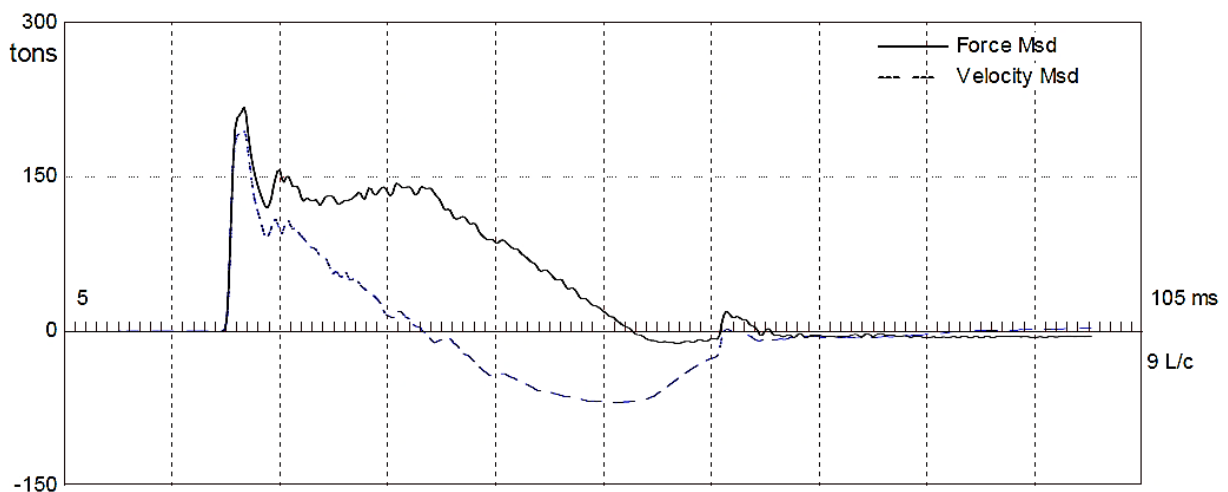


Figure 2.11: Typical signals recorded by the PDA® in dynamic testing.

The signals obtained from the sensors are processed using the simplified CASE method. This method provides information for each applied impact and during the test about the mobilized geotechnical resistance, structural integrity, maximum compression and tension stresses, maximum energy transferred to the pile, and maximum displacement. The CASE method results in a closed-form solution. This method will not be explained in detail because it is applicable only to uniform piles without joints, such as single-segment precast concrete

piles. Therefore, this method does not apply to cast-in-place piles, especially CFA piles, where there are variations in cross-section due to the drilling and concreting process. For non-uniform piles, the analysis should be performed using the numerical method CAPWAP, which will be explained later (Andraos et al., 2009).

2.2 CAPWAP METHOD

Once the force and particle velocity signals are recorded and processed in the PDA, the CAPWAP analysis can be performed. The procedure involves an iterative process between the engineer and the software through signal-matching. In this analysis, assuming a pile-soil profile, the parameters of the pile-soil model are adjusted until the calculated force and velocity signals by the CAPWAP closely match the field-recorded signals from the PDA (Souza et al., 2021). Thus, the static resistance mobilized, resistance distribution, soil static stiffness (quake), soil dynamic stiffness (damping factor), simulated load-displacement curve and the forces in the pile at mobilized resistance are determined (Hussein & Mukaddam, 1994). Also, according to works presented by Likins & Rausche (2004) and Green & Kightley (2005) apud Alwalan & Naggar (2020), the CAPWAP is in good agreement with the results of SLT.

The CAPWAP is based on the idea proposed by Smith (1960) and its principle is to determine the unknowns of each pile element in the model: the maximum displacements due to elastic deformations (quake), the maximum static resistances and the damping factors. (Aghayarzadeh et al., 2020). This is possible because the impact hammer serves as a boundary condition and the force and velocity measurements are redundant. Therefore, the model's unknowns can be directly determined in a trial-and-error matching procedure. From this, the signals generated through the parameters help the system achieve dynamic equilibrium (Likins & Rausche, 2000).

Over the years, CAPWAP has undergone a series of improvements that have contributed to simulations of the actual behavior of tested piles. An important improvement in the CAPWAP model occurred when Rausche (1989) incorporated dashpots to support the soil, allowing for a better signal adjustment. In their work, the authors also state that modeling without these dashpots would be impossible. Furthermore, Smith's model has been modified by incorporating other elements such as: damping from the pile material itself, residual stresses, negative skin friction, inertia effects, plugging, unloading quake, among others (PDI, 2014).

Then, the pile and soil model of the CAPWAP method will be briefly presented, as well as the signal-matching technique used to analyze the signals.

2.2.1 PILE MODEL

The numerical analysis CAPWAP is based on the Method of Characteristics to solve the One-Dimensional Wave Equation (Eq. 2.11). As mentioned earlier, the solution can be conceptualized as a downward wave (f) and an upward wave (g). These waves are applied to a sequence of short and uniform segments that could potentially differ from one another, particularly in the context of a non-uniform pile (Figure 2.12).

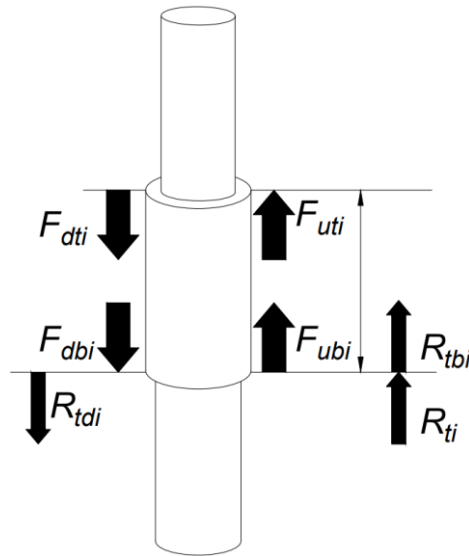


Figure 2.12: Pile model (PDI, 2014).

The fundamental principle of the solution involves applying the waves f and g (Figure 2.3) to each pile segment. Therefore, considering the incidence of a downward wave at the top of a specific segment i (F_{dti}), after a time increment (Δt), the wave will arrive at the base of the segment as F_{dbi} . The F_{dti} and F_{dbi} waves have the same magnitude, but considering that the total resisting force (R_{uti}) acts at the base of the segment, the upward wave at the top of the segment (R_{uti}) will have an intensity equal to $R_{ubi} + 0,5R_{ti}$. Analogously, the resisting force will cause a downward tension wave with a magnitude also of $0,5R_{ti}$, which will affect the magnitude of the downward wave in the segment below (PDI, 2014).

CAPWAP considers that waves should propagate within each segment at constant time intervals (Δt). In other words, the length of each segment is given by $\Delta L_i = c_i \Delta t$, where c_i represents the wave velocity in segment i . As a result, the values of WD and WU are calculated for each element at the moments they reach the base and the top, respectively. On the other hand, the displacement of each segment is calculated through Euler integration based on the velocity.

The pile profile is defined by the cross-sectional area, specific mass, modulus and perimeter of each element, which is used to calculate the unit resistance in the output. Therefore, each segment i has its impedance $Z_i = E_i A_i / c_i$. Additionally, the stiffness of each element is also used for calculating the load-set curve ($E_i A_i / \Delta L_i$). Lastly, CAPWAP also allows for splices in the pile to be modeled and it is possible to consider the damping of the pile material itself.

2.2.2 SOIL MODEL

The resistance of the pile-soil interface is modeled by an elastoplastic spring and a linear dashpot, described by three parameters in each soil segment k : ultimate static resistance (R_{uk}), quake (q_k) and viscous damping (J_k). As previously presented, the total resistance of each soil segment (R_k) is the sum of static (R_{sk}) and dynamic (R_{dk}) resistances mobilized as the wave propagates in the pile:

$$R_k = R_{sk} + R_{dk} \quad (2.21)$$

In the basic Smith (1960) model, the static resistance is a function of displacement and the dynamic resistance is a function of the velocity at which the pile element moves relative to the soil. Consequently, the total resistance before rebound occurs can be calculated in the following manner:

$$R_k = \begin{cases} \frac{R_{uk}}{q_k} u_i + J_k v_i & , \quad u_i < q_k \\ R_{uk} + J_k v_i & , \quad u_i \geq q_k \end{cases} \quad (2.22)$$

Where

u_i : displacement of the pile segment relative to the soil;

v_i : velocity of the pile segment relative to the soil.

Hence, as the displacement and velocity of each pile element are functions of time (vary with the wave propagation), the resistances also vary over time.

The static resistance of the soil (R_{sk}) is represented by a linear spring with a slider element that limits the force on the spring to the R_{uk} during loading and to R_{nk} during unloading. The static resistance during the dynamic event can be represented by the following charts for the shaft and the toe:

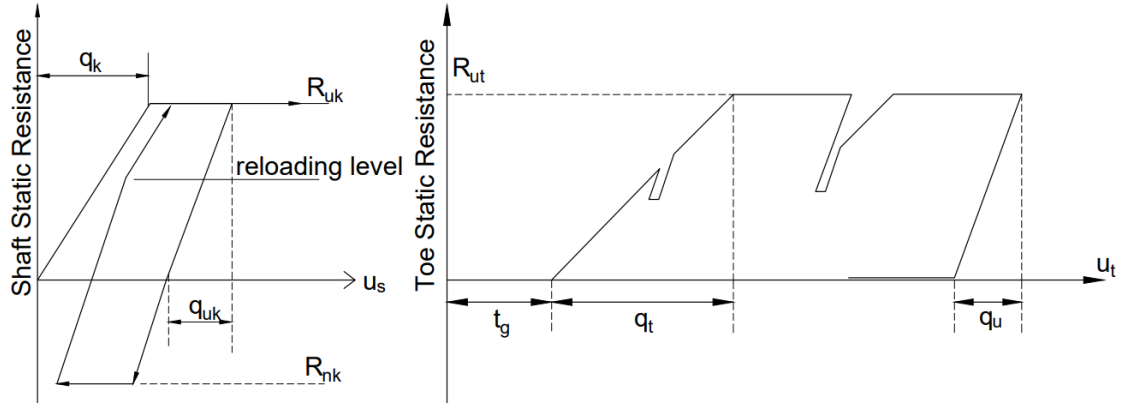


Figure 2.13: Static resistance as a function of shaft displacement (left) and toe displacement (right) (PDI, 2014).

It can be observed that, for the shaft, static resistance is elastically mobilized as displacement increases up to the quake value (q_k), where resistance is maximum ($R_{sk} = R_{uk}$). Beyond this point, there is permanent displacement under the ultimate resistance. Therefore, during the DLT, the pile must displace at least the quake to reach its ultimate capacity. In other words, each segment of the CAPWAP model should have a displacement equal to or greater than the q_k (PDI, 2014). In this context, Hannigan et al. (2016) recommend that the DLT be conducted with sufficient energy resulting in a permanent displacement of at least 2.5mm per blow, with this value limited to 12mm per blow. This ensures an adequate activation of the resistance. Furthermore, according to Rausche et al. (2018), these limits are suitable for low-plasticity soils. Goble & Rausche (1976) recommend that the permanent displacement obtained in the DLT should be at least the diameter of the pile divided by 120.

As observed in Figure 2.13, during unloading the mobilized resistance decreases linearly until it becomes zero, indicating an unloading quake (q_{uk}). The value of q_{uk} is determined by the a_u multiplier in the following equation:

$$q_{uk} = a_u q_k \quad (2.23)$$

CAPWAP considers that $0 < a_u \leq 1$, demonstrating that the unloading stiffness is greater than the loading stiffness. According to PDI (2014), it is common for a_u to be greater than 0.3 and never less than 0.1.

During rebound, the mobilized static resistance can become negative since the pile segment's displacement can be upward. Therefore, the mobilized soil resistance is constrained between these two values (Figure 2.13):

$$R_{nk} \leq R_{sk} \leq R_{uk} \quad (2.24)$$

In Smith's model, the lower limit of shaft resistance (R_{nk}) is equal to $-R_{uk}$, as follows:

$$-R_{uk} \leq R_{sk} \leq R_{uk} \quad (2.25)$$

However, CAPWAP incorporated a multiplier U_n that allows this limit to vary between $-R_{uk}$ and 0. As a result, the value of mobilized shaft resistance varies between $-U_n R_{uk}$ and R_{uk} . This multiplier allows for the consideration of residual driving stresses in the modeling. Another important characteristic is that U_n always has a zero value for the pile's toe (Figure 2.13), ensuring that the toe resistance during unloading is limited to zero.

As seen in Figure 2.13, it is also possible to simulate a remobilization of resistance in CAPWAP. For this, the stiffness in the pile-soil interaction is equal to that of unloading (R_{uk}/q_{uk}) up to a reloading level, beyond which the stiffness decreases, becoming equal to that of the initial loading (R_{uk}/q_k).

Specifically for the pile toe, it is possible to model a gap (t_g) that represents a space left between the pile tip and the soil. In this way, the resistance is activated only after the tip has moved a certain distance (t_g). This gap can be modeled due to loose soil under the pile tip or due to rebound following a previous impact, which causes the pile to lose contact with the tip soil, as the shaft resistance can become negative.

In the basic soil model, viscous resistance forces are considered as a function only of the velocity of the pile segment relative to the soil. These forces oppose penetration and are responsible for decelerating the pile. CAPWAP considers dynamic resistance as a function of both velocity and static resistance. In this regard, the calculation of dynamic resistance can be performed through two distinct approaches: Traditional or Smith-viscous.

Comparing real records to those simulated by the wave equation, it is observed that Smith's traditional approach produces a lesser damping effect. In other words, the calculated dynamic resistance is typically lower than what actually occurs during the dynamic event. This is why CAPWAP utilizes Smith-viscous model, represented by a linear dashpot.

The traditional Smith approach calculates dynamic resistance as follows:

$$R_{dk} = J_{sk} v_i R_{sk} \quad (2.26)$$

Where R_{dk} is the dynamic resistance in soil segment k ; J_{sk} is Smith's dimensional damping factor; v_i is the velocity of pile segment i and R_{sk} is the temporarily mobilized static resistance in soil segment k . The unit of J_{sk} is equal to the inverse of the unit of velocity (seconds/meter).

The second calculation method is the Smith-viscous approach, where dynamic resistance is calculated using the ultimate static resistance (R_{uk}) in soil segment k :

$$R_{dk} = J_{sk} v_i R_{uk} \quad (2.27)$$

It is observed that this approach is similar to the previous one, but it sets R_{sk} equal to R_{uk} . Since the ultimate static resistance is the maximum value that the static resistance can reach, the damping effect is greater, making it closer to reality when field records are observed.

The CAPWAP typically calculates dynamic resistance using Eq. (2.27). However, users can specify how the program performs the calculation, both for the shaft and the pile toe. As a result, the software provides a choice between three alternatives: the Smith-viscous approach (Eq. 2.27), the traditional Smith approach (Eq. 2.26) or a combination of both through the following conditions:

$$R_{dk} = \begin{cases} J_{sk} v_i R_{sk} & , R_{sk} < R_{uk} \\ J_{sk} v_i R_{uk} & , R_{sk} = R_{uk} \end{cases} \quad (2.28)$$

The last calculation option is more recommended for the pile toe, especially when dealing with large quakes or when using the toe gap feature (PDI, 2014).

Smith's fundamental model postulates that the energy associated with soil resistance is exclusively dissipated at the pile-soil interface, assuming rigid soil behavior (Figure 2.14). However, factors like soil type, pile shape, volume and pile surface roughness have a significant influence, causing the soil to strain around the pile as stress is transmitted to the soil mass. As a result, some of the impact energy is dissipated through soil strain. This phenomenon is referred to as "Radiation Damping" in the context of CAPWAP (Likins et al., 1992). Therefore, the soil displacement around the pile represents an inertial resistance that has a significant effect when the pile segment's velocity is low and no true shearing occurs at the pile-soil interface. Furthermore, as pointed out by Likins et al. (1992), the soil model was subsequently enhanced by introducing a mass and a dashpot as separate components from the standard Smith model (Figure 2.15). As a result, soil displacement becomes a function of the dashpot's "stiffness". This effect is typically encountered in displacement piles or drilled shafts installed in fine and dense sands or saturated silts.

Another typical example of this effect occurs in piles embedded in rock. The pile displacement tends to be small, making the mobilized resistance appear to be more dependent on the displacement velocity. Thus, the term "Radiation Damping" is used because energy is radiated from the pile to the geomaterial more than it is used to shear the interface between the pile and the geomaterial (PDI, 2014).

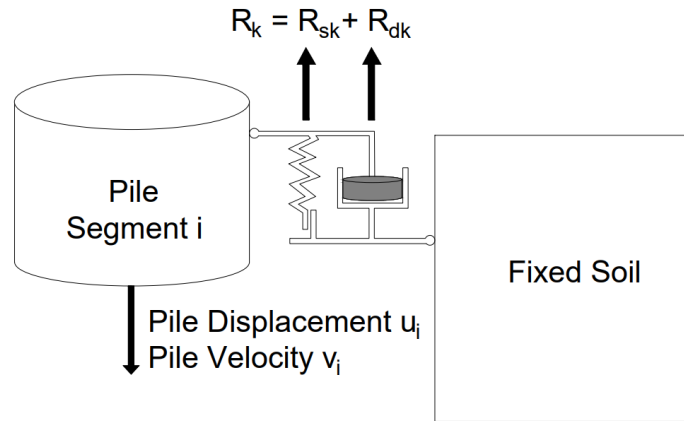


Figure 2.14: Smith's soil model considered fixed.

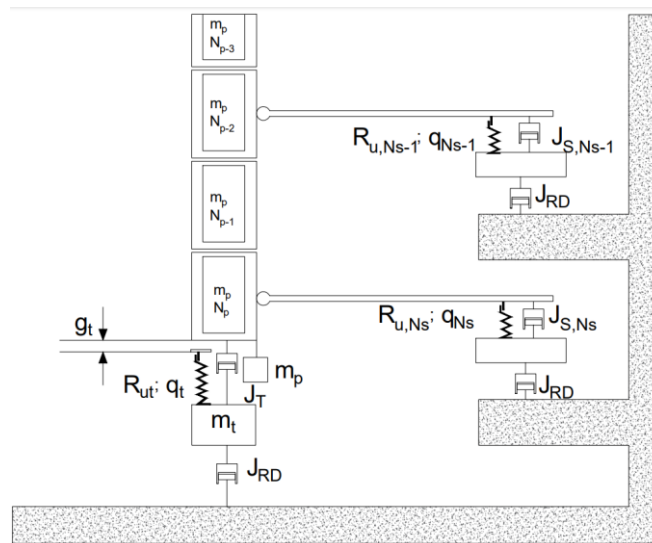


Figure 2.15: The complete CAPWAP's soil model with radiation damping.

2.2.3 CAPWAP PROCEDURE

With both measurements at the top of the pile available (force and velocity), the input and response at the pile's top are known (Wave Down and Wave Up, see Eqs. 2.18 and 2.19). However, the part of the system responsible for producing the response, the soil, is unknown. To determine the soil properties, a reverse analysis is performed, typically referred to as "signal-matching." This solution is achieved iteratively until the assumed soil parameters result in a sufficiently satisfactory fit between the measured signals and those calculated by the pile-soil model (Rausche et al., 2000).

To assess the fit between the signals and, consequently, to evaluate if the proposed soil model is reasonably adequate, CAPWAP employs a measure called Match Quality (MQ). The lower the MQ value, the better the fit between the signals. To calculate the MQ , CAPWAP

divides the signal used in the analysis (typically WU) is divided into four different time periods: I, II, III, and IV (Figure 2.16).

Period I is the time from the onset of impact (t_0) to the instant $t_0 + 2L/c$. This segment highlights the distribution of resistance along the pile, with the rate of change in WU numerically equal to the skin friction developed in the pile. Period II, on the other hand, begins from $t_0 + 2L/c$ and continues until $t_r + 3\text{ ms}$ later. The value of t_r is the time between the beginning of the impact and the corresponding peak velocity. Period II is characterized by the development of toe resistance. Period III is defined between the times $t_0 + 2L/c$ and $t_r + 5\text{ ms}$ later. This period represents the development of the total mobilized resistance. Finally, Period IV occurs between $t_0 + 2L/c$ and 25 ms later, representing the unloading (rebound) behavior.

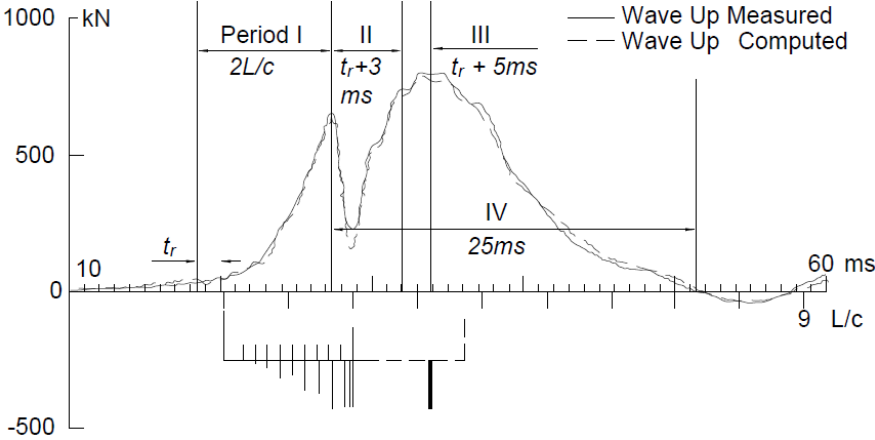


Figure 2.16: MQ time periods (PDI, 2014).

It is observed that Periods II, III, and IV overlap in the vicinity of the time $t_0 + 2L/c$. Consequently, this region of the record will receive additional influence in the MQ calculation (PDI, 2014). For each of the periods, an error is calculated as the sum of the absolute differences between the calculated quantity and the field-measured data with sensors. These quantities can be WU , average force or even particle velocity measured at the pile head. Typically, WU is used since its behavior exhibits the developed resistance most clearly.

Including the overlap of the periods, the four error values are summed, and then an average is calculated. This average is computed by dividing the sum by the number of points involved in the signal. Then, this value is divided by the maximum force measured at the top of the pile, and it can be expressed as a percentage by multiplying it by 100.

The maximum force measured at the top of the pile is used to make MQ dimensionless and also because it serves as a reference in the field-measured signal. The maximum force occurs at the beginning of the signal and is directly related to the downward force developed

by the hammer blow. This force is equal to the maximum particle velocity times the impedance of the pile.

Given the explanation above, mathematically MQ is calculated by the following equation:

$$MQ = \left\{ \frac{\sum_{l=1}^4 (\sum_{i=1}^{N_l} |WU_{mi} - WU_{ci}|)}{\sum_{l=1}^4 N_l} \right\} \frac{100}{F_{m\acute{a}x}} \quad (2.29)$$

N_l : number of points in each time period;

WU_{mi} : wave-up measured at time i ;

WU_{ci} : wave-up calculated at time i ;

$F_{m\acute{a}x}$: maximum force measured at the top of the pile.

In summary, the signal-matching procedure can be summarized as follows:

- I) Select a force/velocity record from a significant blow for analysis;
- II) Set up a mechanical pile model by discretizing it into small segments, with the model's top being the point where force and velocity are measured;
- III) Configure a mechanical soil model, representing the distribution of its resistance as concentrated forces on the pile segments;
- IV) Perform the initial attempt at soil resistance parameters (ultimate static resistances, quakes and damping factors);
- V) Analyze the pile-soil system, prescribing one of the three measured quantities: force, velocity or downward force (WD). Calculate the complementary quantity: velocity, force or upward force (WU);
- VI) Compare the calculated signal with the measured signal, calculating the MQ ;
- VII) Assess the differences between the measured and calculated curves and adjust the soil resistance parameters and/or pile model to improve the MQ . Repeat the process from step V until a satisfactory MQ is achieved;
- VIII) When the MQ is satisfactory (less than 5.0), the distribution of static resistance and the pile-soil model are defined, enabling a t-z/q-z analysis to simulate a SLT.

According to Rausche et al. (2000), in general, MQ values greater than 5.0 are considered unreliable. Furthermore, according to PDI (2014) and Rausche et al. (2018), the CAPWAP procedure should not be simply aimed at minimizing the MQ value, as there are several effects related to the CAPWAP result that need to be considered by the analyst. Therefore, the MQ should be as low as possible, but the pile-soil model must have a physically meaningful connection with reality.

According to Bruno & Randolph (1999), a perfect match is not possible since the rheological models are simple (springs and dashpots). As a result, the distribution of soil parameters should not be considered unique but rather a better match by a particular software operator. In this regard, as mentioned by Kuei et al. (2020), the reasons for the non-unique solution in CAPWAP can stem from various sources, including the numerous unknown parameters that are estimated from limited measurements.

2.3 QUAKE AND DAMPING FACTOR VALUES

For the pile toe quake (q_t), Thompson & Goble (1988) understand that there is a clear relationship with the pile tip diameter. Rausche et al. (2008) further notes that q_t is also a function of the pile material, soil densification or loosening due to pile installation, the stiffness and resistance of the geomaterial.

Smith (1960) states that a 2.5mm pile q_t is valid as long as the pile is of small diameter whereas Islam et al. (2022) recommends q_t to be equal to the pile diameter divided by 120 for piles driven into soil and 1mm for piles close to a rocky top. However, Authier & Fellenius (1980), Likins (1983) and Hannigan & Webster (1987) apud Rausche et al. (2010) recommended that q_t should be equal to the pile diameter divided by 60.

According to Flynn & McCabe (2019), q_t varies between $D/120$ and $D/60$, depending on the pile type. Randolph & Deeks (1992) suggest that this range is between $D/100$ and $D/50$, where D represents the pile toe diameter.

Through a theoretical approach, q_t can be calculated according to the equation presented by Randolph & Deeks (1992):

$$q_t = \frac{0.2D}{G} \sigma_{ubr} \quad (2.30)$$

Where

D : pile diameter;

σ_{ubr} : is the unit base resistance.

Authier & Fellenius (1980) presented three interesting case studies in which q_t was high (around 20mm) in driven piles. The occurrence of high q_t is not well understood, but it is believed to be related to pore pressure developed during pile installation. According to these authors, a practical significance of high q_t is that a given hammer may not be able to mobilize the necessary resistance in the DLT.

Similarly, Likins (1983) also discussed three cases in which q_t were high, both in sandy and clayey soils. The only common aspect among the three cases is that the soils were saturated. Therefore, as with Authier & Fellenius (1980), it is likely that the high q_t occurred due to excess pore pressure developed during pile driving in poorly drained soils.

Murakami (2015) stated that the q_s has a significant influence on the determination of the friction distribution along the pile. With an increased q_s , more time is needed to mobilize the lateral resistance towards the pile tip. In this regard, according to Allin et al. (2021), a significant limitation of CAPWAP is the determination of shaft resistance near the pile tip. For example, Fellenius (1988) stated that usually the obtained static resistance varies little for different CAPWAP operators, but the distribution of shaft resistance and toe resistance can vary considerably.

Based on a theoretical formulation involving shear strength and shear modulus, Randolph & Deeks (1992) as cited in Rausche et al. (2008) estimate that the q_s should be in the range of 0.2 to 0.5% of the pile diameter. Murakami & Massad (2016) presented a methodology to determine the q_s through SLTs and DLTs on driven piles. These authors used the "displacement matching" technique, which can be studied in detail in Murakami (2015).

Based on the theoretical load transfer relationship developed by Randolph & Wroth (1978) apud Sakr (2013), the shaft quake (q_s) can be calculated using the following equation:

$$q_s = \frac{\tau_u r_0}{G} \ln \left(\frac{r_m}{r_0} \right) \quad (2.31)$$

Where

τ_u : is the yield shear stress at pile interface;

r_0 : is the radius of the cross-section of the pile;

r_m : is the radius at which the shear stress becomes negligible;

G : is the shear modulus of soil.

Murakami & Massad (2014) state that q_s between 1.0 and 7.5mm is acceptable; however, there is a q_s value that results in a better signal match (a lower MQ).

According to Souza & Albuquerque (2016), the q_s depends on the soil type, pile type, pile material, and impact energy. Additionally, the q_t is greater for piles supported in clays, silts, fine sands, and saturated soils.

According to PDI (2014), it is recommended that J_s be between 0.08 and 1.30 s/m. This recommendation is valid for typical driving velocities and moderately plastic soils commonly encountered in test practice. However, for small velocities (less than 0.3 m/s), Coyle & Gibson

(1970) suggest that dynamic resistance should be calculated as follows, where n is approximately 0.2:

$$R_{dk} = J_{CG} v_i^n \quad (2.32)$$

Where J_{CG} is the Coyle & Gibson (1970) damping factor. For a more detailed study, it is advisable to refer to the original work.

In general, Flynn & McCabe (2019) suggest that J_s should range from 0.16 to 0.65 s/m, while the value should be on the order of 0.15 s/m for the toe (J_t). Rausche et al. (2008) state that damping factors can vary widely, often with little correlation to soil types. Nevertheless, values obtained through CAPWAP analyses show good agreement with SLT results. Therefore, these authors suggest that the J_s should be in the range of 0.65 s/m for clay and 0.16 s/m for sands as indicative values.

Thompson & Goble (1988) investigated the occurrence of high damping factors in piles driven into sands. These authors concluded that there is no clear relationship between soil type and density with the damping factor, although it is more likely to be related to the depositional and mineralogical characteristics of the sands. Furthermore, it is recommended that the investigation of J_s and J_t be carried out through CAPWAP analyses and SLTs.

The overestimation of soil static resistance due to velocity effects is a concern because deep foundations predominantly supported by lateral friction in highly plastic soils tend to exhibit plunging failure, at best. In the worst-case scenario, they demonstrate peak resistance behavior (softening). Additionally, the effects of pile acceleration must be considered, as they can generate high temporary soil resistance, especially at the tips of piles in cohesive soils. This inertial effect has not been thoroughly studied (Rausche et al., 2018).

In addition to the previously suggested values, articles, theses, and dissertations were consulted to evaluate typical values of shaft quake and damping for CAPWAP analyses. In these studies, the values presented in Table 2.1 were mostly considered constant along the pile shaft, neglecting the variation in soil properties across different layers along the shaft.

In studies that provided results from multiple CAPWAP analyses on different piles, the mean value and coefficients of variation for each parameter were calculated. Additionally, Table 2.1 presents the type of pile used, the predominant soil type along the shaft and the location of the studies.

It is observed that the mean values for q_s were around 2.5mm. However, similar to J_s , q_s showed high coefficients of variation. Although the study by Marchezini (2013) resulted in values very close to those suggested by Coyle et al. (1973) and Hannigan et al. (1998) for

clayey soil, the works of Souza & Albuquerque (2016) and Generoso (2014) resulted in J_s values very different from those suggested by Coyle et al. (1973) and Smith (1960) for silty soil.

Table 2.1: Typical shaft quake and damping according to different authors.

Pile Type	Soil Type	q_s		J_s		Source	Location
		Mean (mm)	CV (%)	Mean (s/m)	CV (%)		
CFA	Silt	2.91	37	0.98	41	Souza & Albuquerque (2016)	São Paulo, Brazil
Driven Precast	Clay	2.61	74	0.70	47	Marchezini (2013)	Federal District, Brazil
CFA	Silt	2.13	67	1.29	21	Generoso (2014)	Belo Horizonte, Brazil
Driven Steel	Sand	1.56	38	-	-	Lima (1999)	São Carlos, Brazil
Driven	Any	2.54	-	0.16	-	Smith (1960)	USA
-	Clay	2.54	-	0.66	-	Coyle et al. (1973)	USA
-	Silt	2.54	-	0.33	-	Coyle et al. (1973)	USA
-	Sand	2.54	-	0.16	-	Coyle et al. (1973)	USA
-	Cohesive	2.54	-	0.66	-	Hannigan et al. (1998)	USA
-	Cohesionless	2.54	-	0.16	-	Hannigan et al. (1998)	USA
Driven Pipe	Any	2.50	-	0.1-1.4	-	Rausche et al. (2009)	USA

2.4 FOUNDATION ENGINEERING PRACTICE IN SINOP

Mato Grosso is one of the largest states in Brazil, with an area of approximately 903,357 km². Consequently, there are naturally different geological formations that directly influence the soil properties in various regions of the state. Specifically, in Sinop - MT, as will be detailed in section 3.1.1, there is a predominance of alluvial soil characterized by poorly consolidated sediments, very soft to soft clay, clayey silt and poorly to moderately compacted silty sand, with significant thicknesses, exceeding 50 meters from the perspective of foundation engineering.

In this regard, the foundations of buildings and grain storage structures are predominantly deep, reaching depths of 30 to 50 meters, depending on the terrain's peculiarities and the magnitude of the loads. Generally, there is a preference for using cast-in-situ piles such as CFA and drilled shafts with stabilizing fluid, with nominal diameters ranging from 50 to 120 cm.

These piles have been preferred by foundation engineers because the groundwater table is close to the surface and they possess satisfactory structural strength and rigidity, capable of reaching depths above 30 meters, where there is an increase in soil resistance according to the SPT. Another factor contributing to the use of these two types of piles is the availability of machinery in the region. Alternative options, such as steel piles, are out of use in the city due to the lack of equipment suppliers and mainly due to the high transportation costs of these piles from supplier states like Sao Paulo and Minas Gerais to Sinop.

The foundation projects for buildings and storage structures in Sinop have a fundamental concern with the occurrence of admissible displacements. Since the soil is relatively compressible, the projects generally rely not only on SPT results. For project definitions, static load tests are conducted to obtain the load-displacement behavior of a single pile. Once the project is defined, additional tests are usually conducted to verify performance and analyze overall foundation reliability.

SLT are predominantly conducted using a reaction system composed of robust steel beams and reaction piles cast in situ or helical piles. Tests of up to 10,000 kN have been conducted with these characteristics on CFA piles and drilled shafts at depths of 40 to 50 meters.

DLT is typically conducted using impact application devices with hammers weighing between 60 and 200 kN. As previously mentioned, reinforced concrete extensions with dense reinforcement are constructed to receive the hammer impacts. Blows with increasing energy are applied to ensure that the pile tip displaces sufficiently to mobilize the required design resistance.

2.5 LITERATURE REVIEW COMMENTS

In this chapter, the main characteristics of the DLT and the theoretical framework involved in the propagation of stress waves in piles and CAPWAP analyses were presented. For CAPWAP analyses, the influence and importance of selecting q_s and J_s in the signal-matching technique were highlighted. In addition to influencing Match Quality (MQ), these parameters can affect the determination of mobilized static resistance and its distribution along the pile shaft. Consequently, they are related to predicting the displacement of the pile when subjected to compression.

However, despite this importance, the variation of q_s and J_s depending on soil type and its properties is still not well understood by the technical community. This scenario is more noticeable in Brazil, where there is a limited number of research studies addressing the topic. Even in the consulted works, the variability of parameters for different soil types and piles is evident.

Therefore, given the literature review presented, it is imperative that this dissertation addresses the determination of correlations between soil properties and q_s and J_s along the shaft, especially for CFA piles. This is expected to provide a better understanding of the variation of CAPWAP model parameters based on soil type and its properties, thereby increasing the reliability of the analysis results and reducing the sole influence of subjectivity and professional experience in signal analysis.

3. METHODOLOGY

3.1 SINOP CITY: LOCATION AND CLIMATE

The research was conducted in the city of Sinop, state of Mato Grosso, Midwest region of Brazil. The urban area of the city is bounded from north to south by parallels $11^{\circ}48'$ and $12^{\circ}00'$, and from west to east by meridians $55^{\circ}35'$ and $55^{\circ}26'$. Sinop is approximately 310 miles from the state capital Cuiabá and 870 miles from the federal capital Brasília.

According to Miranda & Amorim (2000), the city is situated in the transition between the Cerrado biome to the south and the Amazon Rainforest to the north (Figure 3.1). The climate is markedly hot and humid equatorial, with an average temperature of 25°C . The rainfall regime is well-defined in two periods: the rainy season, which occurs between January and March, and the dry season between June and August. The average annual precipitation is approximately 2500mm. (SEPLAN, 2007 apud Knechtel, 2015).

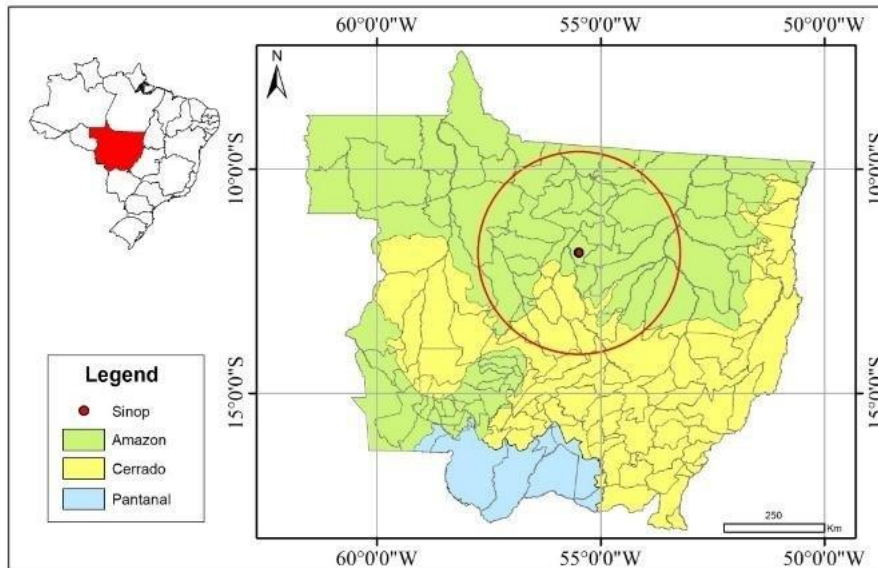


Figure 3.1: Location of Sinop (Martim et al., 2020).

The territory is predominantly situated within the geomorphological unit of the Parecis Plateau, where the terrain is flat and gently undulating (Melo & Franco, 1980). This topography, combined with the climate, has directly contributed to the region's economic prominence in agribusiness, particularly with soybean and corn cultivation.

3.1.1 GEOLOGICAL ASPECTS

According to Cutrim et al. (2021), Sinop is located in the Parecis Sedimentary Basin. In this basin, the Parecis Group is composed of the Rio Ávila, Salto das Nuvens, Utariti, and Ronuro formations.

The Rio Ávila formation, from the Jurassic period, underlies the other formations. This formation is characterized by medium bimodal pink sandstone with cross-bedding. Next is the Salto das Nuvens formation from the Cretaceous period, which is also characterized by bimodal sandstone with cross-bedding, but with polymictic conglomerate of fine red sandstone. According to Bahia (2007), the conglomerate also contains pebbles of gneiss, slate, and quartz interbedded with fine sandstone.

The Utiariti formation overlies the Salto das Nuvens formation. This formation is composed of bimodal sandstone with cross-bedding at the base and fine sandstones on top. In its middle position, there are pebbles and lenses of argillite, while at the upper portion, there is bimodal sandstone also with cross-bedding (Bahia, 2007). According to Cutrim et al. (2021), the Utiariti formation is from the Cretaceous period and has a fluvial origin, consisting of fine to medium sandstone with red, yellow, and white colors, with occurrences of siltstones. This formation outcrops over 92% of the area of Sinop city.

Finally, overlying the Utiariti formation is the Ronuro formation, which is of Tertiary/Quaternary age and consists of poorly consolidated sediments including sand, silt, clay, gravel, and laterites. This formation outcrops over approximately 8% of the surface, mainly in well-drained areas such as rivers. These sediments have an alluvial origin.

The Table 3.1 summarizes the characteristics of the Parecis Group that define the subsurface of Sinop.

Table 3.1: Stratigraphic chart of Sinop (Cutrim et al., 2021).

Era	Geochronology		Lithostratigraphy		
	Period	Epoch	Units		
			Group	Formation	
				Lithology	
Cenozoic	Tertiary	Neogene		Ronuro	Sand, silt, clay, gravel and laterites.
				Utiariti	Fine to medium-grained sandstone, with yellow, red, and white colors. Small-scale cross-bedding, with scattered pebbles.
Mesozoic	Cretaceous		Parecis	Salto das Nuvens	Polymictic conglomerate, coarse sandstone, red fine sandstone, coarse sandstone with large-scale cross-bedding, siltstone, claystone, calcareous claystone, and marl; fossiliferous. Fluvio-lacustrine evaporitic sequence.
					Rio Ávila
	Jurassic				

3.2 TEST SITES

Figure 3.2 shows the location of the test sites used for the development of this research. Site A is located in the Florença Residential District, while Site B is in the Northern Residential Sector of the city of Sinop. There is a distance of approximately 3.3 km between the two locations. Site A will be used as a reference and was geotechnically characterized through SPT, VST, particle size distribution, and determination of Atterberg limits. Additionally, at Site A, a SLT and two DLTs were performed for the development of the analyses. Site B was used to validate the results obtained at Site A, also receiving SPT and VST field tests, in addition to DLT. These tests will be described in detail later in this dissertation.

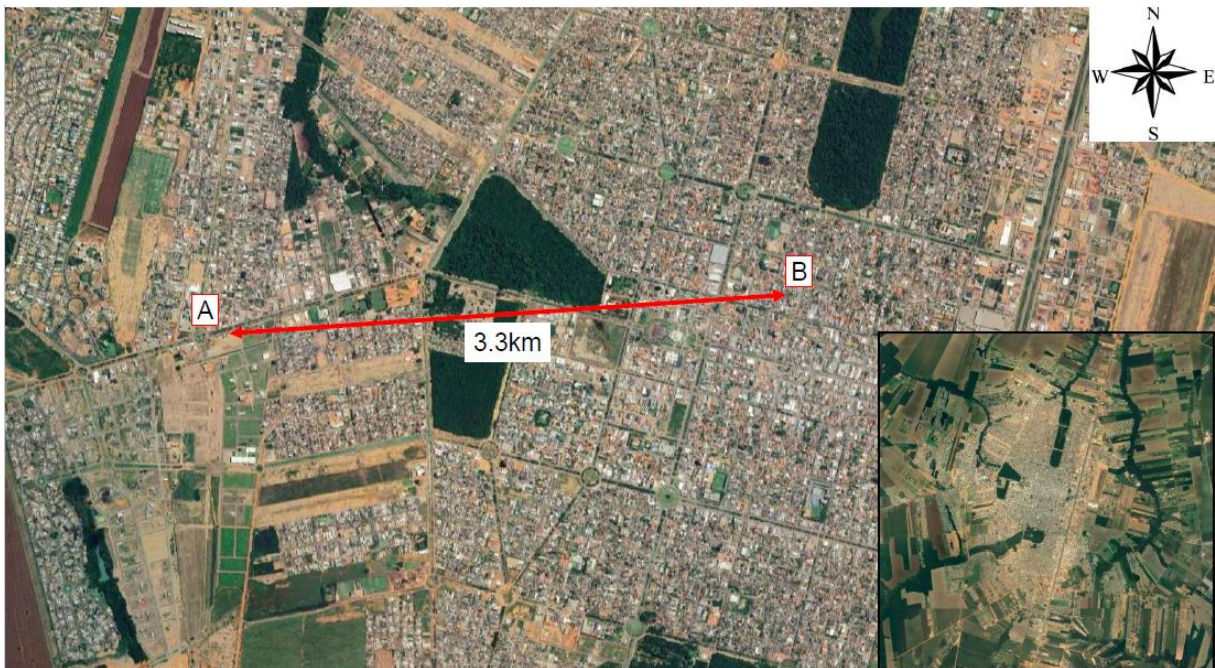


Figure 3.2: Location of testing sites.

Both sites received the construction of residential buildings. Site A received a 28-story building with a foundation solution consisting of 312 CFA piles with nominal diameters of 50 and 60 cm and depths of 32 meters. The project was based on SPTs with semi-empirical correlations for determining the foundation's load-bearing capacity, as well DLT and SLT at the beginning of the foundation construction.

Site B will have a 42-story building whose foundation is currently under study (as of June 2024). The choice of foundation solution has undergone several changes, and the initial estimate is that a total of 483 CFA piles with nominal diameters of 50 and 60 cm and depths of 30 and 32 meters will be used. The initial studies were based on SPT (Standard Penetration Test) to

predict the behavior of the piles and will be supplemented with SLT (Static Load Testing) and DLT (Dynamic Load Testing) to verify the performance of the piling system. The tests conducted in this dissertation were performed on CFA piles initially executed for preliminary studies that did not advance, as the foundation solution had not yet been defined.

Figure 3.3 presents the area of these two constructions. The land areas of Sites A and B are, respectively, 2430m² and 4990 m².



Figure 3.3: Areas of sites A and B

3.3 GEOTECHNICAL INVESTIGATION

In agreement with the companies responsible for the construction projects, two experimental fields were established for this dissertation to conduct field tests, sample collection, and load testing.

At Site A, a small experimental field of approximately 72m² was set up, where 3 SPT boreholes with a maximum depth of 32m were drilled, along with 3 VST boreholes reaching 15 meters deep. Additionally, 3 CFA piles with a depth of 32 meters and a diameter of 60cm

were installed, of which 2 were used for DLT and 1 for SLT. Furthermore, during the installation of the 4 reaction piles for the SLT, samples were collected for laboratory tests aimed at determining the specific gravity of particles, grain size distribution, and Atterberg limits. Figure 3.4 shows the locations of the tests conducted at Site A.

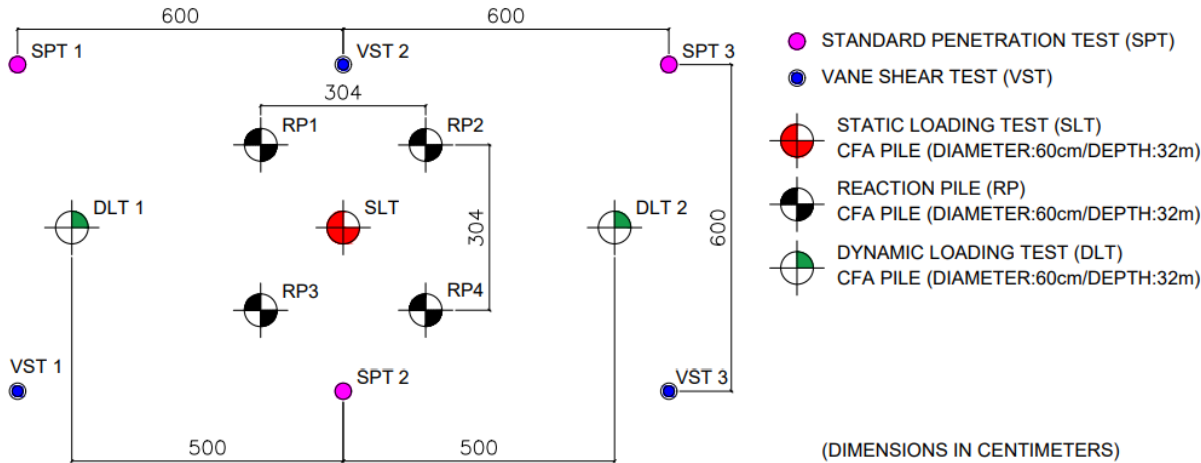


Figure 3.4: Experimental field at Site A (see Appendix A).

An experimental field was also utilized at Site B, although only SPT and VST boreholes were conducted, as the objective at this site is to validate the results and correlations found in the analyses at Site A. In total, 2 SPT boreholes and 2 VST boreholes were carried out. Additionally, 4 DLTs were performed on CFA piles with a depth of 32 meters and a nominal diameter of 60cm. Figure 3.5 depicts the experimental field at Site B used for the validation of the results from Site A.

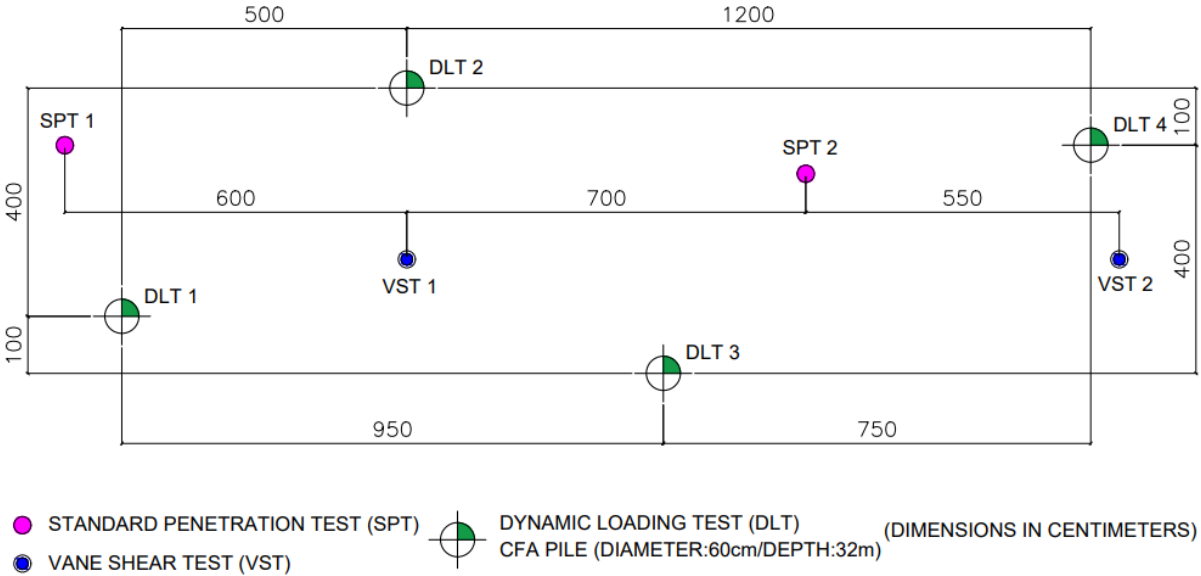


Figure 3.5: Experimental field at Site B (see Appendix A).

Appendix A presents the two experimental fields at Sites A and B, allowing observation of their positions relative to the terrain and buildings. The drawings include a scale to assist the reader in measuring the distances between the piles, boreholes, and the building foundations. Table 3.2 summarizes the tests conducted at each site, as well as their specific objectives.

Table 3.2: Summary of tests carried out at each site.

Test	Quantity	Depth (m)	Specific Objective
Site A			
SPT	3	32	- Soil type identification - Soil color - Soil origin - Groundwater Table (GWT) - Index N
VST	3	3 to 15	- Undrained shear resistance (S_u)
Particle-size Distribution	4	7, 15, 21 and 28	- Grain size distribution - Uniformity Coefficient (C_u) - Coefficient of Gradation (C_c)
Atterberg Limits	2	7 and 15	- Liquid Limit (LL) - Plastic Limit (PL) - Plasticity Index (PI)
Natural Moisture Content	1	7 and 15	- Liquidity Index (LI)
SLT	1	-	- Static load capacity of the pile - Static resistance distribution
DLT	2	-	- CAPWAP analyses - Quake and damping distribution
Site B			
SPT	2	50	- Soil type identification - Soil color - Soil origin - Groundwater Table (GWT) - Index N
VST	2	4 to 10	- Undrained shear resistance (S_u)
DLT	4	-	- CAPWAP analyses - Quake and damping distribution - Validation of results

The SPTs were conducted following the procedures and equipment established by NBR 6484 (ABNT, 2020). A manual system was utilized, employing a 65kg hammer operated by a textile cable, which passed through a pulley installed at the top of a tripod. In addition to obtaining SPT N -value, the tests allowed for the identification of soil type at each meter of depth, as well as the groundwater table (GWT). Soil type identification was done through

tactile-visual inspection, considering the grain size, plasticity, color and origin of the soil. It is worth noting that soil type identification is subjective in this context. The SPTs tests were carried out by a company located in Sinop - MT.

At depths where SPT investigations indicated the presence of cohesive soil below the GWT, VSTs were conducted to determine S_u . To conduct the tests, a vane with dimensions specified in NBR 10905 (ABNT, 1989) was manufactured.

Figure 3.6 shows the design of the vane, while Figure 3.7 shows its real image. The VSTs were conducted at every meter with prior drilling using water circulation, as employed in SPT tests. As a result, each drilling advanced by 50 cm, and the vane was inserted without rotation for about 50 cm for each test (the vane was driven with the weight of the 65 kg hammer used in the SPT).

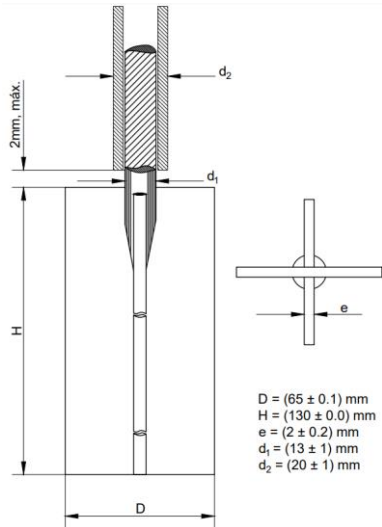


Figure 3.6: The vane design.



Figure 3.7: The vane used in the tests.

Torque was applied using a manual torque wrench (Figure 3.8) attached to the metal rod of the vane. Although difficult to control, an attempt was made to maintain an average rotation speed of $6^\circ/\text{min}$ manually using a stopwatch (Figure 3.9 and Figure 3.10).



Figure 3.8: The torque wrench used in the VSTs.

After determining the maximum torque (T_{max}), 10 complete revolutions were applied to determine the torque under the disturbed soil condition (T_r). Thus, using Eq. (3.1) of NBR 10905 (ABNT, 1989), S_u of the soil can be calculated as follows:

$$S_u = 0,86 \frac{T_{max}}{\pi d_{vane}^3} \tag{3.1}$$

Where d_{vane} is the vane's width.

The undrained shear strength under disturbed soil conditions (S_{ur}) can also be calculated using Eq. (3.1), but replacing T_{max} with T_r .



Figure 3.9: Torque application in the VST.



Figure 3.10: Vane with tested soil.

The laboratory tests were conducted on samples collected during the installation of the first reaction pile of the SLT at Site A, at depths of approximately 7, 15, 21 and 28m. These depths were determined to obtain the soil properties in the three distinct layers of the geotechnical profile identified in the SPT boreholes at Site A. The results will be presented later in a specific chapter. The following standards were used for these tests:

- NBR 6457 (ABNT, 2024) for determining the natural moisture content of the soil;
- NBR 6459 (ABNT, 2017) for determining the liquid limit;
- NBR 7180 (ABNT, 2016) for determining the plastic limit.
- NBR 7181 (ABNT, 2016) for determining the grain size distribution of the soil.

These tests were conducted at the geotechnical laboratory of the Federal University of Mato Grosso do Sul (UFMS), located in the city of Campo Grande (Figure 3.11 and Figure 3.12).



Figure 3.11: Application of vacuum for determination of grain specific gravity.



Figure 3.12: Samples used in sieving for determination of Atterberg's limits

As mentioned earlier, both at Site A and Site B, CFA piles were installed for this research. At Site A, 3 piles were installed, and 2 DLTs and 1 SLT were conducted. At Site B, 4 piles were installed, and only DLTs were conducted. The locations of the piles can be seen in Figure 3.4 and Figure 3.5. The following Table 3.3 summarizes the main characteristics of the tested piles, where the diameters are nominal, as there are variations in cross-sectional area due to the drilling and concreting process of this type of pile.

Table 3.3: Characteristics of the CFA piles according to monitoring.

Pile	Diameter (cm)	Depth (m)	Concrete Volume (m ³)	Overconsumption (%)	Concrete Pressure (kPa)
Site A					
SLT - 1A	60	32	12.0	32	30 to 110
DLT - 1A	60	32	15.0	66	40 to 90
DLT - 2A	60	32	12.0	32	40 to 110
Site B					
DLT - 1B	60	32	10.5	15	50 to 105
DLT - 2B	60	32	9.3	3	45 to 70
DLT - 3B	60	32	9.9	9	35 to 75
DLT - 4B	60	32	10.8	18	45 to 80

The installation monitoring reports of the piles can be viewed in Appendix B. These reports contain information regarding the torque developed during pile drilling, as well as the rotation speed and drill rate. Additionally, there is information about the concrete pressure and lifting rate during concreting.

In this regard, it is recommended to read the doctoral thesis by Silva (2011), in which the author details the limitations of these measurements and suggests an interesting procedure for correlating the drilling energy of a CFA pile with its load-bearing capacity.

The "torque" measurement presented in Figure 3.13 is the pressure of the hydraulic pump responsible for rotating the continuous auger of the drilling machine. As mentioned by Silva (2011), the pressure on the graph is related to the torque developed during pile drilling, but it is an indirect measurement that must be corrected for energy losses in the system, mechanical and hydraulic characteristics of the equipment, auger cutting angle, and procedures adopted during drilling.

Furthermore, the concrete pressure is obtained through a sensor positioned at the top of the drilling rig tower. In other words, the pressure is not read at the bottom end of the auger, where the concrete exits. Therefore, the pressure presented in the report is not strictly accurate due to the sensor's positioning.

Finally, the overconsumption indicated is determined by correlating the number of concrete pulses generated by the pump per minute with the concreting time. This measure should be calibrated even before the start of pile installation, by timing one minute, recording the number of pulses, and the corresponding volume of consumed concrete. It is important to note that these measurements can be controversial if not approached with caution (Almeida

Neto, 2002). Another work that can be consulted for better understanding is that of Rausche et al. (2004).

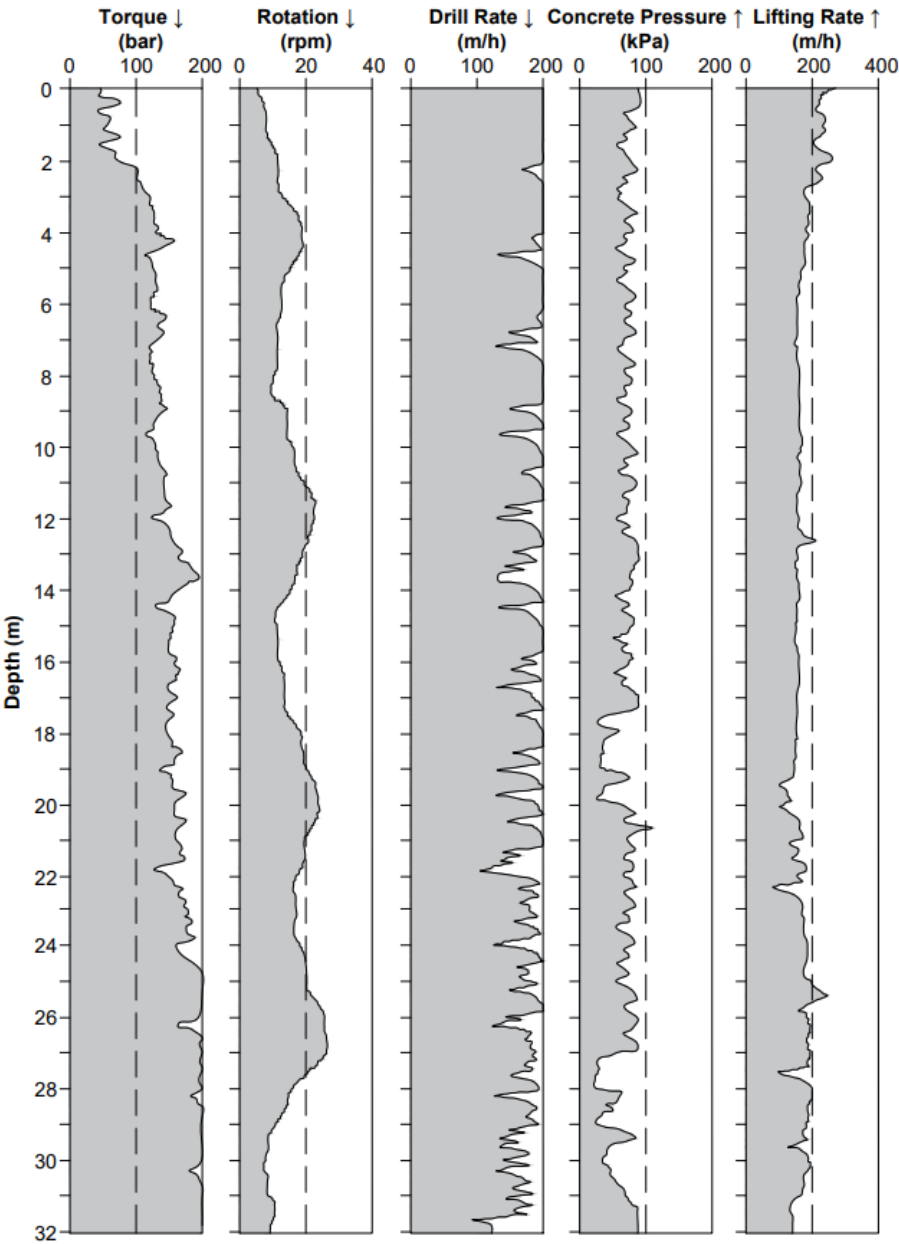


Figure 3.13: Pile monitoring record for DLT - 1A pile (see Appendix A).

3.4 STATIC LOADING TEST (SLT)

As seen in Figure 3.4, the SLT reaction system consisted of four CFA piles. These piles were connected to two steel beams measuring 110 cm in height via welded steel bars. For applying loads to the test pile, two hydraulic cylinders connected to a high-pressure hydraulic pump were utilized. Load readings were taken using a load cell and a load indicator calibrated by the São Paulo Institute of Technological Research. Displacements were measured using four digital deflectometers placed on the pile cap. These deflectometers were attached to magnetic

bases that remained fixed to two reference beams throughout the test. Figure 3.14 provides a side view of the static load test setup. Figure 3.15 and Figure 3.16 show real images of the SLT assembly. These images demonstrate the system's protection against sunlight, rain, and wind, which could affect load and displacement measurements.

In addition to the precautions taken during assembly and the equipment used in the test, the load test was performed following the procedures outlined in NBR 16903 (ABNT, 2020). During the test, the pile was loaded up to the maximum compression load of 2940kN at its top by two hydraulic cylinders. The adopted loading method was slow with maintained load, where the load increments were equal to 20% of the working load expected for the tested pile (1470kN), totaling 10 loading stages. At each stage, the load was maintained until displacement stabilization occurred, for a minimum of 30 minutes according to the following Eq. 3.1:

$$\frac{\Delta_{ZCR} - \Delta_{ZPR}}{\Delta_{ZCR} - \Delta_{ZPS}} \leq 5\% \quad (3.1)$$

Where:

Δ_{ZCR} : is the average displacement of the current reading;

Δ_{ZPR} : is the average displacement of the previous reading;

Δ_{ZPS} : is the final average displacement of the previous stage.

Displacement readings were taken at intervals of 5, 10, 15 and 30 minutes after the application of each load. In stages where displacement stabilization did not occur, readings were taken every 15 minutes and for a minimum duration of 60 minutes.

At the maximum load stage (2940kN), in addition to the readings up to 30 minutes, a final displacement reading was taken at the time of 12 hours. Subsequently, unloading was initiated in 4 stages with the same displacement stabilization criteria, but with a minimum reading time of 15 minutes. Upon reaching zero load, a final reading was taken at 30 minutes. In Appendix C, the displacement readings for each load stage in the test are presented.

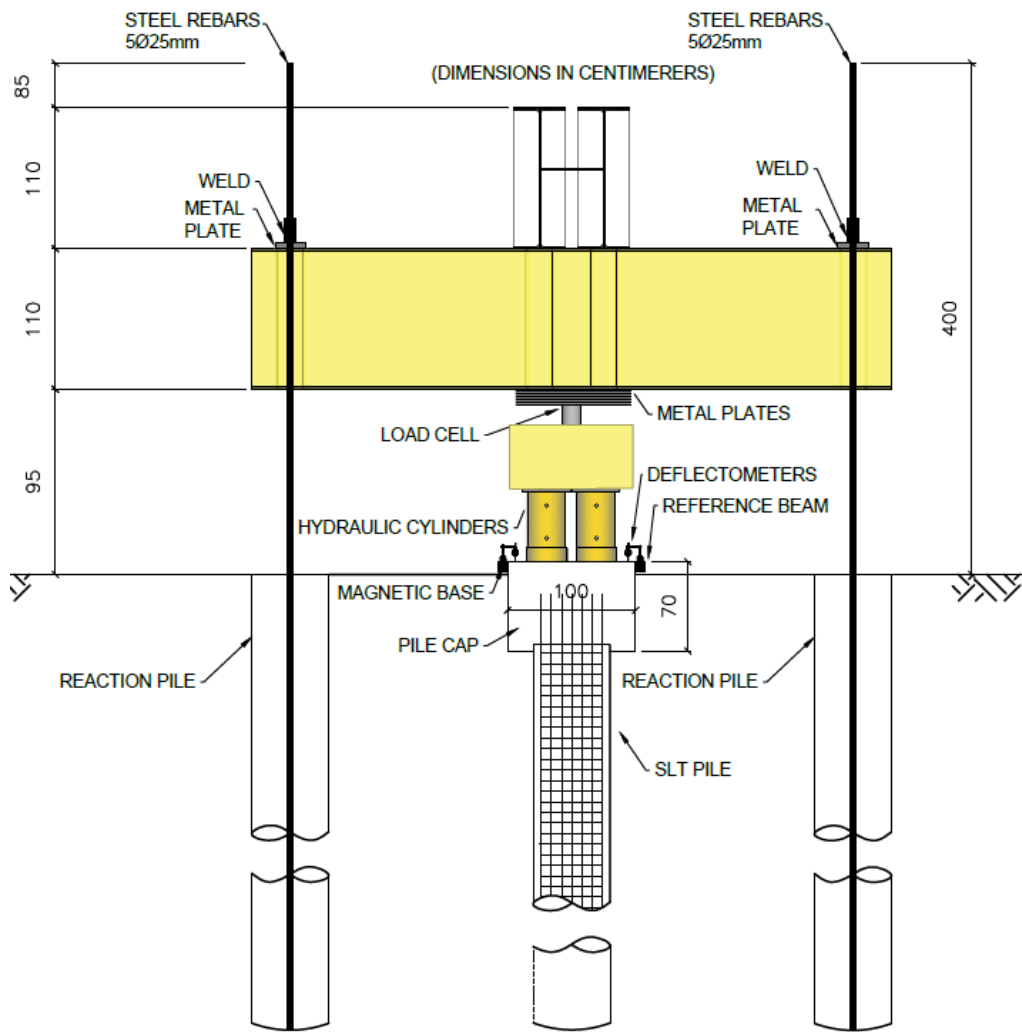


Figure 3.14: SLT setup.



Figure 3.15: External view of the load test covering.



Figure 3.16: Internal view of the load test setup.

3.4.1 STIFFNESS METHOD (DÉCOURT, 1998)

The Stiffness Method (Décourt, 1998) was utilized for the interpretation of the load-displacement curve obtained in the SLT. In this method, stiffness (k_{SM}) is defined as the ratio of load (Q) to the corresponding displacement (Δ_z) obtained in the test (measured at the top of the pile):

$$k_{SM} = \frac{Q}{\Delta_z} \quad (3.2)$$

Therefore, an indication that the pile is nearing failure occurs when the ratio tends to zero (when there are incessant displacements for approximately constant loads). By plotting a load-stiffness curve, it's possible to visualize the proximity of the pile to failure. Additionally, it's also possible to ascertain if there was any pre-loading prior to the load test (when stiffness increases).

Besides indicating the proximity of ultimate load and the presence or absence of pre-loading, the stiffness curve can indicate the domains of skin friction and tip resistance. For the development of the method, Décourt (1998) divides foundations into two cases: those in which physical failure can occur and those in which it cannot.

In the first case, the reduction behavior of stiffness is clear and, most of the time, follows a straight line intersecting the load axis. According to Décourt (1998), this behavior is rare, limited to displacement piles such as precast concrete and steel piles. In these cases, physical failure can occur (Figure 3.17).

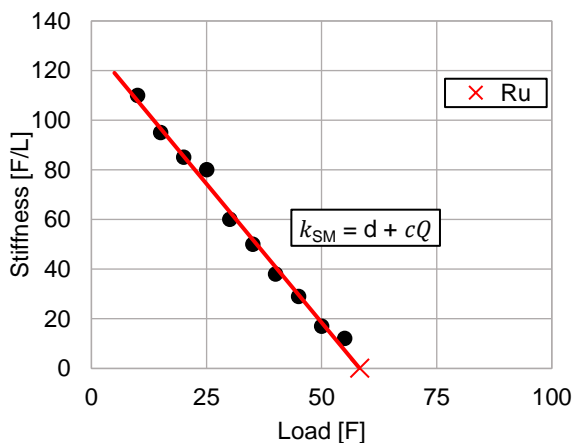


Figure 3.17: Foundation stiffness graph with physical failure.

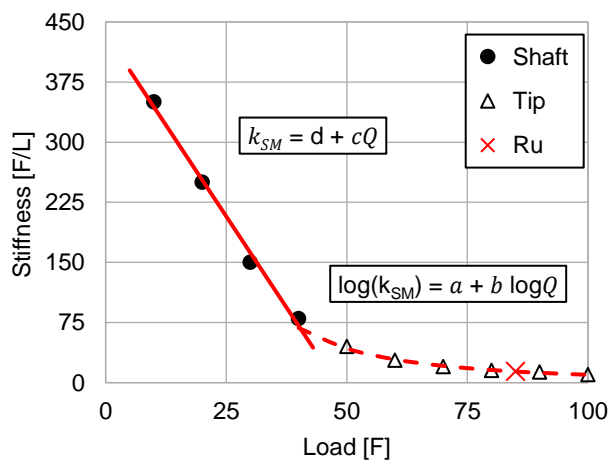


Figure 3.18: Foundation stiffness graph without physical failure.

In the second case, physical failure hardly ever occurs. According to Décourt (1998), the majority of foundations exhibit this type of behavior (cast-in-situ piles, including continuous flight auger piles). For these foundations, there's a significant reduction in stiffness with increasing load (high mobilization of resistance with small displacements), followed by smaller reductions in stiffness with increasing loads (large increase in displacements with smaller increments of mobilized resistance). Thus, the load-stiffness curve has a hyperbolic shape with a sub-horizontal asymptote (Figure 3.18)

Once failure is not clearly defined for most piles, a failure criterion is used, which is nothing more than fixing a point on the load-displacement curve that conventionally denotes failure. In the Stiffness Method, the failure criterion is a displacement equal to 10% of the diameter of the pile cross-section (measured at the top of the pile).

As well noted by Décourt (2008) and Carvalho & Albuquerque (2023), the criterion of 10% of the diameter does not consider the elastic shortening, which can be considerable for long and flexible piles. In other words, this method does not account for the elastic shortening of the pile shaft, nor the load transfer at depth. Therefore, since the method considers the pile as rigid, as the piles become shorter and have larger diameters, the error associated with the failure criterion tends to be smaller, as the elastic shortening is reduced. Furthermore, the ideal would be the direct measurement of displacement at the pile tip using tell-tales, for example.

The domain of skin friction occurs in the linear portion at the beginning of the stiffness curve, while the end of the curve determines the tip domain through a log-log equation. Thus, the method is applied based on the best fit of the two equations to the set of load-stiffness points obtained in the SLT. Once the two domains are determined, the conventional failure load (R_u) on the log-log curve is determined as follows:

$$\log k_{SM} = a + b \log Q \quad (3.3)$$

$$k_{SM} = 10^{(a+b \log Q)} \quad (3.4)$$

$$\frac{Q}{\Delta_z} = 10^{(a+b \log Q)} \quad (3.5)$$

According to the failure criterion, $\Delta_z = 10\%D \Rightarrow Q = R_u$.

$$R_u = 0.1D \times 10^{(a+b \log R_u)} \quad (3.6)$$

Where D is the diameter of the tested pile tip, and a and b are the adjustment coefficients obtained for the log-log function. Therefore, it is sufficient to iteratively determine the value of R_u that satisfies Eq. 3.6. This step can be performed using an automated calculation spreadsheet.

Once R_u is determined, the shaft resistance component (R_s) of the pile is determined by the intercept of the line on the load axis ($k_{SM} = 0 \Rightarrow Q = R_s$):

$$k_{SM} = cQ + d \quad (3.7)$$

$$0 = cR_s + d \quad (3.8)$$

$$R_s = -\frac{d}{c} \quad (3.9)$$

Where c and d are the adjustment coefficients obtained from the linear regression of the first domain of the stiffness curve. Therefore, the tip resistance component (R_b) is determined by the difference between the conventional (R_u) and shaft resistances (R_s).

$$R_b = R_u - R_s \quad (3.10)$$

In this regard, it is important to clarify that the shaft and tip resistances are approximate, since there will always be a portion of tip resistance mobilized in the skin friction domain (Carvalho & Albuquerque, 2023).

This method was used to determine the shaft and tip resistance components of the tested pile in the SLT. For a more detailed study, it is suggested to read the mentioned papers and the work by Melo (2019).

3.5 DYNAMIC LOADING TESTS (DLT)

As mentioned earlier, DLTs were conducted on CFA piles with depths of 32 m and diameters of 60 cm following the procedures outlined in NBR 13208 (ABNT, 2007). A drop weight hammer with 49kN was used for impact application (Figure 3.19). The impacts from the drop weight hammer were cushioned by a reinforced concrete extension with a cross-sectional diameter of 60 cm and a height of 1.80 m. The concrete used in it had a compressive strength of 40 MPa at the time of the tests. Additionally, during the tests, a 2 cm thick plywood cushion was placed on top of the reinforced concrete.

Two accelerometers and two strain transducers were fixed directly onto the shaft of the pile at a distance of 2.10m from the top. During this stage, it was necessary to treat the lateral surface of the pile to ensure it was clean, smooth and uniformly flat in the region of the sensors (an electric grinder was used for this purpose). Furthermore, the top of the reinforced concrete extension was leveled to ensure a flat surface and uniform distribution of the hammer impact.

For the acquisition of force and velocity signals, impacts with increasing energy were used. As the impacts were applied, readings of permanent displacements were conducted using a reference beam and a digital deflectometer positioned on a steel plate bolted to the pile.

In total, 5 impacts were performed with drop heights of 30, 60, 90, 120 and 150cm for each pile. The impacts with the lowest energy were used to verify the proper installation of sensors, the correct positioning of the hammer and the wave velocity in the instrumented section of the pile. Subsequently, impacts were applied ensuring that the compression and tension stresses did not exceed the limits imposed by the pile material. Additionally, the tests were conducted considering the criteria of Goble & Rausche (1976), Hannigan et al. (2016) and Rausche et al. (2018) mentioned in section 2.2.2: sufficient energy resulting in a permanent displacement of at least 2.5mm per blow, with this value limited to 12mm per blow and that the permanent displacement obtained in the DLT should be at least the diameter of the pile divided by 120.

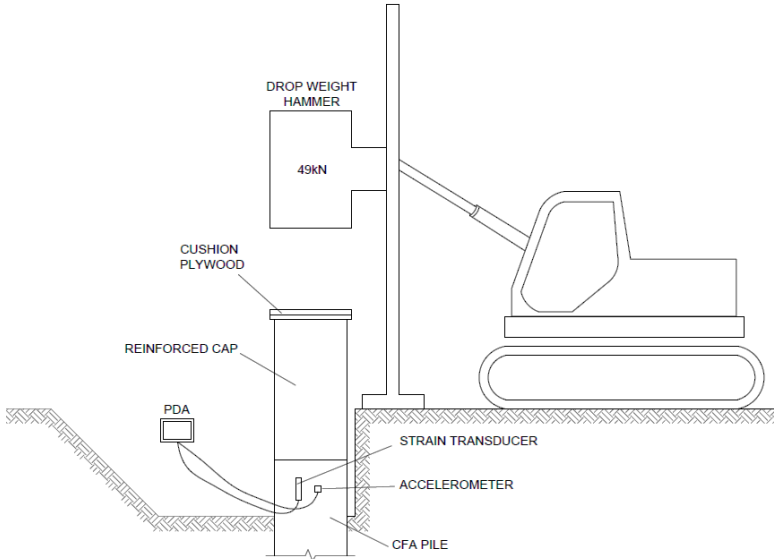


Figure 3.19: Drop weight hammer used.

3.5.1 CAPWAP ANALYSES

The CAPWAP analyses were conducted following the methodology presented by Ng & Sritharan (2013) titled "Improved Signal-matching Technique". In the original work, these authors studied driven steel piles. Thus, the geometric and mechanical properties of the piles were thoroughly known (known impedance), unlike CFA piles where there are impedance variations with depth. The consideration of impedance variation with depth for CFA piles will be presented later.

The first step of the CAPWAP analyses was the selection and preparation of the signal corresponding to the impact of the hammer that mobilized the necessary resistance. In this regard, signals meeting the criteria of Goble & Rausche (1976) and Hannigan et al. (2016) were

chosen. Additionally, another criterion for selection was the quality of the acquired signals: proportionality between force and velocity signals at the beginning of the records, minimal variability among individual force and velocity signals, and the return of the force signal to zero at the end of the records (indicating that the section instrumented by the sensors deformed elastically as stress waves propagated).

The following figures present the force and particle velocity signals selected for CAPWAP analyses in the piles at sites A and B. As mentioned in the literature review chapter, the force and velocity signals are equal to the average of the respective signals individually read by each sensor in a section near the top of the pile. Therefore, F is numerically equal to the average of F_1 and F_2 , and V corresponds to the average of V_1 and V_2 .

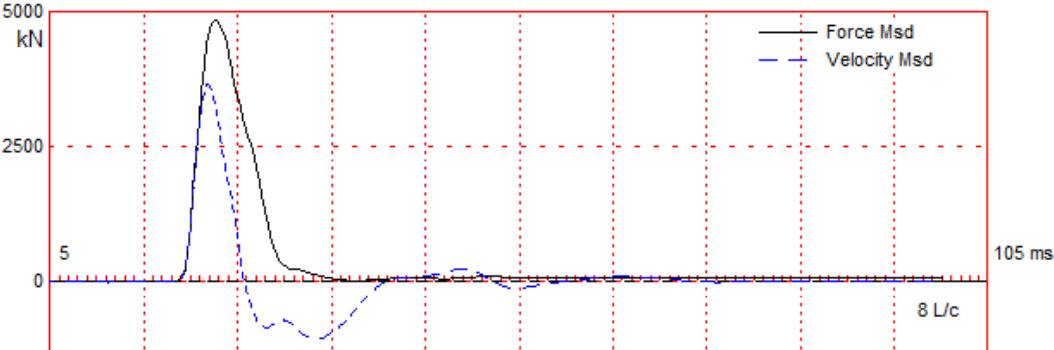


Figure 3.20: Force and particle velocity - DLT 1A.

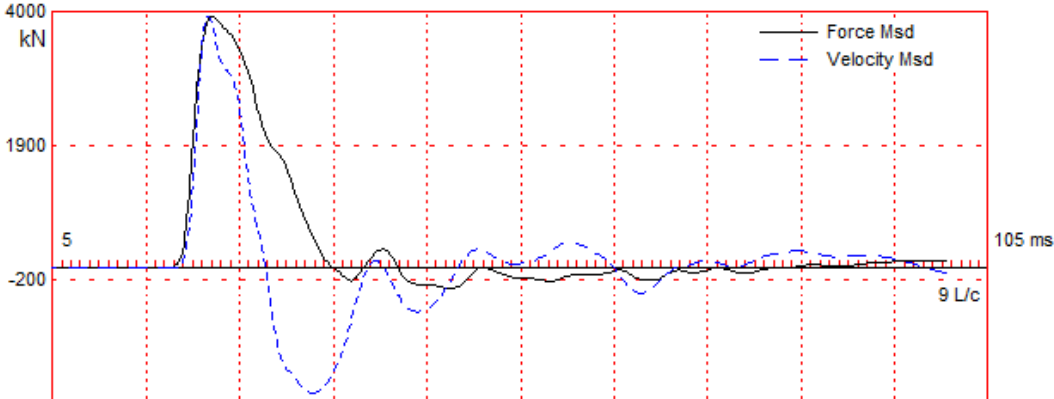


Figure 3.21: Force and particle velocity - DLT 2A.

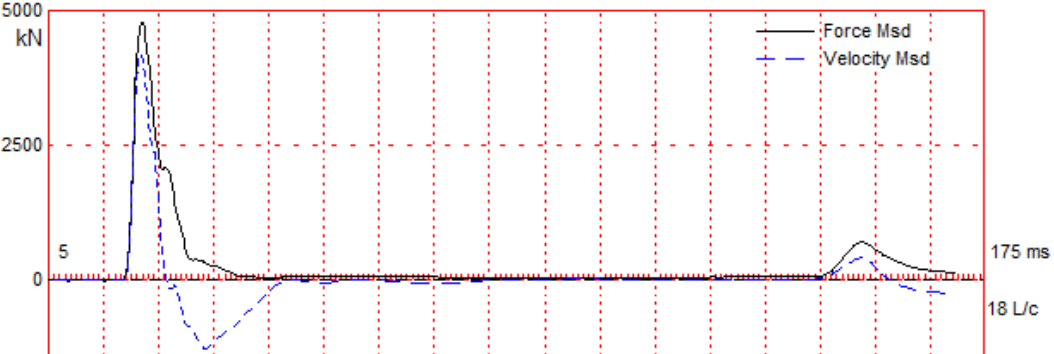


Figure 3.22: Force and particle velocity - DLT 1B.

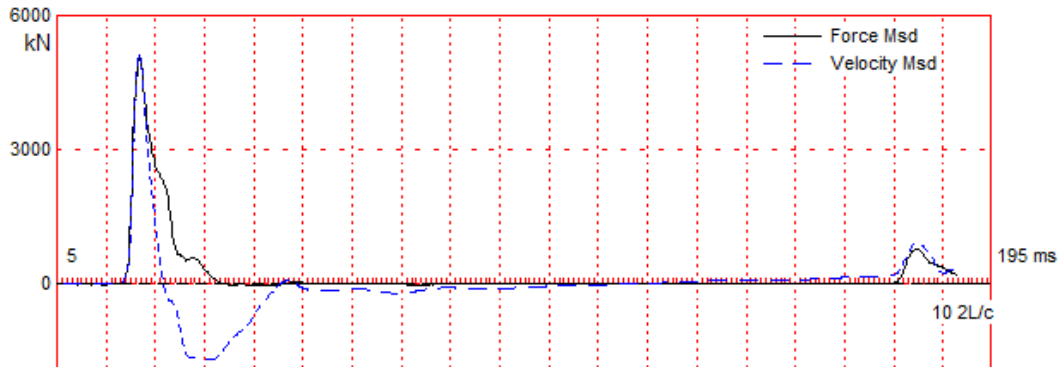


Figure 3.23: Force and particle velocity - DLT 2B.

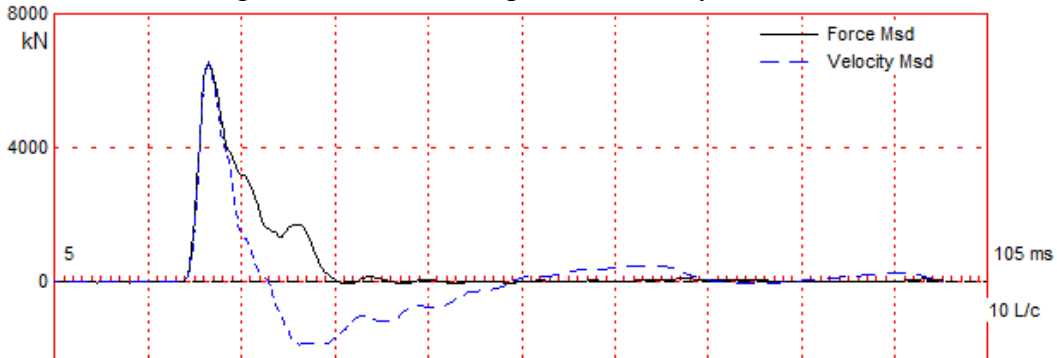


Figure 3.24: Force and particle velocity - DLT 3B.

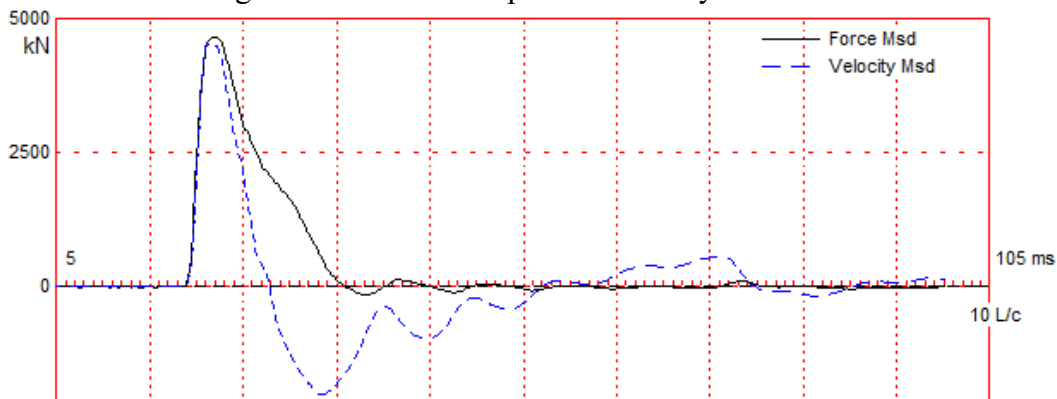


Figure 3.25: Force and particle velocity - DLT 4B.

Once the signals to be analyzed by CAPWAP have been selected, a permanent displacement measured in situ by a digital deflectometer must be assigned. This displacement is applied to the final segment of the displacement signal, which the PDA calculates as the Eulerian integral of the velocity signal. Therefore, the velocity signal is adjusted so that its integral at the end of the dynamic event matches the permanent displacement measured in situ. Thus, like the force and velocity signals read at the top of the pile, the set per blow serves as a boundary condition in CAPWAP analysis.

Table 3.4 contains a summary of the signals selected for analysis development.

Table 3.4: Summary of blows selected for CAPWAP analyses.

Pile	Diameter (cm)	Depth (m)	Blow Number	Drop Height (m)	Maximum Energy (kJ)	Permanent Displacement (mm)	Set (mm/blow)
Site A							
DLT - 1A	60	32	3	0.9	23.1	6.0	2.0
DLT - 2A	60	32	3	0.9	25.1	5.4	1.8
Site B							
DLT - 1B	60	32	3	0.9	23.7	4.8	1.6
DLT - 2B	60	32	3	0.9	27.1	3.0	1.0
DLT - 3B	60	32	5	1.5	43.8	16.0	3.2
DLT - 4B	60	32	4	1.2	30.6	5.2	1.3

The next step was defining the pile model. To achieve this, the impedance of the pile was adjusted in depth based on the concrete pressure and overconsumption (Table 3.3) obtained from the pile monitoring records. It was assumed, as a simplification, that the concrete consumption was directly proportional to the injection pressure. Thus, the pile models were adjusted by changing the impedance of each element based on the concrete pressure at their respective depths. Therefore, in the end, the theoretical volume of the pile coincided with the volume obtained in the monitoring report.

The next step was to assign static resistances to the piles in the CAPWAP analyses. The resistance values inserted into the Site A analyses were those obtained using the Stiffness Method, presented earlier in Section 3.4.1. The proportion between the shaft and tip resistances relative to the total resistance was maintained. As will be seen in the results chapter, the total static resistance obtained from the SLT at Site A was 3467 kN, with 65% of this value corresponding to shaft resistance and 35% to tip resistance. Therefore, these values were inserted into the CAPWAP analyses at Site A as boundary conditions.

At Site B, the shaft and tip resistances were determined using the method proposed by Décourt-Quaresma (1978), which relies on the SPT N -values. The mathematical representation of the method is provided by Eq. 3.11 below:

$$R_u = \alpha C N_p A_p + 10\beta UL \left(\frac{N_L}{3} + 1 \right) \quad (3.11)$$

R_u : is the geotechnical ultimate static resistance of the pile;

N_p : is the average value of the standard penetration resistance at the pile tip;

N_L : is the average value of the standard penetration resistance along the shaft of the pile;

α : is the factor depending on the pile type and the soil type at the pile tip;

- β : is the factor depending on the pile type and the soil type along the shaft of the pile;
- C : is the characteristic coefficient of the soil (Table 3.5);
- U : is the perimeter of the cross-sectional area of the pile along its length;
- L : is the length of the pile;
- A_p : is the area of the pile tip.

Table 3.5: C-parameter for tip resistance (Décourt & Quaresma, 1978).

Soil Type	C (kPa)
Clay	120
Clayey Silt	200
Sandy Silt	250
Sand	400

For CFA piles, regardless of the soil type, Décourt (1996) suggests $\alpha = 0.3$ and $\beta = 1.0$, using a failure criterion corresponding to a displacement of 10% of the pile diameter (as Stiffness Method). It is important to emphasize that the factors α and β derive from the influence of the pile installation process and the foundation soil type. Therefore, their values are conditioned to the geotechnical characteristics of the locations where the load tests used by Décourt (1996) were conducted, in addition to the effects of pile installation processes. Thus, the resistance factors cannot be taken as a rule and should only be used as preliminary estimates. Therefore, it is advisable that the factors be readjusted based on new load tests, according to each situation (Aoki & Cintra, 2010).

Subsequently using an automated spreadsheet, the values of α and β were adjusted to ensure that the total shaft and tip resistances matched those obtained by the Stiffness Method (Décourt, 1998) presented in section 3.4.1. Thus, the distribution of static resistance was refined proportionally based on the results of the analysis obtained from the SLT. An interesting outcome was the establishment of new α and β values for CFA piles in the soil of Sinop - MT, enabling better predictions of load capacity for future foundation designs.

Therefore, the static shaft and tip resistances of the piles at Site B were determined using the SPTs conducted on-site and also with the α and β factors determined by the Stiffness Method from the SLT at Site A.

Next, the dynamic parameters of the soil model (q_s and J_s) were adjusted for each depth interval along the length of the piles at Site A. This process began with the soil element closest to the surface and was repeated for consecutive elements until reaching the pile tip. For each determination of q_s and J_s , the MQ was recalculated to define the best soil model parameters. Once a preliminary distribution of the dynamic soil parameters in depth was determined, there

was a proportional refinement in their values until the lowest possible MQ values were obtained. This process allowed for the definition of q_s and J_s along the analyzed piles.

Finally, the correlations established between q_s and J_s and the soil properties at Site A were validated at Site B. The procedure adopted was identical to that at Site A, but defining q_s and J_s based on the SPTs and VSTs conducted at Site B. The criterion adopted for validation was $MQ < 5.0$, a value considered satisfactory by the developers of the CAPWAP method (PDI, 2014).

3.6 METHODOLOGY SUMMARY

Therefore, the methodology employed in this research can be summarized through the flowchart presented in Figure 3.26.

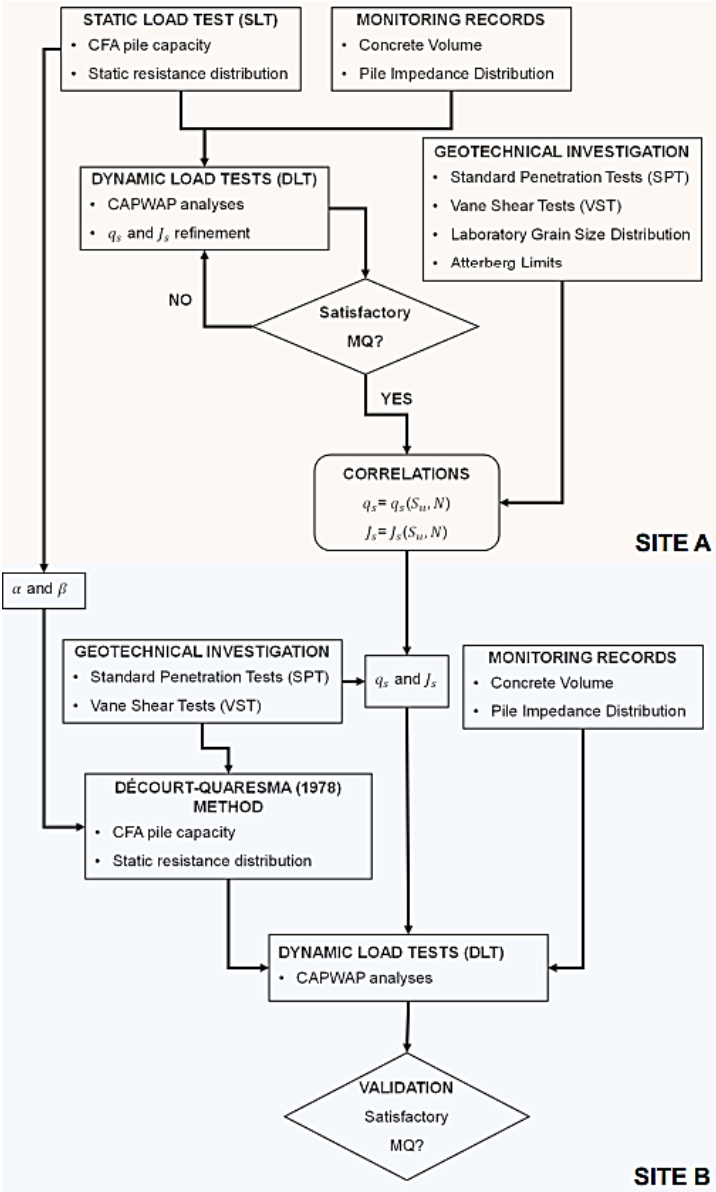


Figure 3.26: Flowchart summarizing the methodology used in this dissertation.

4. RESULTS

4.1 SITE A

4.1.1 SOIL PROPERTIES

At Site A, the 3 SPT boreholes identified the occurrence of soft yellow clayey silt with thickness ranging between 13 and 14m. Below this layer, the same type of soil with medium consistency was observed, with a thickness varying between 1 and 2m. Next, a more resistant layer with a thickness of 1 meter of yellow silt with gravel was identified. Beneath this gravel layer, there was a change in soil type to moderately compact red sandy silt with thicknesses between 7 and 12m. The last stratum identified in the SPT boreholes was a moderately compact red sand. Additionally, the groundwater table (GWT) identified in all 3 boreholes was at a depth of 2.10m. The soil types mentioned were identified through tactile-visual inspection of the SPT. As will be seen, the Unified Soil Classification System (USCS) was used with the results of laboratory tests to identify the soil type and its main characteristics. As stated in section 3.3, laboratory tests on the soil from Site A were conducted on samples taken at depths 7, 15, 21 and 28m.

At a depth of 7m, the grain size distribution indicated that 58% of the soil passed through the #200 sieve (0.075mm). Additionally, according to the NBR 6502 (ABNT, 1995) classification, considering only the soil's particle size distribution, 38% consists of clay, 20% of silt, 28% of sand, and 14% of gravel. Additionally, the liquid limit (LL) in this layer was 37%, while the plastic limit (PL) was 19%, resulting in a plasticity index (PI) of 18%. The moisture content determined was 32.9%, resulting in a liquidity index (LI) of

At a depth of 15m, 79% of the sample passed through the #4 sieve, and 15% passed through the #200 sieve. Furthermore, according to the NBR 6502 (ABNT, 2015) classification, 61.55% of the sample is sand, 24.41% is gravel, 9.34% is silt, and 4.70% is clay. The uniformity coefficient (C_u) was 25, while the coefficient of gradation (C_c) was 5. Since C_c is not between 1 and 3, the soil is considered poorly graded. The LL of this sample was 23%, and it was not possible to form the 3mm cylinder for the PL.

At a depth of 21m, 97% of the sample passed through the #4 sieve, and 24% passed through the #200 sieve. According to the Brazilian standard, 72.50% is sand, 18.58% is silt, 5.35% is clay, and 3.57% is gravel. Again, the soil is poorly graded with C_u and C_c values of 140 and 18, respectively. The LL of this sample was 20%, and it was not possible to form the 3mm cylinder for the PL, which agrees with the high sand fraction.

Finally, at a depth of 28m, 96% of the soil passed through the #4 sieve, and 20% passed through the #200 sieve. According to the Brazilian sieve analysis standard, 76.70% of the soil

is sand, 9.62% is silt, 8.98% is clay, and 4.70% is gravel. The obtained C_c was 33, and C_u was 130, indicating a poorly graded soil. The LL was 24%, while it was not possible to form a 3mm cylinder for the determination of the PL.

Figure 4.1 shows the grain size distribution obtained from the sieve and sedimentation tests for the four sampled depths.

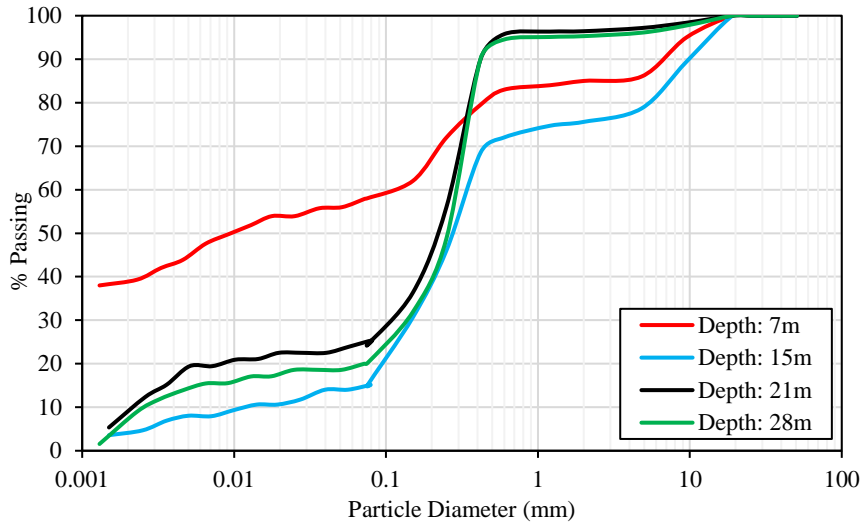


Figure 4.1: Grain size distribution at Site A.

According to the USCS, the soil at a depth of 7m is classified as a fine-grained soil in group CL, indicating inorganic clay with low plasticity. However, at other depths, the soil is classified as a coarse-grained soil, specifically sand with an appreciable amount of fines, belonging to group SM, which indicates silty sands or sand-silt mixtures. The 3 VST boreholes were limited to the first layer characterized by the USCS as inorganic clay with low plasticity, belonging to group CL. The VSTs revealed an approximately constant average undrained strength between 3 and 8m depth, with its value linearly increasing up to 15m. This variation in strength aligned with the evolution of SPT resistance with depth.

Figure 4.2 presents the geotechnical profile of Site A with the results of SPTs and VSTs. In this profile, the soil layers are those defined by the SPT, where the relative density or consistency are determined based on N -values according and the soil types are determined through tactile-visual inspection by the professional responsible for issuing the test report according to NBR 6484 (ABNT, 2020).

Figure 4.3 shows the average geotechnical profile of Site A used in this research. In this profile, in addition to the classification of soil layers according to the USCS, the clay, silt, sand, and gravel fractions according to NBR 6502, the Atterberg limits, C_c , C_u , the average values of N and S_u are presented, which were synthesized into their mean values and their range of variation for 95% confidence.

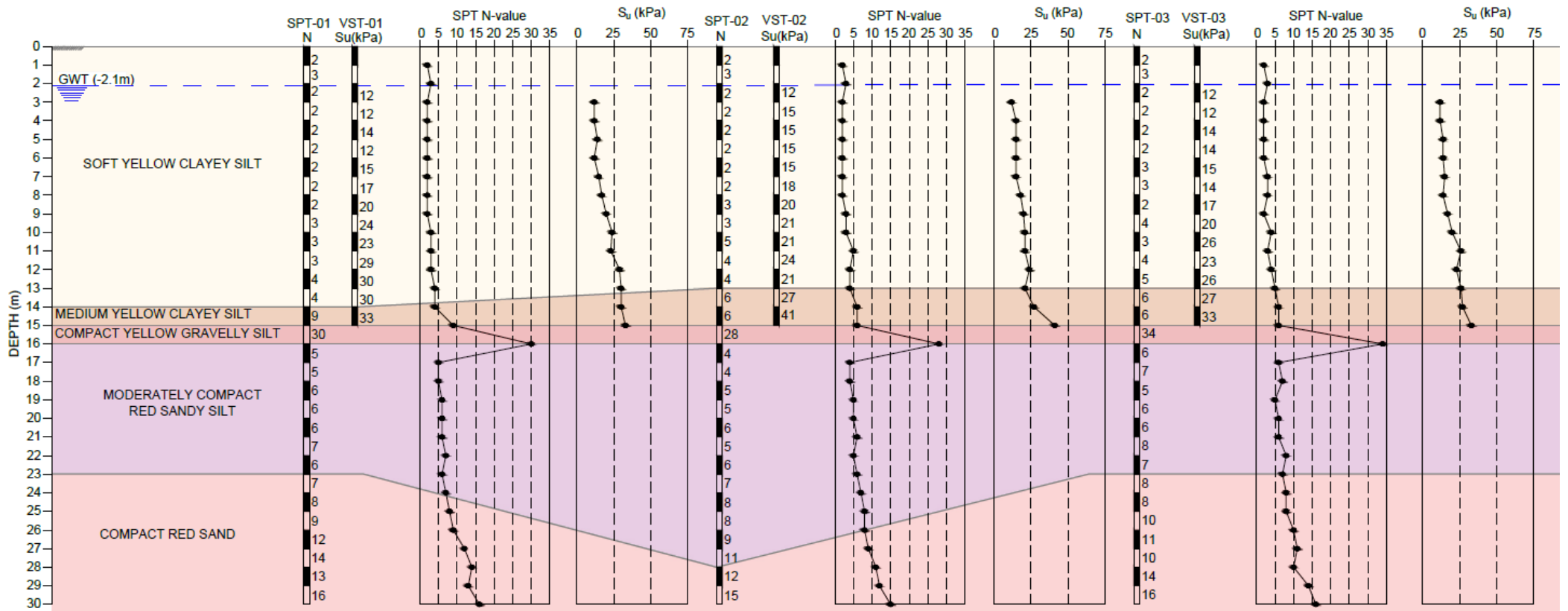


Figure 4.2: Geotechnical profile of Site A with the results of SPTs and VSTs (no scale).

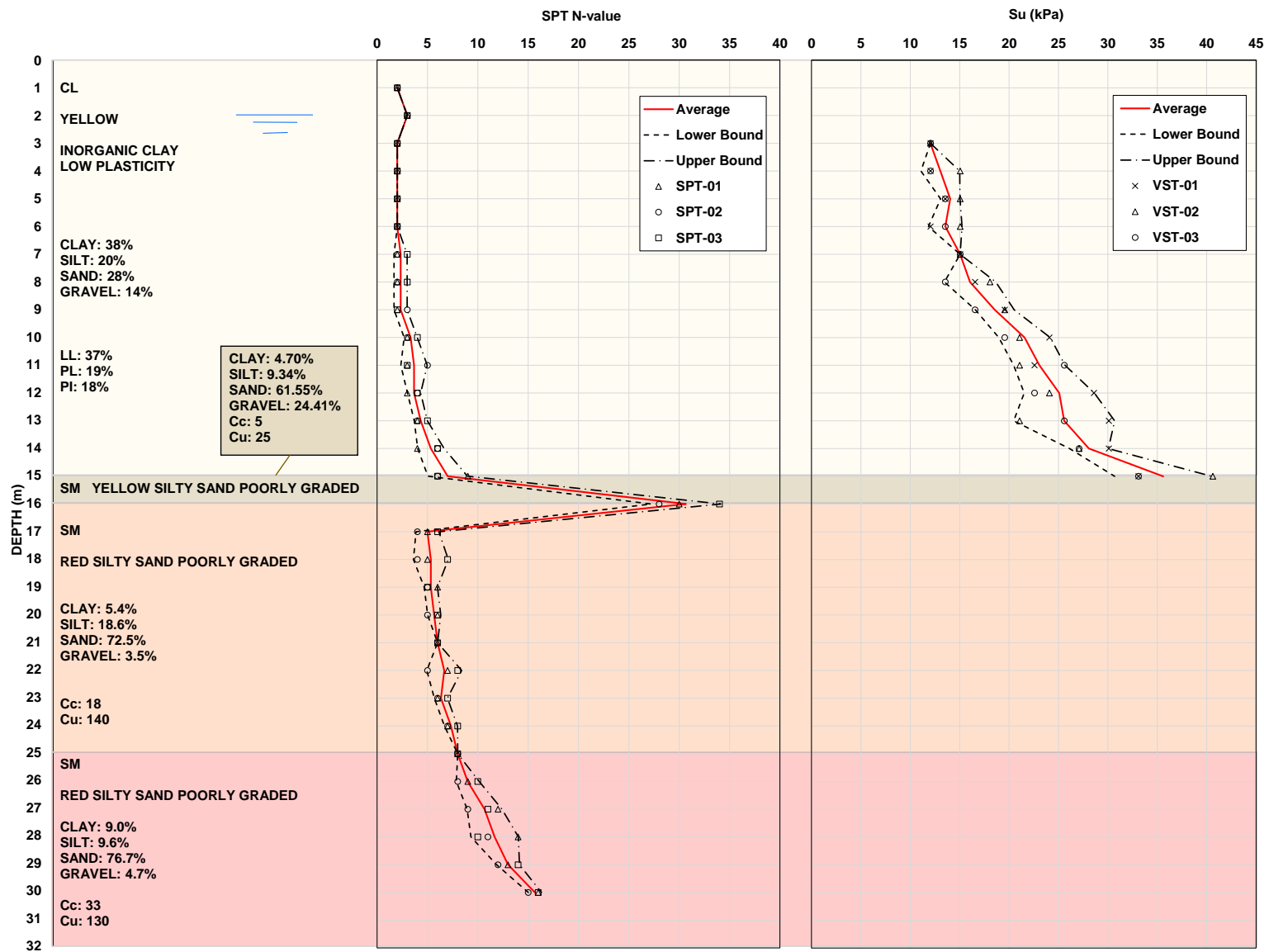


Figure 4.3: Average geotechnical profile of Site A.

4.1.2 SLT ANALYSIS

Figure 4.4 presents the load-displacement curve obtained from the SLT conducted on a CFA pile with a diameter of 60cm and a depth of 32m. As expected for the CFA pile and as seen in the load-displacement curve, there was no clear failure during the test, characterizing a typical behavior of cast-in-situ piles. Therefore, four failure criteria were applied to determine the ultimate resistance. The Offset Limit proposed by Davisson (1972), the criterion of NBR 6122 (2019), Van der Veen (1953), and 10%D Criterion (Terzaghi, 1943) applied to the load-displacement curve extrapolated by the Stiffness Method proposed by Décourt (1998) were used. Figure 4.5 presents the results of the application of these methods, and Table 4.1 summarizes the corresponding values.

These failure criteria were briefly discussed in Melo (2009), where their applicability and limitations were highlighted.

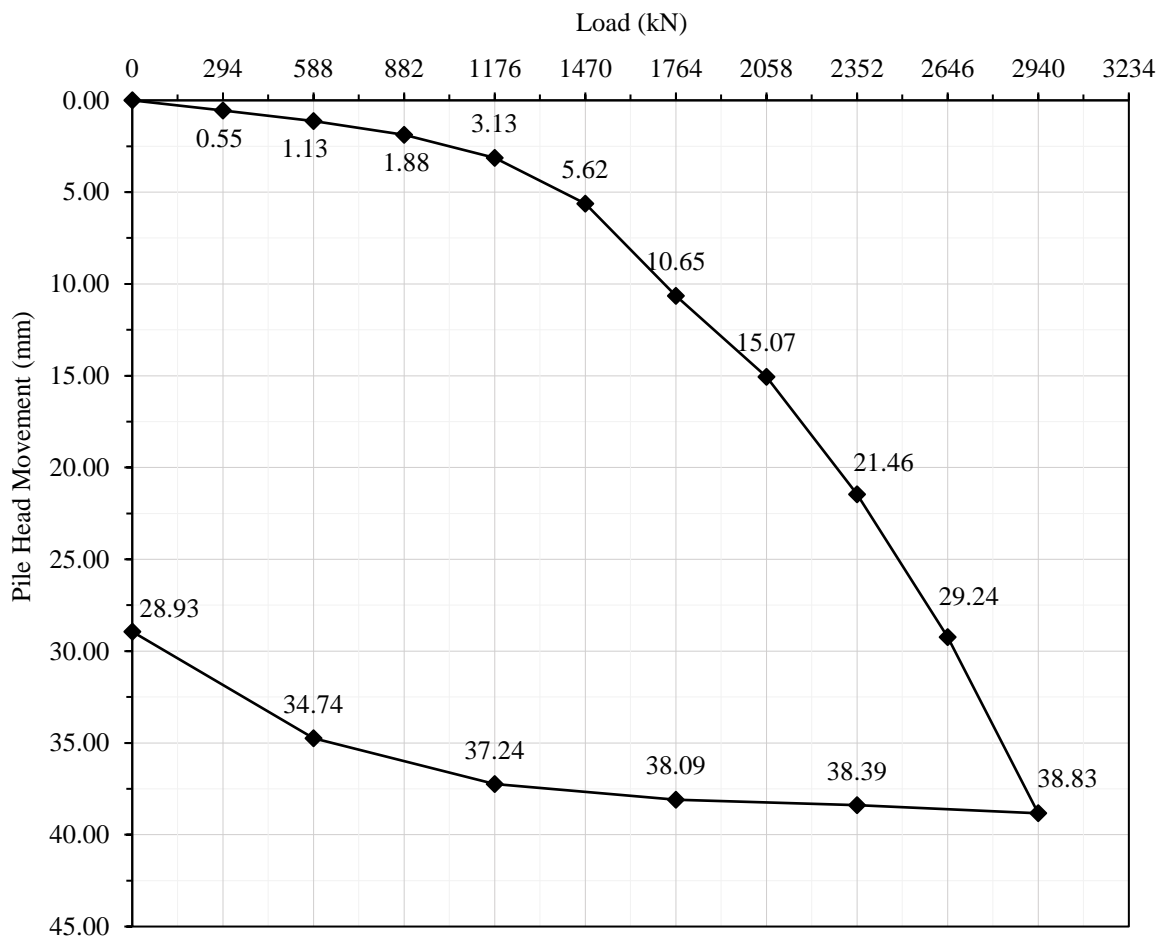


Figure 4.4: Load-displacement curve from the SLT.

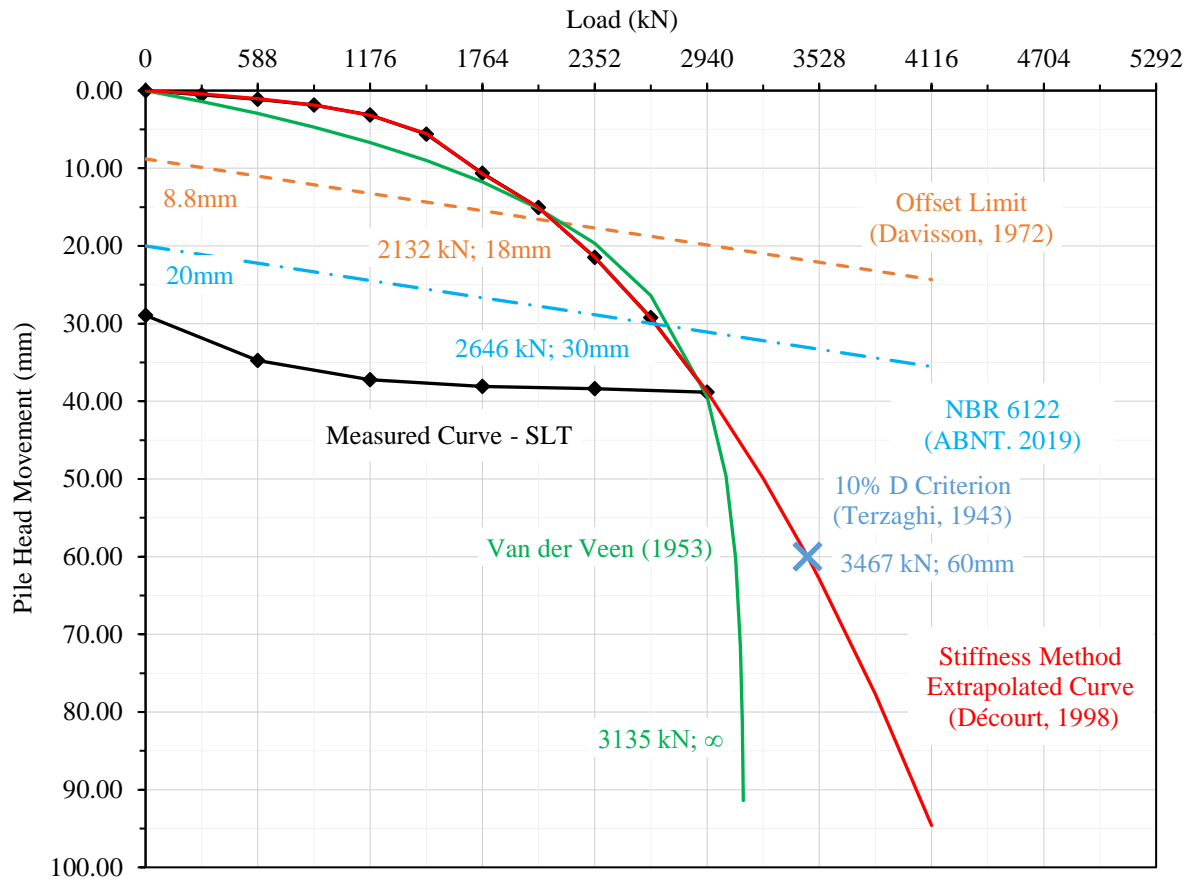


Figure 4.5: Four failure criteria applied to the SLT curve.

Table 4.1: Summary of the four failure criteria.

Failure Criterion	Displacement (mm)	Load Capacity (kN)	Load Test / Load Capacity
Offset Limit (Davisson, 1972)	18	2132	1.38
NBR 6122 (ABNT, 2019)	30	2646	1.11
Van der Veen (1953)	∞	3135	0.94
10%D (Terzaghi, 1943)	60	3467	0.85

The Van der Veen (1953) method is one of the most used in Brazil and resulted in a bearing capacity of 3135kN. However, it is noticed that at the beginning of the curve, there was not a good fit compared to the values measured in the SLT. This poor adjustment of the load-displacement curve was also affirmed by Guimaraes et al. (2002) as a defect of the method. Furthermore, according to Niyama & Decourt (1994), this method is applicable for displacement piles, since the bearing capacity of cast-in-situ piles is underestimated. In other words, with the development of larger displacements, the mobilized resistance tends to increase at a rate greater than that of the Van der Veen (1953) method, which adjusts the curve with a

vertical asymptote. However, Mota (2003) advocates and suggests the use of Van der Veen (1953) in the soil of Brasília.

The criteria of NBR 6122 (ABNT, 2019) and Davisson (1972) are very similar. Both criteria consider an elastic shortening of the shaft calculated as that of an axially loaded bar (QL/EA), where Q is the applied load, L is the length of the pile, E is the modulus of elasticity, and A is the cross-sectional area. Therefore, as they assume that the normal stress on the cross-section of the pile is constant, these two criteria do not consider the transfer of load from the pile to the soil through the shaft. In other words, by formulating these two methods, the resistance distribution along the pile shaft is not considered, considering that there will be a shortening like that of a free bar. The difference between the two criteria is the displacement of the tip necessary to determine the intercept of each line on the displacement axis. It is noted that the Davisson criterion (1972) considered a tip displacement (8.8mm) inferior to the value considered of 20mm by NBR 6122 (ABNT, 2019).

According to Melo (2009), the Davisson criterion (1972) is widely used in North America for load tests conducted with rapid loading. This explains the conservative load capacity associated with a smaller displacement, compared to other criteria.

Finally, the Terzaghi (1943) failure criterion is one for which the displacement is equal to 10% of the diameter of the pile tip. Since the curve measured in the SLT was not sufficient to reach such displacement (60mm), it was decided to extrapolate it according to the Stiffness Method by Décourt (1998). It is observed that the extrapolated curve agreed with the expected behavior for a cast-in-situ pile, where the mobilized resistance increases with the increase of displacements following a sub-horizontal asymptote, without showing a clear failure as Van der Veen (1953) method.

As will be seen later, the Stiffness Method allowed the estimation of the shaft and tip resistances of the tested pile. Therefore, due to the deficiencies and applicability of the methods presented, the Terzaghi (1943) failure criterion applied in the extrapolation of the curve by the Stiffness Method by Décourt (1998) was considered for the subsequent analyses.

Therefore, Figure 4.6 presents the application of the Stiffness Method with the Terzaghi (1943) failure criterion to the tested pile. It can be observed that there was a good fit both in the linear section characterizing the mobilization of shaft resistance and the curved section related to the mobilization of tip resistance.

The summary of the results from the method application can be seen in Table 4.2. It is observed that the total resistance is 3467 kN for a displacement of 60mm, whereas the shaft resistance is 2237 kN and the tip resistance is 1230kN. In other words, according to the failure

criterion and the method used, the shaft and tip resistances correspond to 65% and 35% of the total resistance of the pile, respectively.

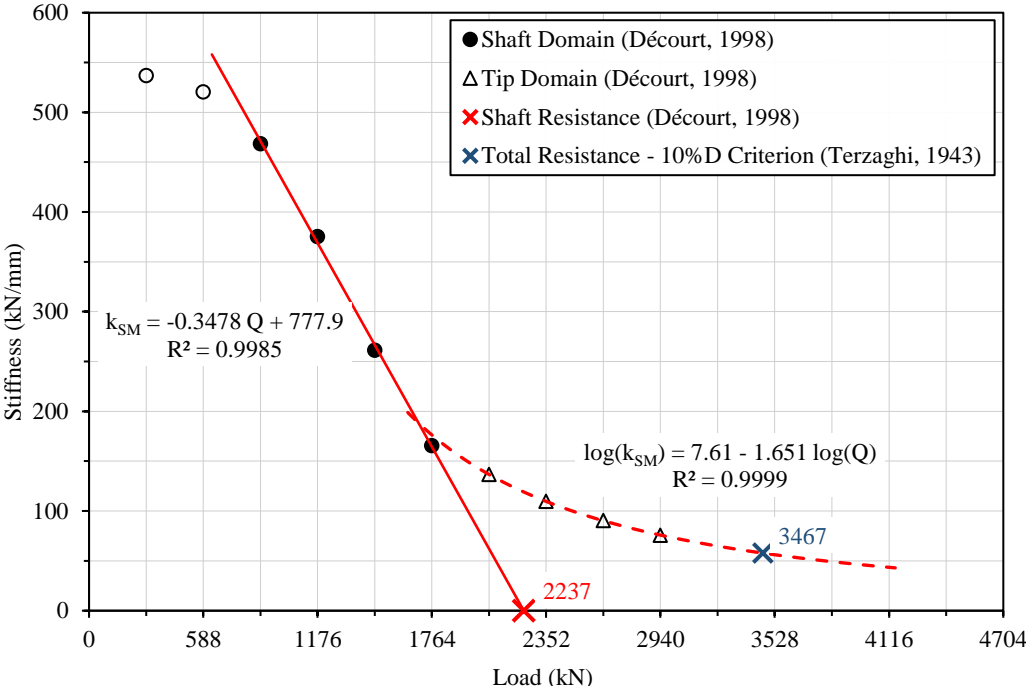


Figure 4.6: Application of the Stiffness Method for the SLT.

Table 4.2: Resistance components obtained by the Stiffness Method.

Resistance	Value (kN)	Percentage (%)
Total	3467	100
Shaft	2237	65
Tip	1230	35

The CAPWAP analyses on the piles at Site A were conducted using the estimated shaft and tip resistance values based on the SLT. However, since no SLT was performed at Site B, it is necessary to retro-analyze the semi-empirical method Décourt & Quaresma (1978) for predicting the load-bearing capacity of the piles at Site B. To achieve this, at Site A, the resistances obtained from the SLT were inserted into the formulation of the semi-empirical method as known variables. Subsequently, the load capacity factors α and β were determined to be used in predicting the load-bearing capacity of the piles at Site B.

The shaft and tip resistance values resulted in α and β values of 0.68 and 1.15, respectively, in the Décourt & Quaresma (1978) method applied to the soil at Site A. With the calibration of these factors, it is possible to determine the distribution of static resistance along the shaft under failure conditions.

The following two figures present the resistance distribution considering the calibrated factors compared to those initially suggested by the authors of the method for preliminary analyses ($\alpha = 0.3$ and $\beta = 1.0$). Additionally, the distribution of axial load in the shaft of the pile due to the transfer of load by lateral friction is presented. For the distribution of axial force, the average resistance distribution between the SPT boreholes was considered.

It is important to note that the determination of the values of α and β , as well as the resistance distribution, were obtained considering the nominal diameter of the CFA pile (60cm) and a 10%*D* failure criterion. In other words, variations in the cross-sectional area with depth were not considered, as usually done in practice, and the resistance is a function of the failure criterion.

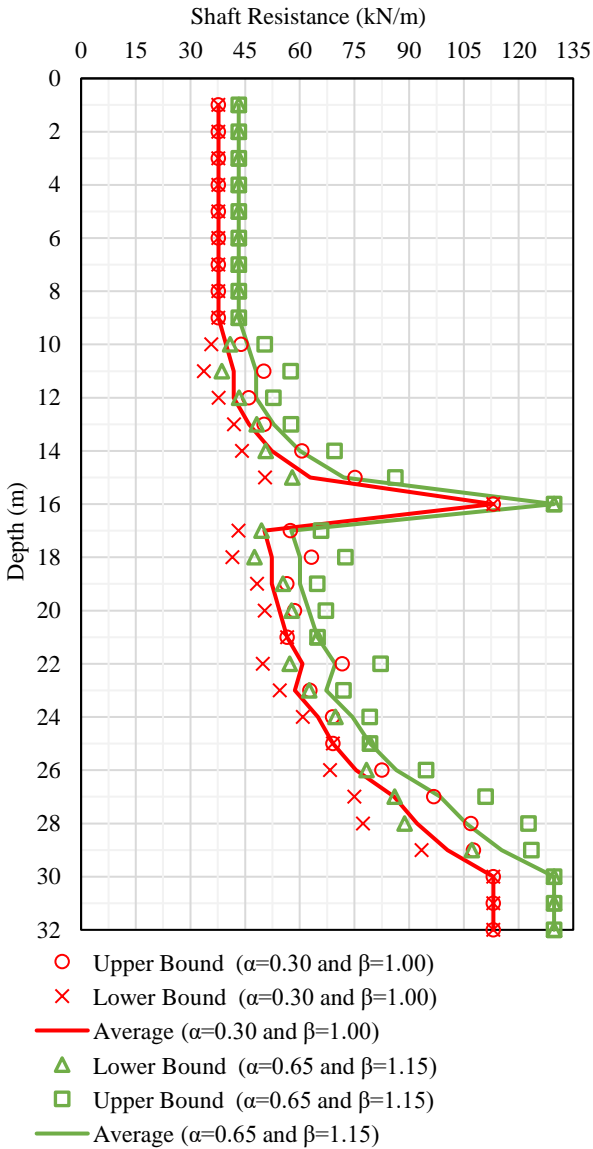


Figure 4.7: Shaft resistance – Site A.

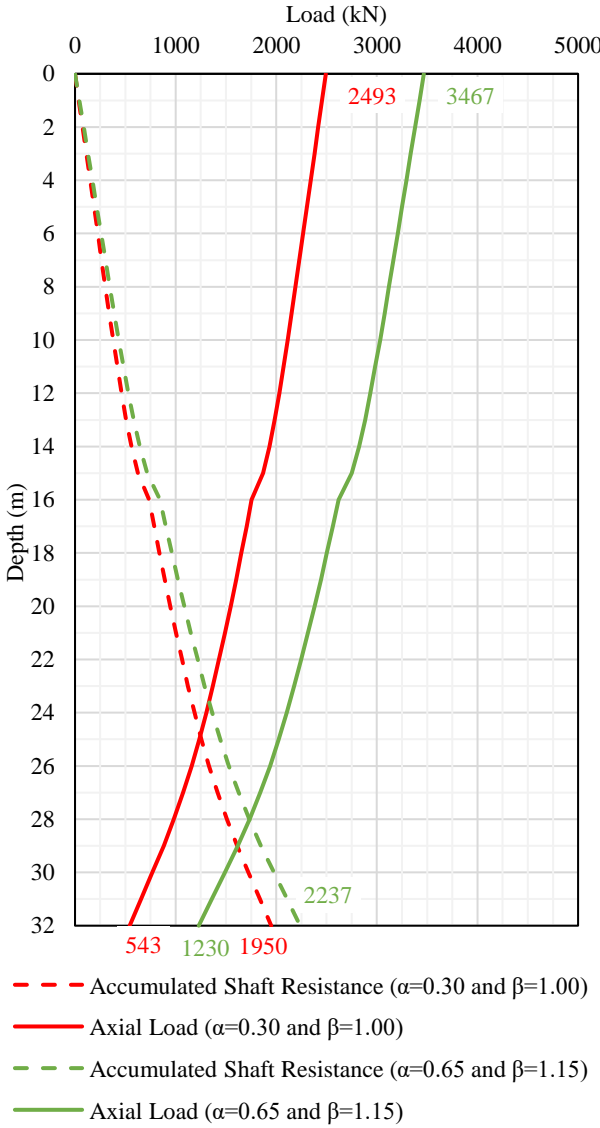


Figure 4.8: Load transfer - Site A.

4.1.3 CAPWAP ANALYSIS

Once the distribution of static resistance and the variation of impedance of the piles with depth at Site A were determined, the CAPWAP analyses aimed to achieve an MQ less than 5 by varying only the parameters q_s and J_s for each soil segment of the model. In other words, other CAPWAP parameters were kept constant with their default values. The reports of each analysis in standard format, exported from the CAPWAP software, can be found in the appendices. In these appendices, the results are detailed with all the parameters used for the adjustment between the measured and computed signals.

Once an MQ less than 5 was achieved, the analyses were considered satisfactory. The following figures from the CAPWAP standard output present the measured Wave Up (Wup Msd) compared to the computed Wave Up (Wup Cpt) as a function of the pile-soil model fit. On the vertical axis, the scale is force dimensioned, and the horizontal axis is time scaled. The derivative of the Wave Up is numerically equal to the unit shaft friction developed in the pile. The standard report of the results of each analysis can be found in Appendix D.

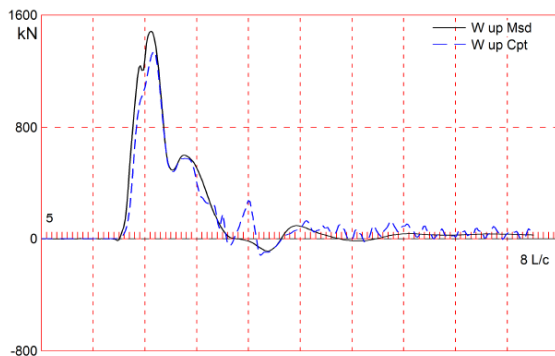


Figure 4.9: DLT – 1A - Measured and computed WU signals.

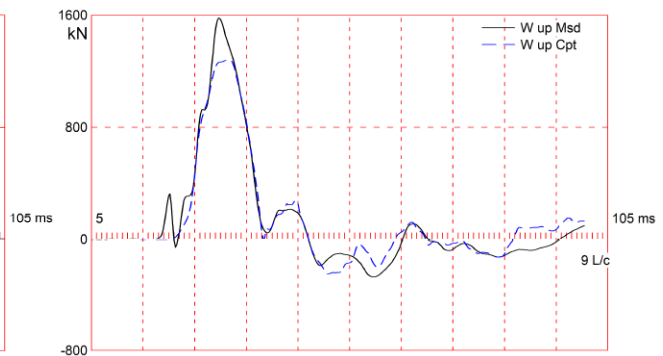


Figure 4.10: DLT – 2A - Measured and computed WU signals.

With the satisfactory MQ , the parameters q_s and J_s were considered representative of the pile-soil system and the dynamic wave propagation event. A set of q_s and J_s data was determined as a function of depth. For each depth, the mean values and their ranges of variation for 95% confidence were determined and are presented in Figure 4.11.

In the first graph of Figure 4.11, it is observed that the q_s predominantly exhibited higher values in the clay layer compared to the lower layers of silty sand. Additionally, the quake showed a tendency to decrease with increasing depth, which may suggest a relationship with the soil's resistance, as will be discussed later.

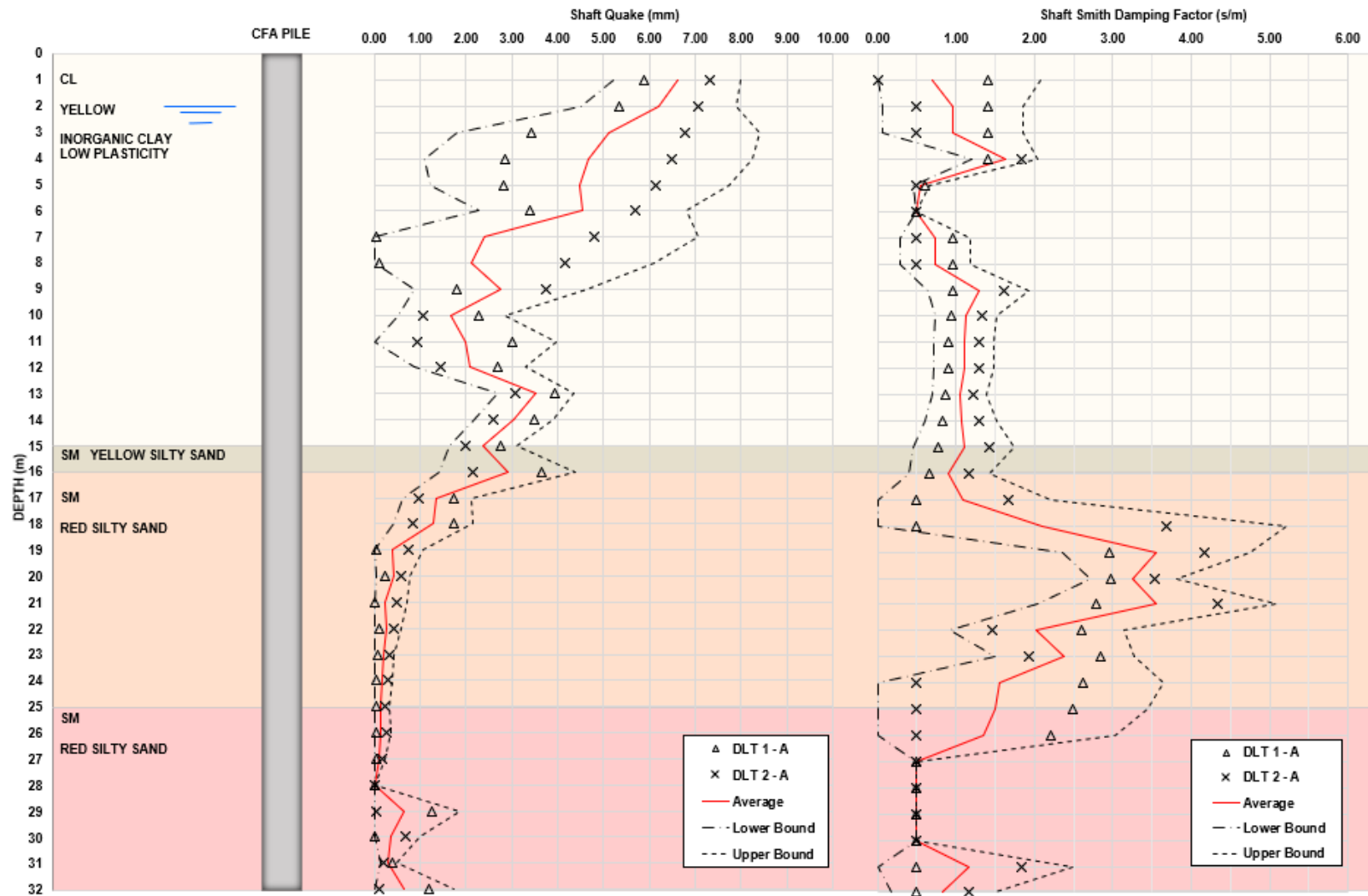


Figure 4.11: Variation of q_s and J_s as a function of depth - Site A.

The distance between the variation limits for 95% confidence, the confidence interval of the quake, is greater in the clay layer than in the silty sand layers, ranging between 8mm and 1mm. In the silty sand layers, the confidence interval is much smaller, and the q_s is practically restricted to 1mm, with values close to 4mm and 2mm between 15 and 18m.

Analyzing the 2nd graph of Figure 4.11, J_s exhibited mean values close to 1s/m in the clay layer and a significant increase in the silty sand layer between 16 and 25m depth. The J_s in the clay layer reached values of up to 2s/m, while in the other layers, they reached values close to 4.5s/m. Regarding the confidence intervals, the clay layer showed less dispersion around the mean compared to the silty sand layers, where the variability was greater.

Figure 4.12 again presents the variation of quake and damping in depth, but with information regarding the variation of resistance to SPT and VST. In addition, the quake and damping values suggested in the literature by Smith (1960), Randolph & Deeks (1992) and Hannigan et al. (1998). As seen in section 2.3, Smith (1960) suggests a constant quake of 2.54mm and Randolph & Deeks (1992) state that the quake varies between $D/500$ and $D/200$ (1.20 and 3.00mm). As for damping values, Smith (1960) suggests 0.16s/m regardless of soil type and Hannigan et al. (1998) suggests 0.66s/m for cohesive soils and 0.16s/m for non-cohesive soils.

In Figure 4.12, it is observed that the shaft quake values tended to be higher than those predicted in the technical literature, especially for $S_u < 15kPa$, up to 7m deep in clay. This disparity likely arose because Smith (1960) and Randolph & Deeks (1992) based their studies on driven piles, where the setup effect can be significant. That is, during pile driving, there is a decrease in clay resistance due to excess pore pressure and structure breakage, which is partially recovered after a period of rest (setup). Additionally, driven piles generally have smaller cross-sectional areas compared to CFA piles, meaning that the relative displacement between the pile and the soil must be greater for a given resistance to be mobilized (displacement to mobilize skin friction as a function of the pile diameter).

In the transition between the clay and silty sand layers, the quake values respected the expected limits by Randolph & Deeks (1992). However, in the silty sand layer, they assumed values much lower than expected. Therefore, unlike what is generally considered in CAPWAP analyses, the quake values are not constant.

There is an inverse relationship between q_s and SPT N-value. While there is an increase in SPT resistance, there is a decrease in quake values with depth. The same trend is observed when analyzing undrained resistance relative to quake values up to 15m. This result aligns with the concept that less deformable soil requires less displacement to mobilize a certain resistance.

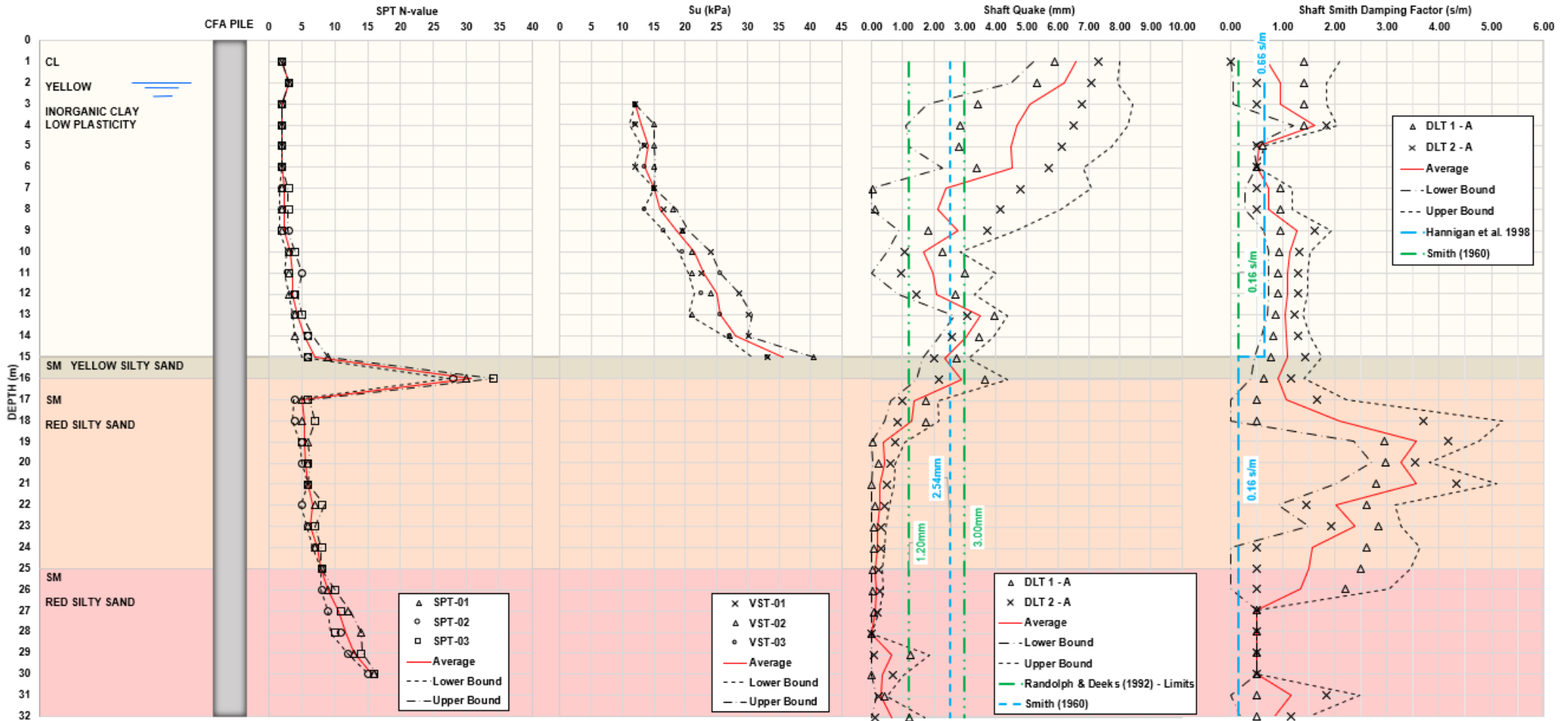


Figure 4.12: Variation of q_s , J_s , SPT N -value and S_u as a function of depth - Site A.

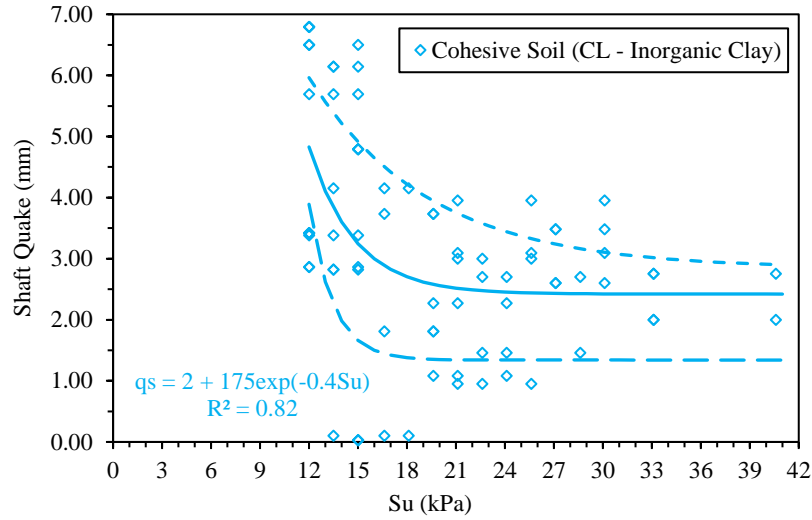


Figure 4.13: Shaft quake as a function of undrained shear strength.

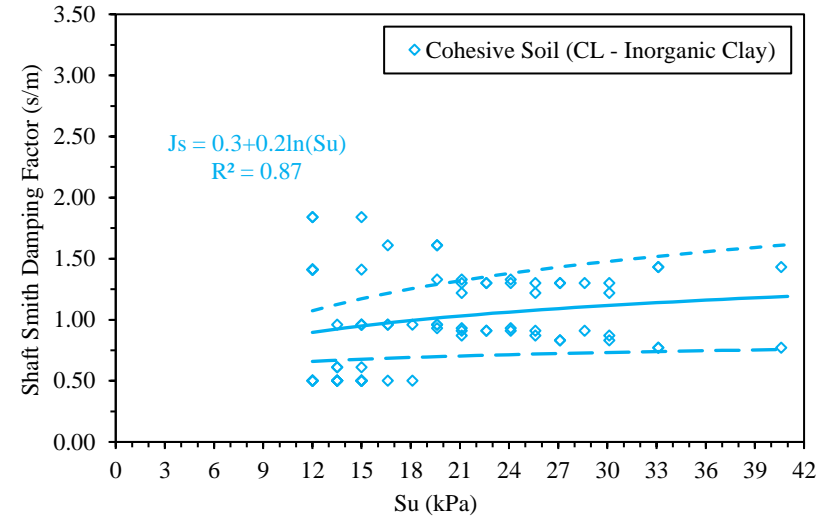


Figure 4.15: Damping factor as a function of undrained shear strength.

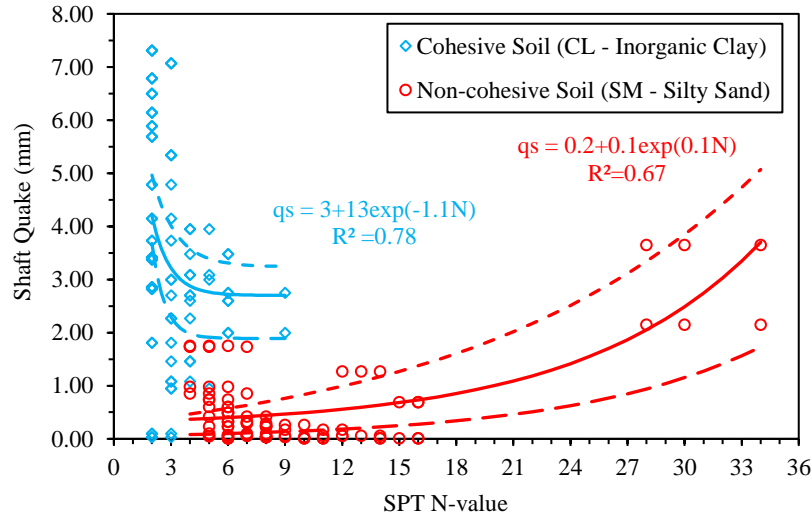


Figure 4.14: Shaft quake as a function of SPT N-value.

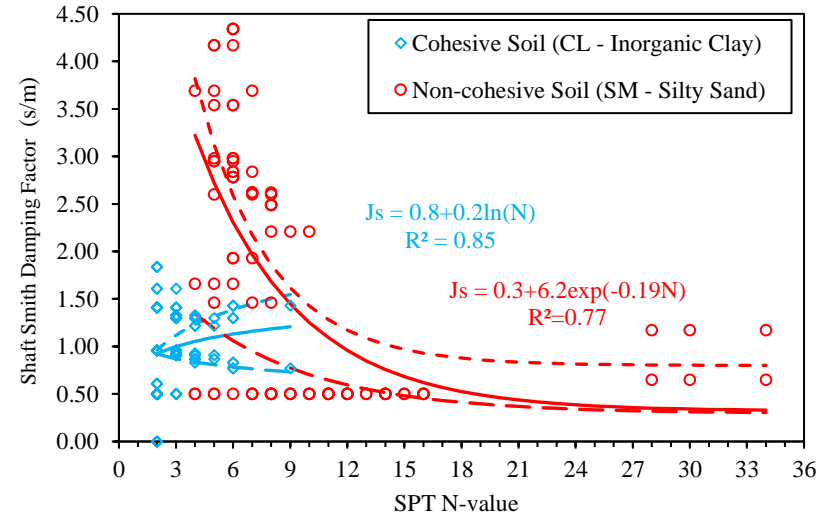


Figure 4.16: Damping factor as a function of SPT N-value.

In the same Figure 4.12, it is noted that the damping factor values were predominantly higher than those expected in the literature, especially in the silty sand layer. This indicates greater damping (dynamic resistance) mobilized during the DLTs. As the surface of the CFA pile tends to be rougher and more irregular than that of driven piles, a shaft plug may have occurred. This shaft plug is characterized by the adhesion of a mass of soil to the shaft, resulting in a shear failure that does not occur at the pile-soil interface. In other words, the shear failure occurs within the mass of soil. Thus, since the diameters of the tested CFA piles are relatively large (60cm), the volume (mass) of soil adhered to the shafts may have been considerable. Consequently, inertial forces (as a function of acceleration) may have influenced the values of J_s , as they also cause a damping effect.

The damping factor showed approximately constant average values in the clay layer, even with increasing undrained resistance. However, in the lower layers, this parameter does not assume constant values and appears to be related to the soil type.

Four graphs were plotted to correlate q_s and J_s with the values of S_u and N_{SPT} . In these graphs, the data sets from the cohesive layer, composed of inorganic clay between 0 and 15 meters, were differentiated from those of the non-cohesive layer composed of poorly graded silty sand. In the four previous figures, adjustments were made to the curves to determine correlations, represented by continuous lines, with their equations provided. The upper and lower dashed lines represent the limits within which the values of q_s and J_s have 95% confidence.

In Figure 4.13, it is observed that q_s and S_u have an inversely proportional relationship through an exponential equation. Furthermore, the curve fitting for correlation was relatively good, with an R^2 of 0.82. However, the quake values varied widely between 1 and 7mm. This behavior can also be seen in the distance between the upper and lower limits for a 95% confidence level.

For non-cohesive soil in Figure 4.14, the correlation between N and q_s does not have a good fit ($R^2 = 0.67$). The q_s increases exponentially with the N value, exhibiting behavior opposite to that of cohesive soil, where there is a decrease exponentially as N increases. One explanation may be due to the lower relative density and the poor gradation of cohesionless soil. Therefore, the soil might be in a loose state where resistance is mobilized for greater deformations. Poor gradation is indicative that the non-cohesive soil is not in a compact state.

Analyzing the correlation between S_u and J_s in Figure 4.15, the adjustment using a natural logarithm equation was relatively satisfactory with $R^2 = 0.87$. It is also noted that there is an increase in J_s values with the increase in S_u , albeit at a very small rate. Furthermore, the J_s values exhibited a slight variation between 0.5 and 2.0 s/m, while the confidence limits were also small. Therefore, the correlation between S_u and J_s is considered satisfactory.

For the cohesive soil in Figure 4.16, a relatively good fit using the natural logarithm was achieved. J_s and N were related with an $R^2 = 0.85$. The J_s values varied within a much narrower range compared to non-cohesive soil. It is also observed that there is an increase in J_s values with the increase in N for cohesive soil. Conversely, for non-cohesive soil, a good fit was not achieved ($R^2 = 0.77$) and J_s varied across a wide range of values. However, the data indicate that with an increase in N , there was a reduction in J_s according to an exponential function. This behavior may be related to the increase in the coarse fraction of the soil with depth. The coarser particle size distribution provides lower damping and less excess pore pressure compared to fine soil during DLT.

Table 4.3 summarizes the determined correlations at Site A, the coefficients of determination (R^2), and the ranges of S_u and SPT N -values used.

Table 4.3: Summary of the obtained correlations at Site A.

Soil Test	Soil Type	Parameter	Unit	Correlation	R^2	Validity Range
SPT	Cohesive (CL)	q_s	mm	$q_s = 3 + 13e^{-1.1N}$	0.78	$2 \leq N \leq 9$
		J_s	s/m	$J_s = 0.8 + 0.2 \ln N$	0.85	
	Cohesionless (SM)	q_s	mm	$q_s = 0.2 + 0.1e^{0.1N}$	0.67	$4 \leq N \leq 34$
		J_s	s/m	$J_s = 0.3 + 6.2e^{-0.19N}$	0.77	
VST	Cohesive (CL)	q_s	mm	$q_s = 2 + 175e^{-0.4S_u}$	0.82	$12 \leq S_u \leq 41$ (kPa)
		J_s	s/m	$J_s = 0.3 + 0.2 \ln S_u$	0.87	

The correlations presented above, within their domains of validity and the dispersion of the data used, can be utilized in practical applications in CAPWAP analyses aimed at defining pile designs or even evaluating their performance. The correlations allow for the definition of quake and damping based on the type of soil and its resistance to SPT and VST. These data are easily obtainable and are usually available to the engineer responsible for the analyses.

However, to be used in practice, these correlations must be validated at least at a second site. This will be done later at Site B located in Sinop - MT.

4.2 VALIDATION: SITE B

4.2.1 SOIL PROPERTIES

At Site B, the 2 SPT boreholes identified the occurrence of soft gray silty clay with thickness of 10m. Below this layer, the moderately compact to compact red gravelly sand was observed, with a thickness varying between 6 and 7m. The last layer of soil identified was fine red sand compacted up to 50 meters deep. Additionally, the groundwater table (GWT) identified in all 2 boreholes was at a depth of 3.00m. The soil types mentioned were identified through tactile-visual inspection of the SPT.

Figure 4.17 shows the geotechnical profile in which the layers were classified according to the SPT. It can be seen that the resistance to SPT had approximately constant values in the first layer of soil. In the second layer, there was a variation, possibly due to the gravel mixed with grains of red sand. In the last layer, up to 32 meters, resistance increased at a small rate, then experiencing a significant increase in resistance up to 50 meters.

The same Figure 4.17 shows the variation in undrained resistance obtained in the 2 VSTs. The tests were conducted in the silty clay layer below the GWT. It can be seen that S_u in both holes presented approximately constant values or with a slight increase in resistance up to 10 meters depth, as seen in VST - 02.

To carry out the analyses, an average profile of the soil layers was defined, which is presented in Figure 4.18. In this figure, the average resistance values and their respective limits of variation for 95% confidence depending on depth are presented.

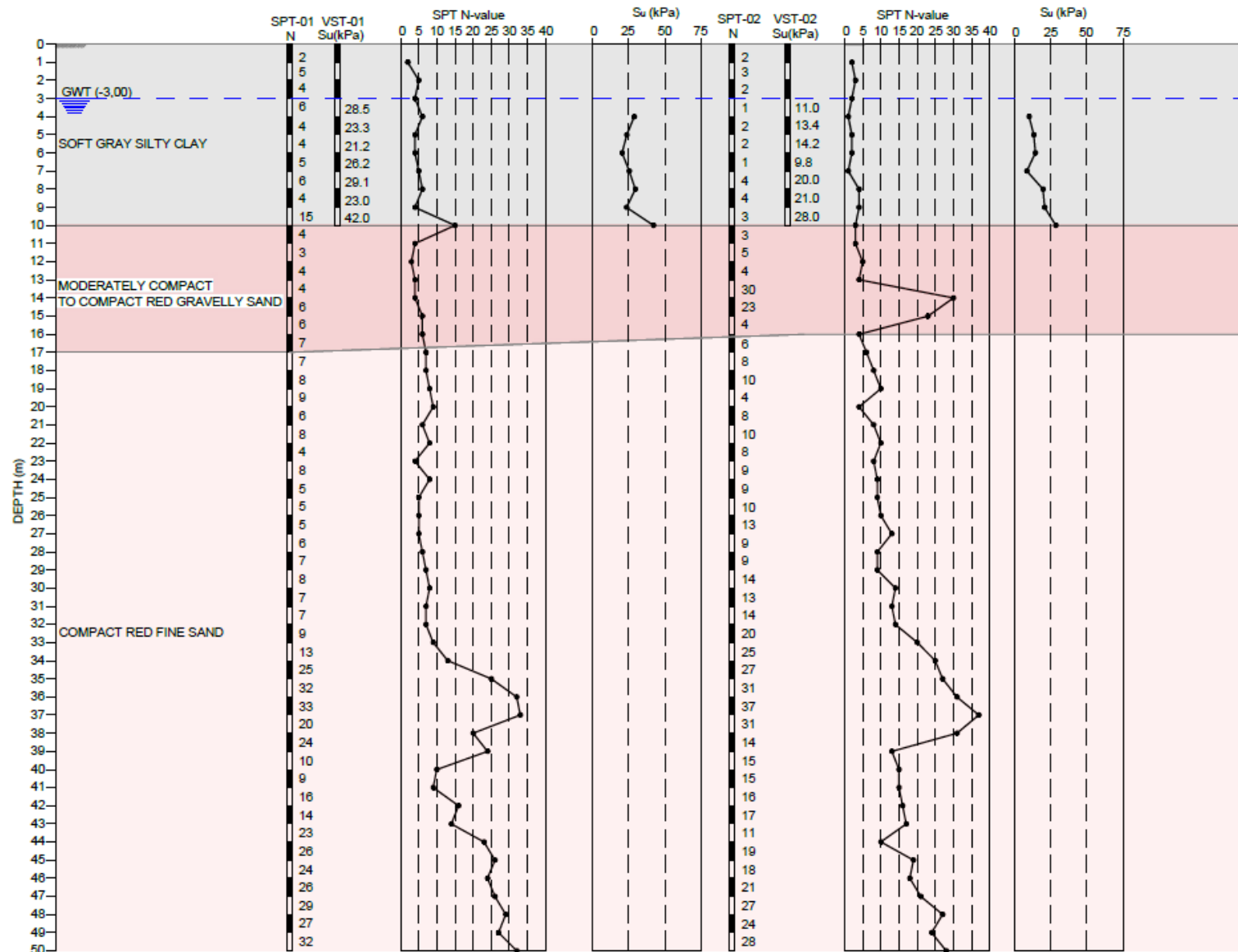


Figure 4.17: Geotechnical profile of Site B with the results of SPTs and VSTs (no scale).

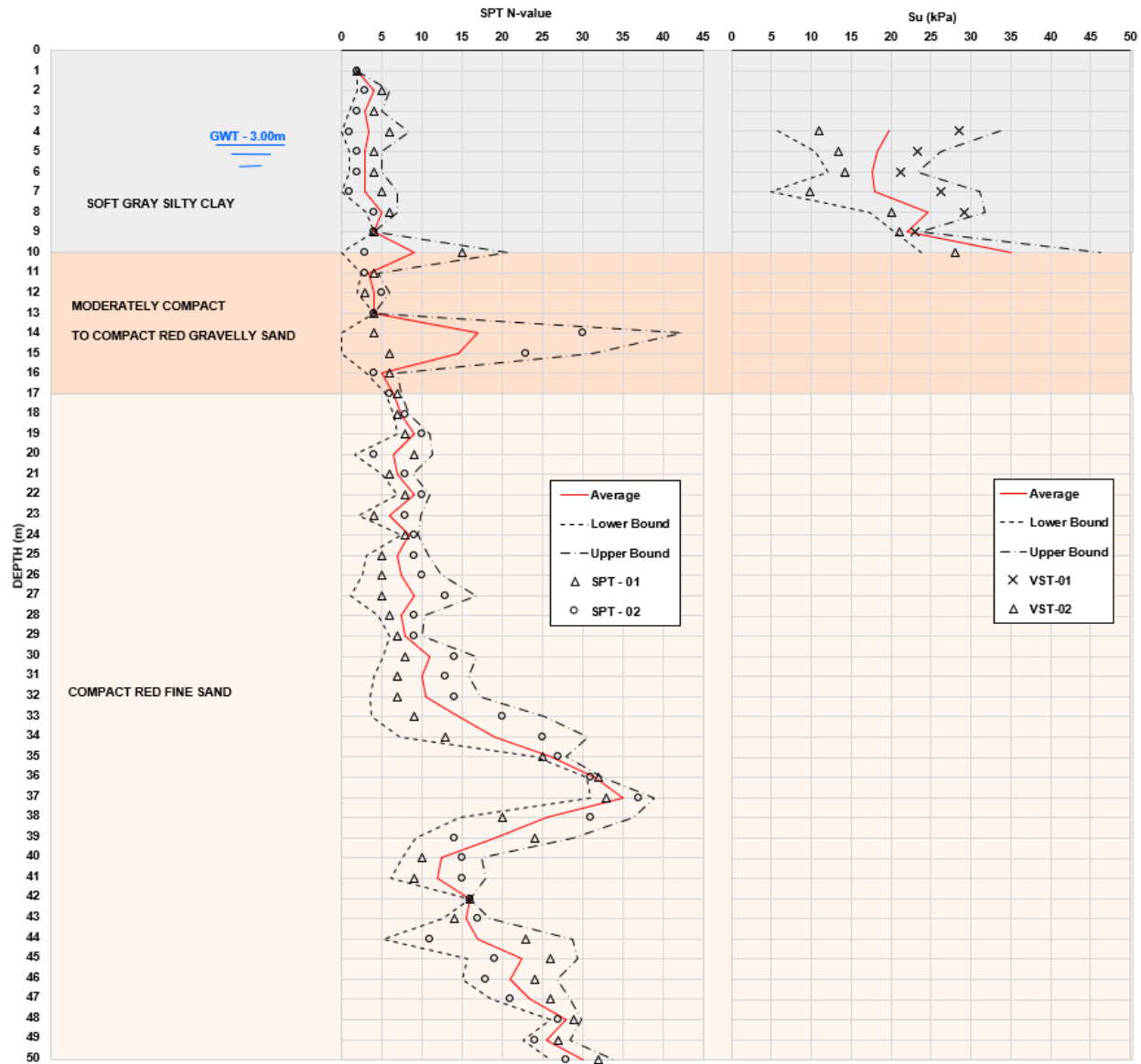


Figure 4.18: Average geotechnical profile of Site B.

4.2.2 STATIC ANALYSIS

As previously presented, the α and β factors of the semi-empirical method of Décourt & Quaresma (1978) were calibrated for the Sinop – MT soil based on the SLT carried out at Site A and the interpretation of the stiffness curve according to the Décourt (1998) method and Terzaghi (1943) failure criterion. The values obtained were $\alpha = 0.65$ and $\beta = 1.15$.

With these load capacity factors and the geotechnical investigation presented in Figure 4.17, the load capacity of a single CFA pile at Site B was estimated. The pile is 32m deep and has a diameter of 60cm.

The following two figures show the distribution of lateral resistance and also the load transfer of the pile in the failure condition. Predicted values are also presented according to the factors suggested in the original work of the authors of the semi-empirical method ($\alpha = 0.3$ and $\beta = 1.0$). In these figures, the upper and lower limits of shaft resistance for 95% confidence are also presented, determined as a function of the resistance variability between the 2 SPT holes.

In Figure 4.19, it can be seen that the variability of shaft resistance increases between 9 and 16 meters depth. Between 16 and 19m the variability decreases, increasing up to 32 meters. Furthermore, as also in Figure 4.20, the shaft and tip resistance are higher for the calibrated α and β factors.

Table 4.4 summarizes the determined static resistance components:

Table 4.4: Resistance components according to adjusted α and β - Site B.

Resistance	Value (kN)	Percentage (%)
Total	3069	100
Shaft	2262	74
Tip	808	26

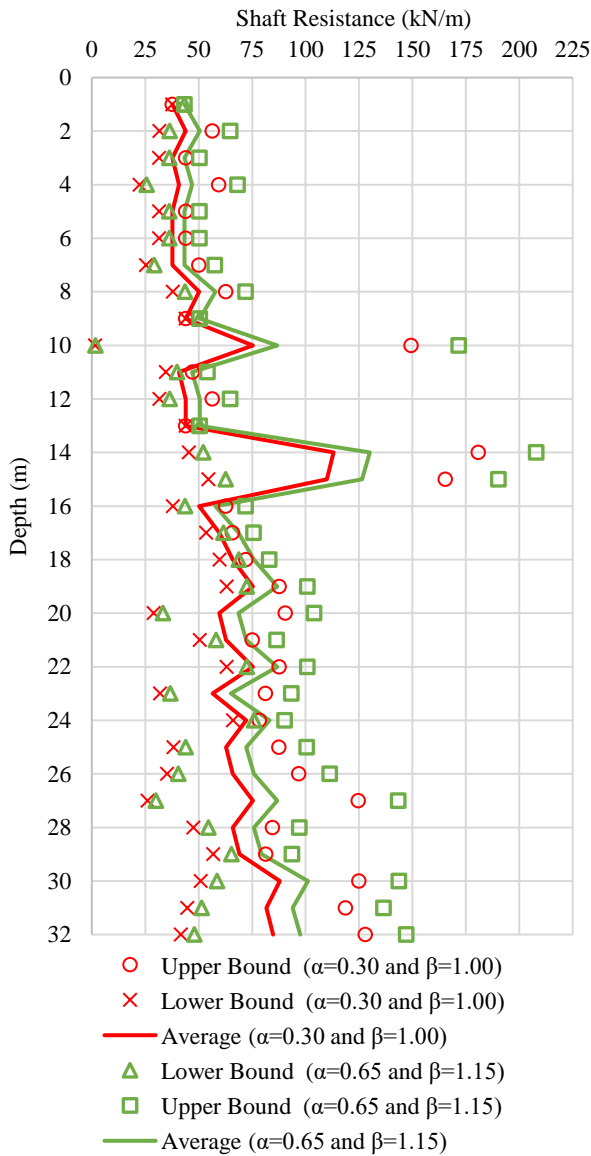


Figure 4.19: Shaft resistance - Site B.

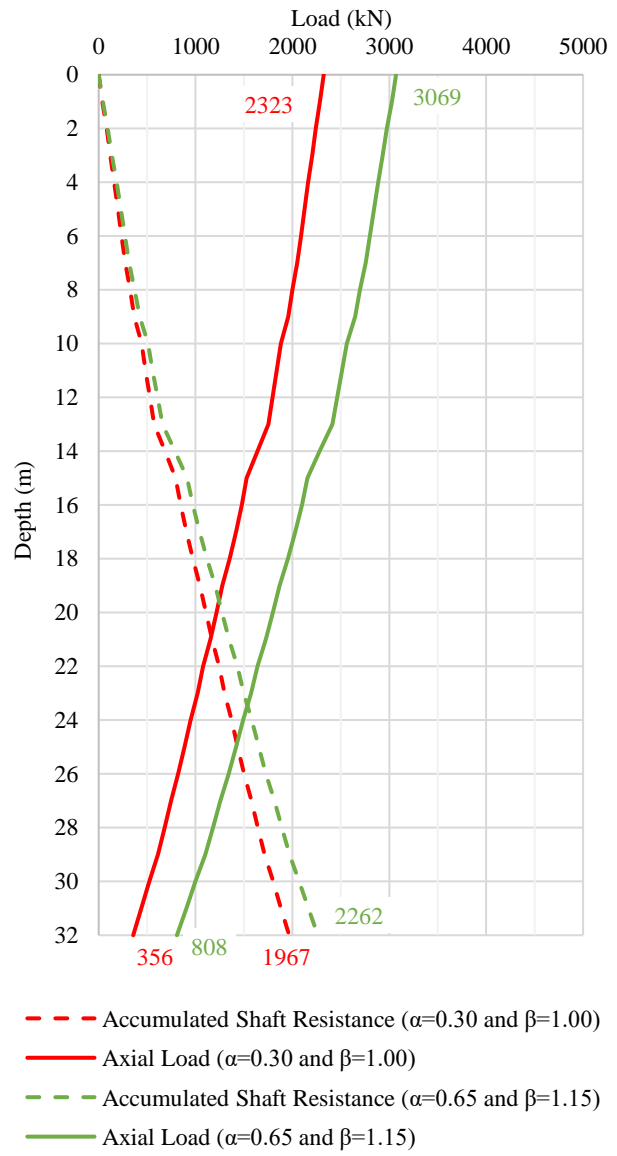


Figure 4.20: Load transfer - Site B.

4.2.3 CAPWAP ANALYSES

With the correlations between N and S_u with q_s and J_s determined at Site A and presented in Table 4.3, the parameters q_s and J_s were determined for the CAPWAP analyses of the four piles at Site B based on the two SPT and two VST boreholes. Figure 4.21 presents the variation of the q_s and J_s parameters based on the pre-established correlations.

In this figure, it is observed that the q_s presented higher values in the soft gray silty clay layer as well as greater variability. Additionally, in this layer, the q_s predominantly exhibits values higher than those suggested by Smith (1960) and Randolph & Deeks (1992). In the red gravelly and fine sand layers, the opposite occurs, and q_s varies very little, presenting lower values compared to the q_s in the clay layer and those proposed by the technical literature.

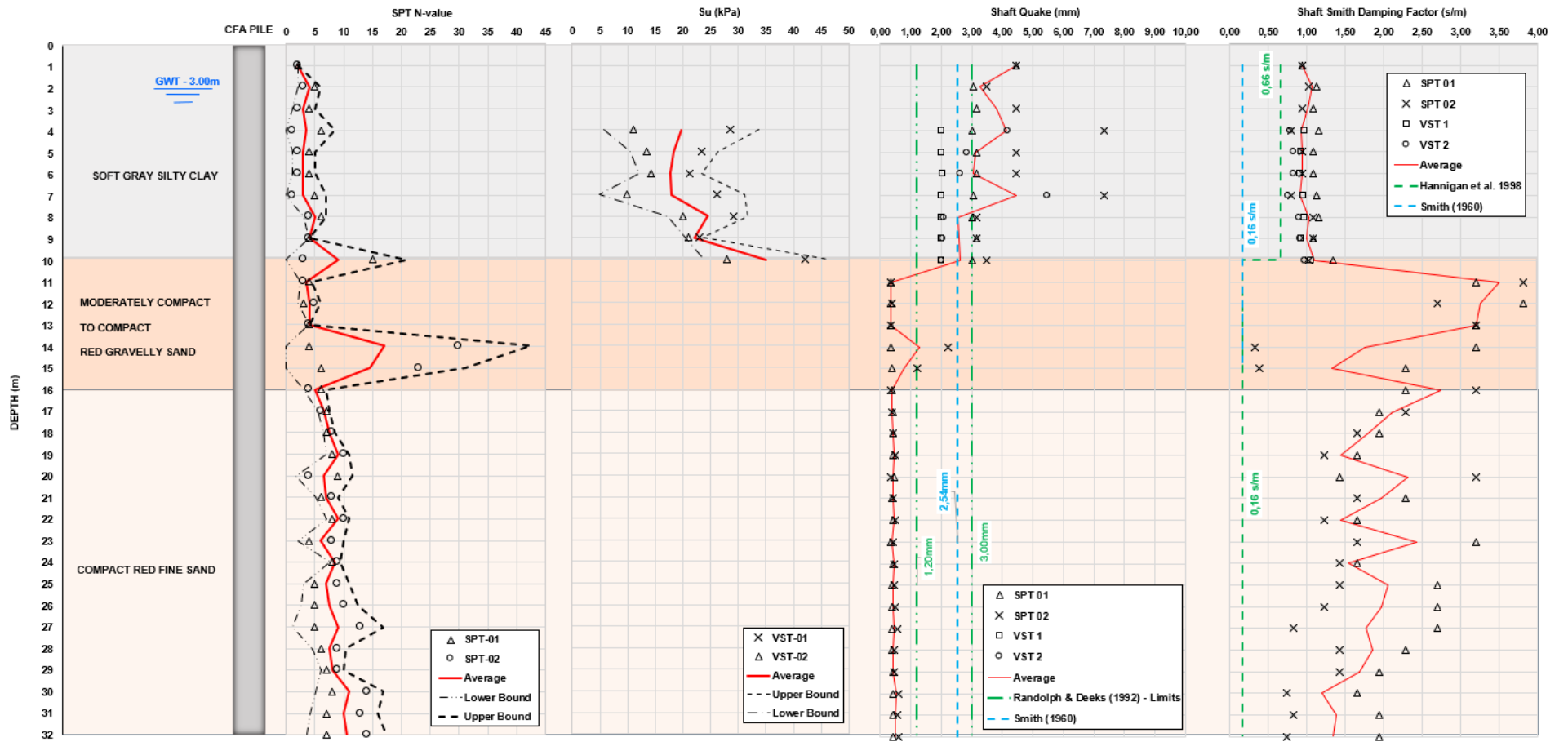


Figure 4.21: Variation of q_s , J_s , SPT N -value and S_u as a function of depth - Site B.

In the last graph of Figure 4.21, J_s has less variability in the clay layer, with average values close to 1 s/m. This value is higher than the predictions of Smith (1960) and Hannigan et al. (1998). In the sand layers, there is significant variability in the values of J_s , with a considerable increase in their average values for each depth. Additionally, J_s is higher in the red gravelly sand layer, further deviating from that suggested in the literature.

Once q_s and J_s were determined, the average values were inserted into the soil model of the CAPWAP for each CFA pile at Site B. Static resistances for each depth were also inserted, estimated according to the semi-empirical method of Décourt & Quaresma (1978) with calibrated alpha and beta factors. Furthermore, the variation of impedance as a function of the variation of pressure and concrete overconsumption recorded in the pile installation monitoring bulletin was introduced as a pile model (Table 3.3 and Appendix B).

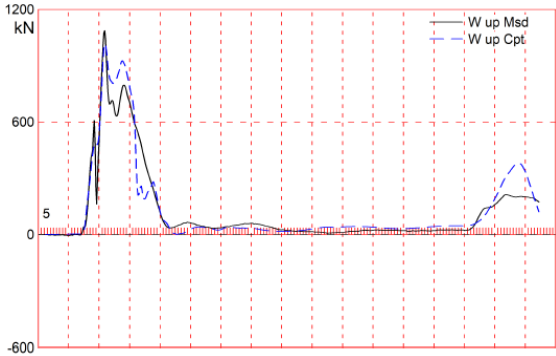


Figure 4.22: DLT 1B - Measured and computed WU signals.

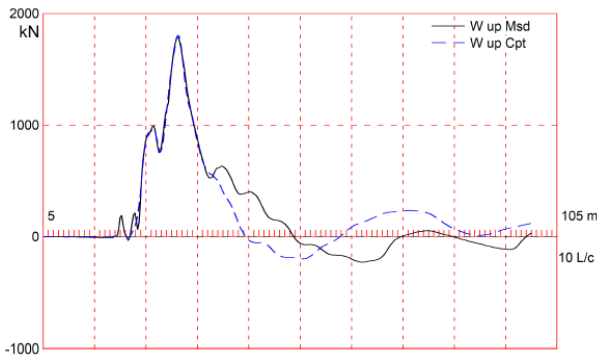


Figure 4.24: DLT 3B - Measured and computed WU signals.

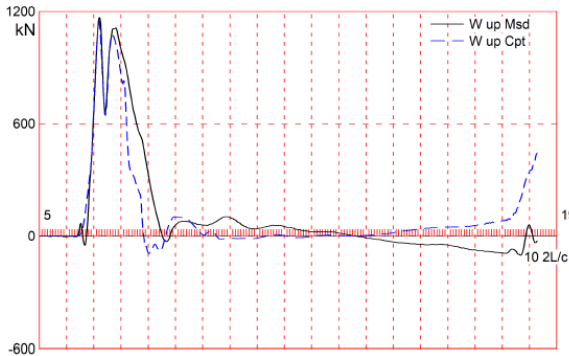


Figure 4.23: DLT 2B - Measured and computed WU signals.

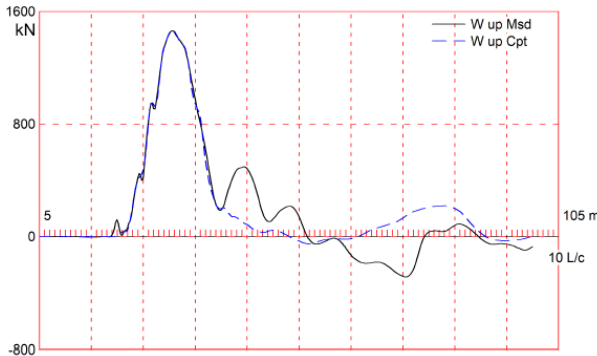


Figure 4.25: DLT 4B - Measured and computed WU signals.

It is noticeable in the previous four figures that the adjustments were better at the beginning and in the intermediate region of the signals, indicating that the adopted parameters were quite satisfactory during the loading phase of the pile. However, the deficiency of the parameters in adjusting signals during the unloading (rebound) phase at the end of the signals is also perceptible.

The values of MQ for the four piles ranged from 2.58 to 5.61 with a standard deviation of 1.37 and coefficient of variation of 30%. The following Figure 4.26 shows that the average MQ of 4.6 was lower than 5.0, which is satisfactory according to the developers of the CAPWAP method (PDI, 2014). However, considering a confidence level of 95%, the lower and upper limits of MQ are 3.26 and 5.94, respectively. Furthermore, of the four analyzed piles, half resulted in satisfactory MQ (DLT 1B and DLT 2B).

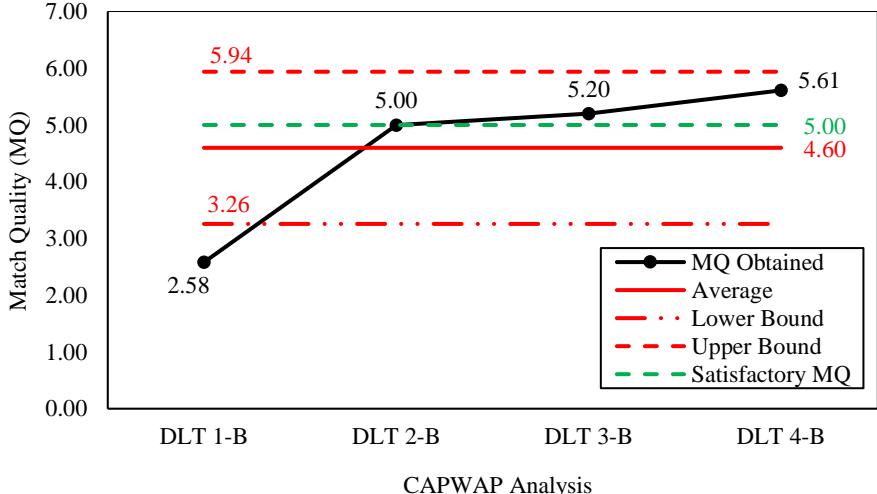


Figure 4.26: Match qualities for CFA piles at Site B.

Based on the average MQ value and its variability, assuming a log normal distribution of probabilities, the probability of $MQ < 5.0$ was determined (Figure 4.27). The results indicate that the probability of $MQ < 5.0$ is 64% considering the methodology presented in this dissertation. In other words, 1 out of 1.57 CAPWAP analyses will have satisfactory MQ if this methodology is considered.

Evidently, the normal distribution of probabilities used only 4 samples for its determination. Unfortunately, this number was limited due to commercial constraints, and it was not possible to conduct more tests at Site B.

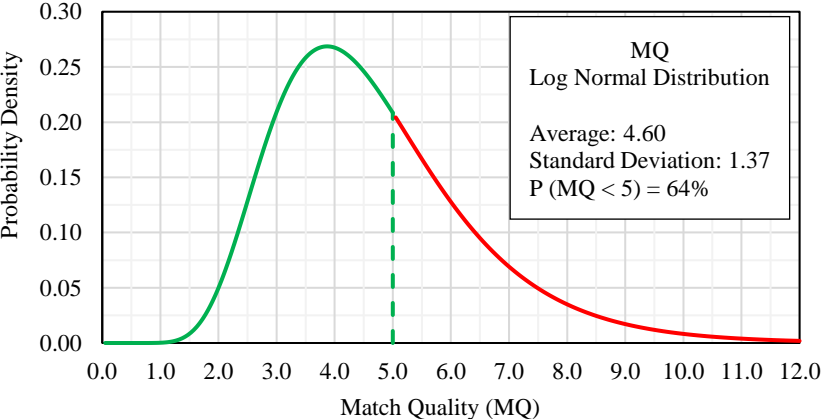


Figure 4.27: MQ Log Normal Distribution - Site B.

5. RECOMMENDATIONS FOR DESIGN PURPOSES

As presented in the literature review, the CAPWAP analysis allows the soil and pile to be modeled for their static and dynamic behaviors. This analysis enables obtaining a static response of the single pile from a short-duration dynamic load in the DLT.

Since the DLT load is of short duration, the pile behavior over the time the loads are maintained is not fully captured. This behavior can be important in the case of displacements over time and in the long term. This deficiency can be mitigated through SLT, where the loading rate and applied loads are controlled according to the criteria of the geotechnical engineer responsible for the foundation design. It was also discussed throughout this dissertation that, for CAPWAP analyses, the soil model variables are not constant with depth but are instead a function of the soil type and its resistance. Additionally, the values obtained at depth differ from those suggested by technical references. Due to this variation from reference values, the methodology presented in this dissertation can contribute to making CAPWAP analyses more rational and reducing deviations from the actual behavior of piles.

Therefore, for practical design purposes, it is recommended to conduct basic soil investigations such as standard penetration test (SPT) to determine the groundwater table, soil types, stratigraphy, and their resistance (N) at depth. If suitable for the local subsoil, vane shear tests (VST) or cone penetration test with pore pressure measurement (CPTu) can also be performed to evaluate the soil's undrained shear strength and its behavior. Based on these initial investigations, the engineer responsible for the design can estimate the most appropriate pile types, diameters, depths, and the necessary capacity with the use of semi-empirical or rational methods and correlations between investigations and soil properties.

Next, once the initial pile characteristics for the design have been estimated, static load tests (SLT) should be conducted in sufficient quantities to be representative of the site. After these static tests are performed, the engineer should interpret the load-displacement curves to determine the pile's load capacity using an appropriate failure criterion. Additionally, if instrumented SLTs at depth are not performed, methods such as Stiffness Method (Décourt, 1998) can be used to estimate the shaft and toe resistance components.

Once the load-displacement behavior and load capacity of the single pile are obtained, the geotechnical engineer will be able to specify the project's piling with types of piles, their diameters, lengths, and installation criteria. For these characteristics to be determined, the design must meet the minimum safety factors, the acceptable probability of piling failure, and also the displacements under service loads, considering the effects of pile group. The deep

foundation design will specify additional tests to verify the performance of the piling. Due to its speed and relatively low cost, the DLT can be used on a larger number of piles to ensure a representative sampling. Since compressive and tensile stresses are monitored by the PDA during the tests, piles belonging to the structure's foundation can be used without the need to install piles exclusively for DLTs. In other words, the tests will be conducted and monitored to ensure they do not damage the tested piles.

The DLTs can be analyzed using the CAPWAP methodology presented in this dissertation, in which the variation of static resistance with depth obtained through SLT is initially introduced, along with the soil model parameters, quake, and damping, inserted with values based on the variable field tests in depth. Specifically for the city of Sinop, the correlations obtained in the previous sections can be used for preliminary analyses as initial input parameters. If a satisfactory Match Quality (MQ) is achieved with the initial input data, the results of the CAPWAP analyses can be used to verify the performance of the piling according to design criteria: safety factors and reliability. If the initial MQ is not achieved, the predicted resistance distribution, soil quake, and damping parameters must be altered until a satisfactory MQ (less than 5.0) is achieved. Thus, the load capacities of the tested piles will be known, and performance verification will be carried out for the geotechnical engineer to approve or reject the results, enabling reliable decision-making.

The methodology is recommended for practical foundation design purposes (Figure 5.1). The quantity of tests should be sufficient to be representative and varies from project to project.

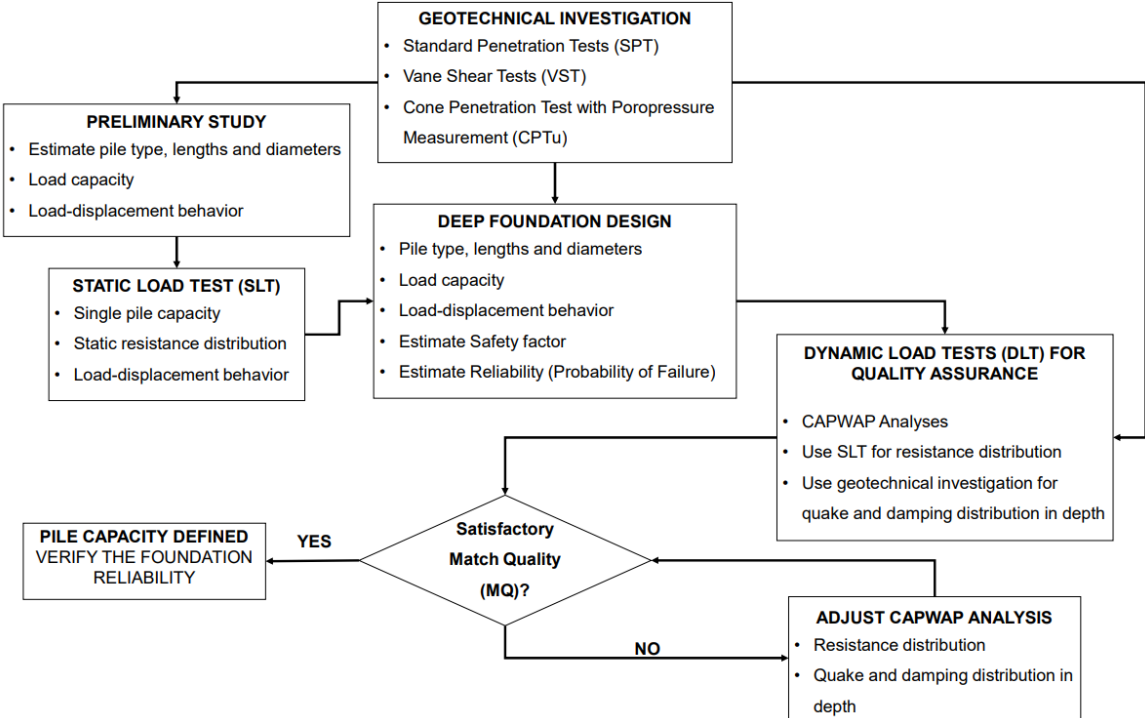


Figure 5.1: Suggested methodology for pile foundation design and quality control.

6. CONCLUSIONS

In this dissertation, due to the limited consideration of constant q_s and J_s for the pile shaft in CAPWAP analyses, neglecting the variability of the soil type and resistance in the geotechnical profile, the objective was to determine their values based on these properties. Therefore, the primary goal of this dissertation was to establish correlations between the SPT N -value, S_u , and the soil type with q_s and J_s for CAPWAP analyses in CFA piles.

To achieve these objectives, an experimental field was created at a site designated as Site A in the city of Sinop - MT. At this location, SPTs and VSTs were conducted, and soil samples were collected at different depths for laboratory characterization. An SLT was also performed to determine the load capacity and resistance domains of the shaft and tip of a CFA pile. Subsequently, using the impedance variation from installation monitoring and the static resistance predicted by the SLT, two piles were subjected to DLTs, allowing for CAPWAP analyses. During this phase, the quake and damping values were varied meter by meter to achieve a satisfactory MQ . Once a satisfactory MQ was achieved, the quake and damping values from the CAPWAP model were compared with the soil stratigraphy measured in the field tests and laboratory characterization.

As a result, correlations between N , S_u , q_s , and J_s were proposed. These correlations were used at a second site, referred to as Site B, where SPTs and VSTs were also conducted, along with four DLTs. The static resistance distribution along the piles at Site B was obtained through a semi-empirical method calibrated by the SLT from Site A applied to the soil in Sinop - MT. The correlations determined at Site A established the values of q_s and J_s inserted into the CAPWAP soil model for Site B. Thus, with the impedance variation of the pile obtained from the installation monitoring report, MQ values were obtained based on the input data, serving as validation criteria for the methodology and the obtained correlations. The validation criterion was $MQ < 5.0$.

In conclusion, the correlations resulted in a satisfactory average MQ but with a 64% probability of achieving a satisfactory value, due to their variability. Moreover, the correlations and methodology employed resulted in a better fit in the initial and intermediate portions of the signals analyzed by CAPWAP, indicating a satisfactory fit for the loading phase but not for the unloading phase of the pile. Therefore, the objectives of this dissertation were practically all achieved, as the previously presented methodology led to results that were mostly satisfactory. In conclusion, given the methodology, results, and conclusions presented, the correlations

determined in this research should be used with caution and good engineering judgment for practical purposes in CAPWAP analyses.

The main conclusions of this dissertation are:

- The correlations for determining q_s and J_s based on the SPT N -value and S_u are more effective in fitting the initial and intermediate portions than the final portion of the analyzed signal.

- The correlations resulted in satisfactory average MQ values lower than 5.0, but with high dispersion, leading to only a 64% probability of a complete signal match.

- For the inorganic clay of Sinop - MT, q_s and S_u have an inverse relationship. That is, an increase in S_u results in a decrease in q_s . The same behavior is observed between q_s and the SPT N -value. The correlations were determined through an exponential equation. The quake values in the clay layer varied widely, from less than 1 mm to close to 7 mm. However, for S_u greater than 20 kPa and N greater than 4, the q_s values tend towards a constant value close to the 2.5mm suggested by Smith (1960) and other authors.

- For the clay in Sinop, J_s varies logarithmically with S_u and N . As S_u and N increase, J_s values also increase. The damping values ranged from 0.5 to 2.0 s/m, with a good data fit. The correlations established for J_s in the clay were satisfactory, with determination coefficients of 0.87 and 0.85.

- For silty sand, q_s is related to the SPT N -value through an increasing exponential equation. The shaft quake varied widely, from less than 1 to 4.5 mm. As N increases, the correlation becomes more dispersed, presenting more reliable values for $N < 15$. Additionally, q_s values for silty sand were lower than those for clay, possibly due to the higher resistance observed in the SPTs.

- For silty sand, J_s did not fit well with the SPT N -value. The best relationship obtained was through a decreasing exponential equation. The increase in N , as shown in the geotechnical profile, is related to the increase in the coarse fraction with depth. Possibly, the decreasing relationship with N indicates that the coarser fraction results in reduced damping.

- Although the correlations presented were obtained, most of the values differed from those predicted in the literature, where other pile types in temperate climate soils were studied. This result probably occurred due to the different installation procedures of the piles, the dimensions of their cross-sections, as well as differing soil properties and drainage conditions of the studied tropical soil.

6.1 RECOMENDATIONS

Due to the limitations of the methodology employed and the objectives that were not fully achieved, the following recommendations are necessary for future research:

- It was observed that the correlations resulted in a good fit for the loading phase of the pile but were deficient for the match in the unloading phase. Therefore, research can be conducted to investigate the soil's unloading quakes in the CAPWAP model.

- Determining the distribution of static resistance in the SLT through instrumentation at various depths (e.g., strain gauges). This would allow for a more accurate representation of resistance distribution in the CAPWAP model.

- Although the monitoring reports of CFA pile installation were used to determine the variation of the impedance of the analyzed piles, it is recommended to improve the accuracy of these measurements. The methodology employed was simplified, where only the cross-sectional area was related to the measured concrete pressure. This could be achieved using technologies that determine the pile profile at depth or through precise measurements of concrete consumption and pressure during CFA pile installation. References such as Pisciak & Likins (2004) are recommended for further reading.

- It is recommended to investigate q_s and J_s using a larger number of DLTs (a larger sample of piles). The methodology can be analogous to that presented in this dissertation, but with a larger number of piles in well-characterized sites that allow for the establishment of reliable correlations, applying a probabilistic treatment to the parameters of the CAPWAP model.

REFERENCES

- AGHAYARZADEH M., KHABBAZ H., FATAHI B., TERZAGHI S. (2020). Interpretation of dynamic pile load testing for open-ended tubular piles using finite-element method International Journal of Geomechanics. ASCE. Vol 20, Issue 2. [https://doi.org/10.1061/\(ASCE\)GM.1943-5622.0001564](https://doi.org/10.1061/(ASCE)GM.1943-5622.0001564)
- ALLIN, R. C., RAUSCHE, F., BRENT, R. R. (2021). Refined Prediction of End Bearing through Multi-Level High Strain Dynamic Measurements. Proceedings: IFCEE. ASCE. 314-329pp. <https://doi.org/10.1061/9780784483404.029>.
- NETO, J. A. A. (2002). A. Análise do desempenho de estacas hélice contínua e ômega – Aspectos executivos. Dissertação de Mestrado, Escola Politécnica, Universidade de São Paulo, SP, 187p.
- ALVAREZ, C., ZUCKERMAN, B., LEMKE, J. (2006) Dynamic Pile Analysis Using CAPWAP and Multiple Sensors. GEO Congress, Atlanta, GA.
- ALWALAN, M. F., EL NAGGAR, M. H. (2020). Analytical models of impact force-time response generated from high strain dynamic load test on driven and helical piles. Computers and Geotechnics. Vol. 128. <https://doi.org/10.1016/j.compgeo.2020.103834>
- ANDRAOS, N. C., KORMANN, A. C. M., ANTONIUTTI, L. N. (2009). Ensaio de carregamento dinâmico em estacas moldadas in loco: contribuições para a seleção do sistema de impacto e amortecimento. Engenharia de Fundações: Passado Recente e Perspectivas – Homenagem ao Prof. Nelson Aoki, São Carlos – SP, EESC-USP, pp. 17-26.
- AOKI, N. (1989). Prediction of the behavior of vertical driven pile and dynamic conditions. Proceedings, 12th International Conference on Soil Mechanics and Foundation Engineering, Rio de Janeiro, RJ, vol. 2, pp. 367-376.
- AOKI, N. (1997). Determinação da capacidade de carga última de estaca cravada em ensaio de carregamento dinâmico de energia crescente. Tese de doutorado, Escola de Engenharia, São Carlos – SP, 130 p.
- ASSOCIAÇÃO BRASILEIRA DE NORMAS TÉCNICAS (1989). NBR 10905: Solo – Ensaio de palheta in situ. Rio de Janeiro, 9p.
- ASSOCIAÇÃO BRASILEIRA DE NORMAS TÉCNICAS (2007). NBR 13208: Estacas – ensaio de carregamento dinâmico. Rio de Janeiro, 12p.
- ASSOCIAÇÃO BRASILEIRA DE NORMAS TÉCNICAS (2016). NBR 7180: Solo – Determinação do limite de plasticidade Rio de Janeiro, 3p.
- ASSOCIAÇÃO BRASILEIRA DE NORMAS TÉCNICAS (2016). NBR 7181: Solo – Análise granulométrica. Rio de Janeiro, 12p.
- ASSOCIAÇÃO BRASILEIRA DE NORMAS TÉCNICAS (2017). NBR 6459: Solo – Determinação do limite de liquidez. Rio de Janeiro, 5p.

- ASSOCIAÇÃO BRASILEIRA DE NORMAS TÉCNICAS (2020). NBR 16903: Solo — Prova de carga estática em fundação profunda. Rio de Janeiro, 11p.
- ASSOCIAÇÃO BRASILEIRA DE NORMAS TÉCNICAS (2020). NBR 6484: Solo — Sondagem de simples reconhecimento com SPT — Método de ensaio. Rio de Janeiro, 28p.
- ASSOCIAÇÃO BRASILEIRA DE NORMAS TÉCNICAS (2024). NBR 6457: Solos — Preparação de amostras para ensaios de compactação, caracterização e determinação do teor de umidade. Rio de Janeiro, 79p.
- AUTHIER, J., FELLENIUS, B.H. (1980). Quake values determined from dynamic measurements. Proceedings 1st International Conference on the Application of Stress-Wave Theory on Piles, Stockholm. A. A. Balkema, Rotterdam, pp. 197-216.
- BAHIA, R. B. C. (2009). Evolução tectonossedimentar da Bacia do Parecis – Amazônia. Tese de doutorado em Ciências Naturais - Universidade Federal de Ouro Preto. Ouro Preto, Minas Gerais.
- BERNARDES, G. P. (1989). Dynamic and Static Testing of Large Model Piles in Sand. Tese de Doutorado, Norwegian Institute of Technology, Noruega.
- BRIAUD, J. L., BALLOUZ, M., NASR, G. (2000). Static capacity prediction by dynamic methods for three bored piles. Journal of Geotechnical and Geoenvironmental Engineering, ASCE, EUA, vol. 126(7): 640-649.
- BRUNO, D., RANDOLPH, M. F. (1999). Dynamic and Static Load Testing of Model Piles Driven into Dense Sand. Journal of Geotechnical and Geoenvironmental Engineering. ASCE. [https://doi.org/10.1061/\(ASCE\)1090-0241\(1999\)125:11\(988\)](https://doi.org/10.1061/(ASCE)1090-0241(1999)125:11(988))
- CARVALHO, D., ALBUQUERQUE, P. J. R. (2023). Ensinando prova de carga estática em fundações: realização – interpretação – projeto - resultados. Campinas, São Paulo, Brasil, 512p.
- CINTRA, J. C. A., AOKI, N. (2010). Fundações por estacas: projeto geotécnico. São Paulo: Oficina de Textos.
- COYLE, H.M., BARTOSKEWITZ, R. E., BERGER, W. J. (1973). Bearing capacity by wave equation analysis – state of art. TX, USA: Texas Transportation Institute, Texas A&M University.
- COYLE, H.M., GIBSON, G. C. (1970). Empirical Damping Constants for Sands and Clays. ASCE. Journal of Soil Mechanics and Foundation Division.
- CUTRIM, A. O., LUZ, J. A. G., MIGLIORINI, R. B. (2021). Avaliação das vulnerabilidades natural, antrópica e total e perigo à contaminação do aquífero Utariti na cidade de Sinop (MT), usando os métodos VAN e POSH. Revista Geociências, vol. 40, n. 3, UNESP, São Paulo, p. 721-733.
- DANZIGER, B.R., COSTA, A.M., LOPES, F.R., PACHECO, M.P. (1996). A discussion on the uniqueness of CAPWAP type analyses. In Proceedings of the 5th International Congress on the Application of Stress-Wave Theory to Piles: Vol. 1. Miami: pp. 394-408.

- DÉCOURT, L. (1996). A ruptura de fundações avaliada com base no conceito de rigidez. In: Seminário de Engenharia de Fundações Especiais e Geotecnia, III SEFE, São Paulo. Anais. ABEF e ABMS, V.1, p. 215-224.
- DÉCOURT, L. (1998). Ruptura de fundações e coeficientes de segurança a luz do conceito de rigidez. In: Congresso Brasileiro de Mecânica dos Solos e Engenharia Geotécnica, XI COBRAMSEG. Brasília. Anais. ABMS, V. 3, p. 1599-1606.
- DÉCOURT, L. (2008). Provas de carga em estacas podem dizer muito mais do que têm dito. Seminário de Engenharia de Fundações Especiais e Geotecnia (SEFE) – VI. ABEF, São Paulo, pp 221-245.
- DÉCOURT, L., QUARESMA, A. R. (1978). Capacidade de carga de estacas a partir de valores SPT. In: CBMSEF, 6. Rio de Janeiro. Anais. V. 1, p. 45-53.
- FELLENIUS, B.H. (1988). Variation of CAPWAP results as a function of the operator. Proc. 3rd Int. Conf. on the Application of Stress-Wave Theory to Piles, Ottawa, pp. 814-825.
- FELLENIUS, H.B. (2023) Basics of Foundation Design. Electronic Edition (The Red Book), 548p.
- FLYNN, K. N., MCCABE, B. A. (2021). Driven cast-in-situ pile capacity: insights from dynamic and static load testing. Canadian Geotechnical Journal, Canada, 58(12): 1870-1883.
- FLYNN, K.N., MCCABE, B.A. (2019). Driven cast-in-situ piles installed using hydraulic hammers: installation energy transfer and driveability assessment. Soils and Foundations. vol 59. Issue 6. pp 1946–1959. <https://doi.org/10.1016/j.sandf.2019.09.003>
- GENEROSO, F. J. (2014). Análise de provas de carga dinâmica e estática em estacas hélice contínua monitoradas em solo residual jovem de gnaiss. Dissertação, Universidade Federal de Viçosa, Viçosa, Minas Gerais, 121p.
- GOBLE, G. G., RAUSCHE, F., (1976). Wave equation analysis of pile driving. WEAP program, Vol. 1 - Background, Vol. 2 - User's Manual, Vol. 3 - Program Documentation, US Department of Transportation, FHWA, Office of Research and Development, Washington, D.C. USA. 371p.
- GONÇALVES, C., ANDREO, C. S., BERNARDES, G. P. (1996). Ensaio de carregamento dinâmico. Estacas Benaton.
- GONÇALVES, G., ANDREO, C. S., BERNARDES, G. P., FORTUNATO, S.G.S. (2000). Controle de fundações profundas através de métodos dinâmicos. 1ª ed. São Paulo, 253p.
- GREEN, T. A. L., KIGHTLEY, M. L. (2005). CAPWAP testing-theory and application. In Proceedings of the International Conference on Soil Mechanics and Geotechnical Engineering. AA BALKEMA Publishers, 16(4): pp. 2115-2118.
- HANNIGAN, P. J., GOBLE, G. G., THENDEAN, G., LIKINS G. E., RAUSCHE, F. (1998). Design and construction of driven pile foundations. FHWA-HI-97-013, vol. II. Washington, D.C. USA: Federal Highway Administration, US Department of Transportation.

- HANNIGAN, P. J., WEBSTER, S. D. (1987). Comparison of static load test and dynamic pile testing results. Proceedings of the 2nd International Symposium. DFI. Luxembourg.
- HANNIGAN, P., RAUSCHE, F., LIKINS, G., ROBINSON, B., BECKER, M. (2016). Geotechnical circular No.12, design and construction of driven pile foundations. GEC 12: Report FHWA-NHI-16-010, vol. I and II. US Department of Transportation, FHWA, Washington D. C., USA.
- HUSSEIN, M., LIKINS, G. & RAUSCHE, F. (1996). Selection of a hammer for high-strain dynamic testing of cast-in-place shafts. In: International Conference Application Of Stress-Wave Theory To Piles, Orlando, EUA, 5:759-772.
- HUSSEIN, M., MUKADDAM, M. (1994). Evaluation of cast-in-place concrete piles from stress wave measurements. Proceedings of the 2nd Geotechnical Engineering Conference, Cairo, Egypt. 13p.
- ISLAM, M. S., KAM, N., WULFF, S. S. (2022). Improved Wave Equation Analysis of Steel H-Piles in Shales Considering LRFD and Economic Impact Studies. Journal of Bridge Engineering. vol 27. ASCE. [https://doi.org/10.1061/\(ASCE\)BE.1943-5592.0001879](https://doi.org/10.1061/(ASCE)BE.1943-5592.0001879)
- KNECHTEL, R. (2015). Study of the physical and chemical quality of Sinop/MT groundwater. Master's Degree Dissertation in Water Resources – Exact and Earth Sciences Institute, Mato Grosso Federal University (UFMT). Cuiabá. Brazil.
- KUEI K. C., DEJONG J. T., GHAFGHAZI M. (2020) Prediction, Performance, and Uncertainty in Dynamic Pile Load Testing as Informed by Direct Measurements from an Instrumented Becker Penetration Test. Journal of Geotechnical and Geoenvironmental Engineering. vol: 146. n: 8, [https://doi.org/10.1061/\(ASCE\)GT.1943-5606.0002290](https://doi.org/10.1061/(ASCE)GT.1943-5606.0002290).
- LIKINS, G. (2015). Pile Testing – State of the Art, 8th Seminar on Special Foundations Engineering and Geotechnics, Sao Paulo, Brazil: 17p.
- LIKINS, G. E., RAUSCHE, F. (2000). Dynamic load testing of augered cast-in-place piles. Deep Foundations Institute, EUA: 9p.
- LIKINS, G. E., RAUSCHE, F., DIMAGGIO, J., TEFERRA, W. (1992). A solution for high damping constants in sands. 4th International Conference on the Application of Stress-wave Theory to Piles. The Netherlands. p. 117-120.
- LIKINS, G., RAUSCHE, F. (2004). Correlation of CAPWAP with static load tests. Proceedings of the Seventh International Conference on the Application of Stress Wave Theory to Piles, Selangor, Malaysia, pp 153-165.
- LIKINS, G., RAUSCHE, F. (2008). What constitutes a good PDA test? Proceedings of the Eighth International Conference on the Application of Stress-Wave Theory to Piles, Lisbon, Portugal, pp 403-407.
- LIKINS, G.E. (1983). Pile Installation Difficulties in Soils with Large Quakes. Dynamic Measurement of Piles and Piers, ASCE Spring Convention. Philadelphia, PA.

- LIMA, F. M. A. (1999). Análise de prova de carga dinâmica em estacas metálicas do tipo trilho. Dissertação de Mestrado, Escola de Engenharia de São Carlos, Departamento de Geotecnia, Universidade de São Paulo, São Carlos, SP, 160p.
- LUSSI, C. Avaliação hidrogeológica do sistema aquífero Parecis na cidade de Sinop – MT e seu entorno. (2013). Dissertação de mestrado em Geologia, UFMT, Cuiabá, Mato Grosso, Brasil.
- MARCHEZINI, S. F. (2013). Comparação entre Métodos Estáticos e Dinâmicos de Previsão de Capacidade de Carga em Estacas Assentes em Solo Tropical. Dissertação de Mestrado, Publicação Departamento de Engenharia Civil, Universidade de Brasília, Brasília, DF, 171p.
- MARTIM, C. C., ZAMADEI, T., SOUZA, A. P., ALMEIRDA, F. T., ZOLIN, C. A. (2020). Coeficientes de Angström-Prescott e a evapotranspiração de referência na transição Cerrado-Amazônia do Mato Grosso. Revista Brasileira de Climatologia, vol. 26, Brazil, 16p.
- MELO, B. N. (2019). Análise de provas de carga à compressão à luz do conceito de rigidez. Dissertação de mestrado. Universidade Estadual de Campinas. Faculdade de Engenharia Civil, Arquitetura e Urbanismo, Campinas, São Paulo, Brasil, 282p.
- MELO, N. P., FRANCO, M. S. M. (1980). Geologia, Pedologia, Vegetação e Uso Potencial da Terra. Folha Juruena, SC. 21. Cuiabá - In: DNPM. Projeto RADAMBRASIL, Rio de Janeiro – RJ. 456 pp.
- MIRANDA, L.; AMORIM L. (2000). Mato Grosso: atlas geográficos. Cuiabá: Entrelinhas.
- MOTA, N. M. B. (2003). Ensaios Avançados de Campo na Argila Porosa Não Saturada de Brasília: Interpretação e Aplicação em Projetos de Fundação. Tese de Doutorado, Publicação G.TD-013A/03, Departamento de Engenharia Civil e Ambiental, Universidade de Brasília, Brasília, DF, 335 p.
- MURAKAMI, D. K. (2015). Novo procedimento para a realização de análise CAPWAP no ensaio de carregamento dinâmico em estacas pré-moldadas. Dissertação de Mestrado em Engenharia Geotécnica, Escola Politécnica, USP, São Paulo. <https://doi:10.11606/D.3.2016.tde-17062016-144914>
- MURAKAMI, D. K., CORGNIER, F., GODINHO, H., SAITO, E. (2022). On the use of wave equation analysis for the hammer selection to install and perform the dynamic test in piles. XX Congresso Brasileiro de Mecânica dos Solos e Engenharia Geotécnica (COBRAMSEG), ABMS, Campinas, Brasil, 7p.
- MURAKAMI, D. K., MASSAD, F. (2016). Determinação do quake de estacas pré-moldadas de concreto através de provas de carga estática e ensaios de carregamento dinâmico. Geotecnia, 137, 79-98. <https://doi.org/10.24849/j.geot.2016.137.05>
- MURAKAMI, D., MASSAD, F. (2014). Determinação do Quake do Fuste de Estacas Pré-Moldadas Através de Provas de Carga Estática e Ensaio de Carregamento Dinâmico. XVII COBRAMSEG, Goiânia.

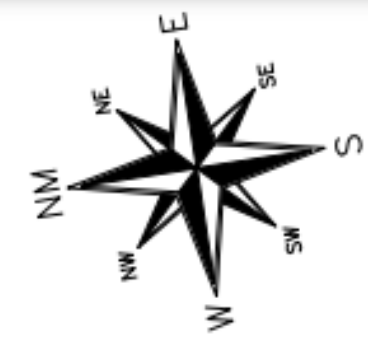
- NG, K. W., SRITHARAN, S. (2013). Improving dynamic soil parameters and advancing the pile signal-matching technique. *Computers and Geotechnics*. vol 54. 166-174pp. <https://doi.org/10.1016/j.compgeo.2013.07.007>
- PEREIRA, J. J. G., SANTOS, J. A., CORREIA, A. G. & SIMÕES, T. N. (2009). Ensaio de carregamento dinâmico – um caso de estudo sobre estacas moldadas. *Geotecnia*, vol. 115: 21-43.
- PILE DYNAMICS, I. (2014). Case Pile Wave Analysis Program, CAPWAP Manual, PDI Inc., Cleveland, OH, EUA: 87p.
- PISCSALKO, G., LIKINS, G. (2004). Automated Inspection Control of Augercast Piles. Proceedings from the 83rd Annual Transportation Research Board Meeting. Washington, D.C. USA. 16p.
- POULOS, H. G. (2017). Tall Building Foundation Design (1st ed.). CRC Press. <https://doi.org/10.1201/9781315156071>
- QUERELLI, A. E. (2019). Monitoração dinâmica na cravação de estacas: aplicabilidade da equação de Energy Approach e estimativas das tensões de compressão. Dissertação de Mestrado. Escola Politécnica, USP, São Paulo: 383p.
- RANDOLPH, M. F., DEEKS A. J. (1992). Dynamic and static soil models for axial response. In: Proceedings of the 4th International Conference on the Application of Stress Wave Theory to Piles. The Hague. p. 3–14.
- RANDOLPH, M. F., WROTH, C. P. (1978). Analysis of deformation of vertically loaded piles. *Journal of the Geotechnical Engineering Division*. ASCE. 1465–88. <https://doi.org/10.1061/AJGEB6.0000729>
- RAUSCHE, F. (1989). CAPWAP capabilities and bored pile testing. PDA Users Day, Pile Dynamics, Inc., Cleveland, OH. USA. 17p.
- RAUSCHE, F. (1997). Hammer design for drilled shaft testing: two case studies. PDA Users Day, EUA: 14p.
- RAUSCHE, F. (2018). Combining static and dynamic loading test results of piles. Symposium: 10th International Conference on Stress Wave Theory and Testing of Deep Foundations. San Diego, USA, 24p.
- RAUSCHE, F., HANNIGAN, P., ALVAREZ, C. (2018). Soil damping and rate dependent soil strength changes due to impact and rapid loads on deep foundations. Symposium: Tenth International Conference on Stress Wave Theory and Testing of Deep Foundations, San Diego, USA.
- RAUSCHE, F., LIKINS, G., LIANG, L., HUSSEIN, M. (2010). Static and dynamic models for CAPWAP signal-matching. *The Art of Foundation Engineering Practice*, Geotechnical Special Publication No. 198, Reston, VA, USA, pp 534-553.
- RAUSCHE, F., LIKINS, G., MIYASAKA, T. & BULLOCK, P. (2008). The effect of ram mass on pile stresses and pile penetration. In: International Conference Application Of Stress-Wave Theory To Piles, Lisboa, Portugal: 389-394.

- RAUSCHE, F., NAGY, M., WEBSTER, S., LIANG, L. (2009). CAPWAP and refined wave equation analyses for driveability predictions and capacity assessment of offshore pile installations. Proceedings of the ASME 28th International Conference on Ocean, Offshore and Arctic Engineering, Honolulu, Hawaii, 9p.
- RAUSCHE, F., ROBINSON, B., LIKINS, G. (2004). Economy, benefits and limitations of ndt for augered-cast-in-place-piles. Proceedings from the 83rd Annual Transportation Research Board Meeting, Washington, D.C. USA. 18p.
- RAUSCHE, F., SEIDEL, J. (1984). Design and Performance of Dynamic Tests of Large Diameter Drilled Shafts. 2nd International Conference on the Application of Stress Wave Theory on Piles: Stockholm, Sweden; 9-16.
- RIBEIRO, D. B. S. Avaliação Hidrogeológica na Cidade de Sinop, MT. (2009). Trabalho de Conclusão de Curso de Geologia, UFMT, Cuiabá, Mato Grosso, Brasil.
- SAKR, M. (2013). Comparison between high strain dynamic and static load tests of helical piles in cohesive soils. Soil Dynamics and Earthquake Engineering. vol 54. pp 20-30 <https://doi.org/10.1016/j.soildyn.2013.07.010>.
- SEPLAN-MT. (2007). Secretaria de Estado de Planejamento e Coordenação Geral. Mato Grosso: Solos e Paisagens. Cuiabá: entrelinhas, 272p.
- SILVA, C.M. (2011). Energia e Confiabilidade Aplicadas aos Estaqueamentos Tipo Hélice Contínua. Tese de Doutorado, Publicação G.TD - 070/11, Departamento de Engenharia Civil e Ambiental, Universidade de Brasília, Brasília, DF, 311p.
- SMITH, E. A. L. (1960). Pile-driving analysis by the wave equation, Journal of the Soil Mechanics and Foundation Division, ASCE, EUA, vol. SM 4, pp. 35-61.
- SOUZA, G. G., ALBUQUERQUE, P. J. R. (2016). Avaliação do emprego de prova de carga estática e ensaio de carregamento dinâmico em estacas tipo hélice contínua. XVIII Congresso Brasileiro de Mecânica dos Solos e Engenharia Geotécnica (COBRAMSEG), ABMS, Belo Horizonte, Brasil, 8p.
- SOUZA, T. J., QUERELLI, A., CRUZ, F. V. A., TREJO, P.C. (2021). Use of the dynamic load test to obtain the pile capacity - The Brazilian Experience. DYNA, 88(217), pp. 169-177. <https://doi.org/10.15446/dyna.v88n217.93416>
- THOMPSON, C., GOBLE, G. (1988). High case damping constants in sand. Third International Conference on the Application of Stress-Wave Theory to Piles. Ottawa. Canada, pp 555-564.
- TU, Y., EL NAGGAR, M.H., WANG, K., RIZVI, S. M. F, QIU X. Dynamic multi-point method for evaluating the pile compressive capacity, Soil Dynamics and Earthquake Engineering, vol. 159, ISSN 0267-7261, <https://doi.org/10.1016/j.soildyn.2022.107317>
- VELLOSO, D. A., LOPES, F.R (2011). Fundações: volume completo. 1ª ed. Oficina de Textos, São Paulo, 568p.

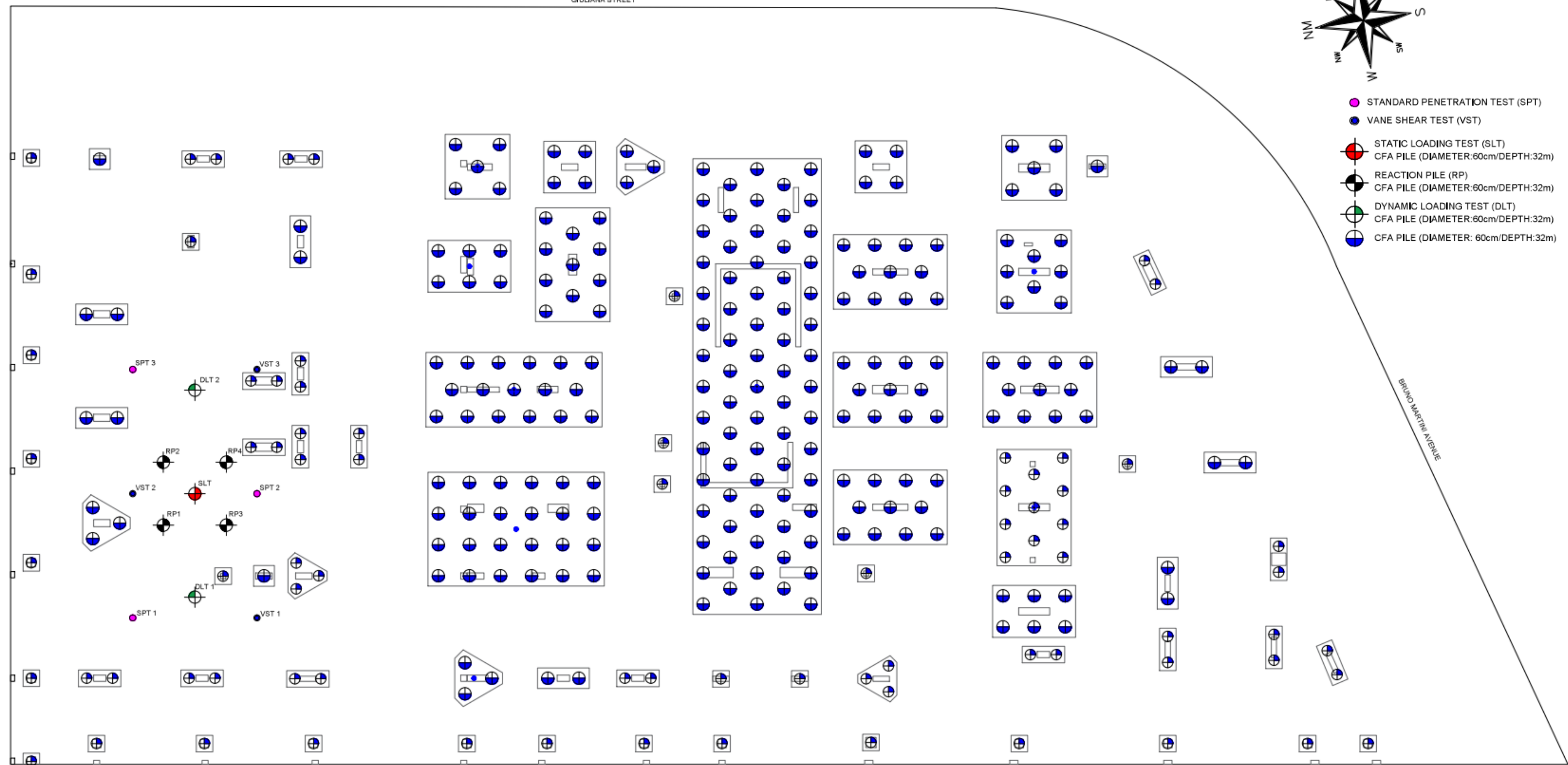
Appendix A

SITE A

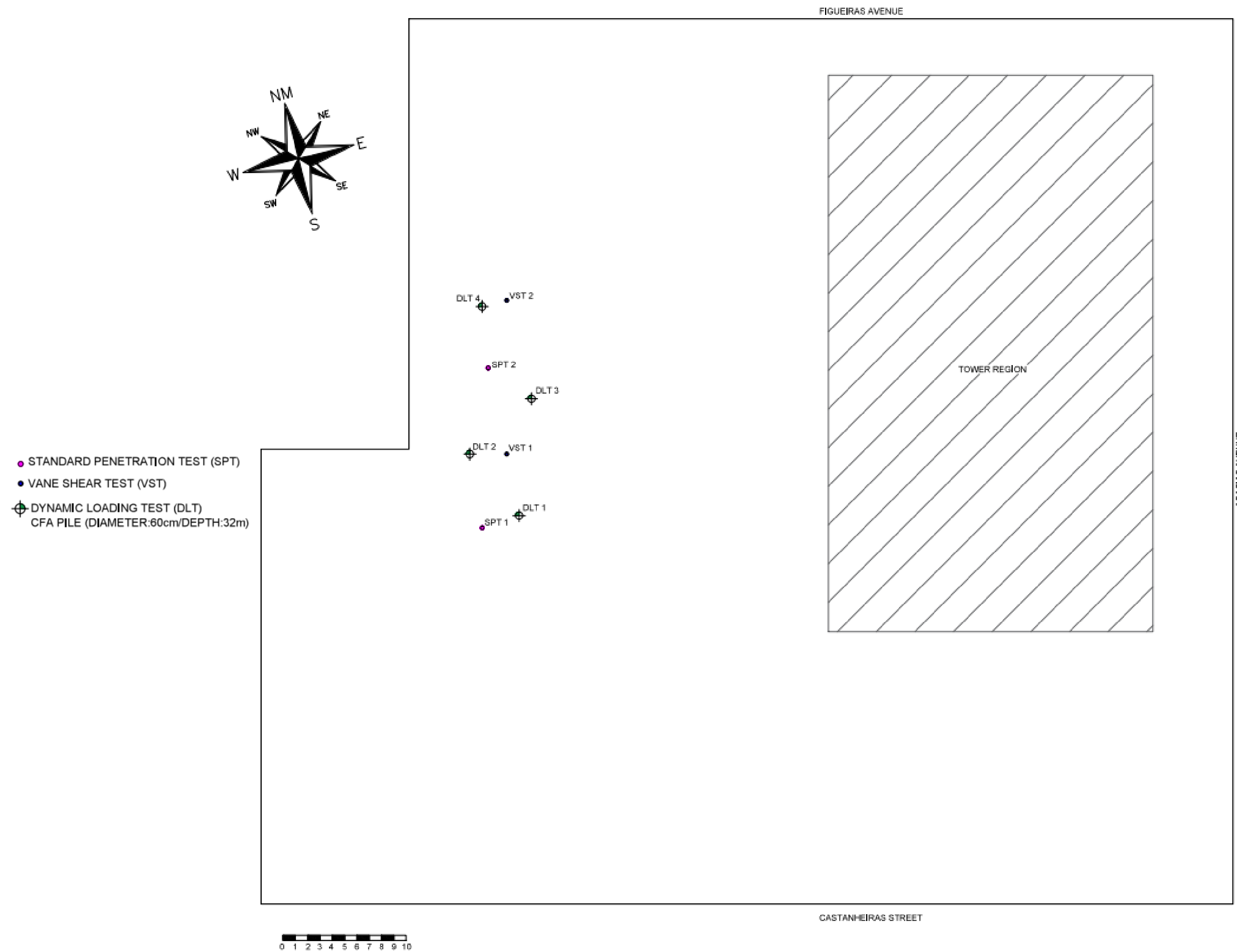
GIULIANA STREET



- STANDARD PENETRATION TEST (SPT)
- VANE SHEAR TEST (VST)
- STATIC LOADING TEST (SLT)
CFA PILE (DIAMETER:60cm/DEPTH:32m)
- REACTION PILE (RP)
CFA PILE (DIAMETER:60cm/DEPTH:32m)
- DYNAMIC LOADING TEST (DLT)
CFA PILE (DIAMETER:60cm/DEPTH:32m)
- CFA PILE (DIAMETER: 60cm/DEPTH:32m)



SITE B



Appendix B

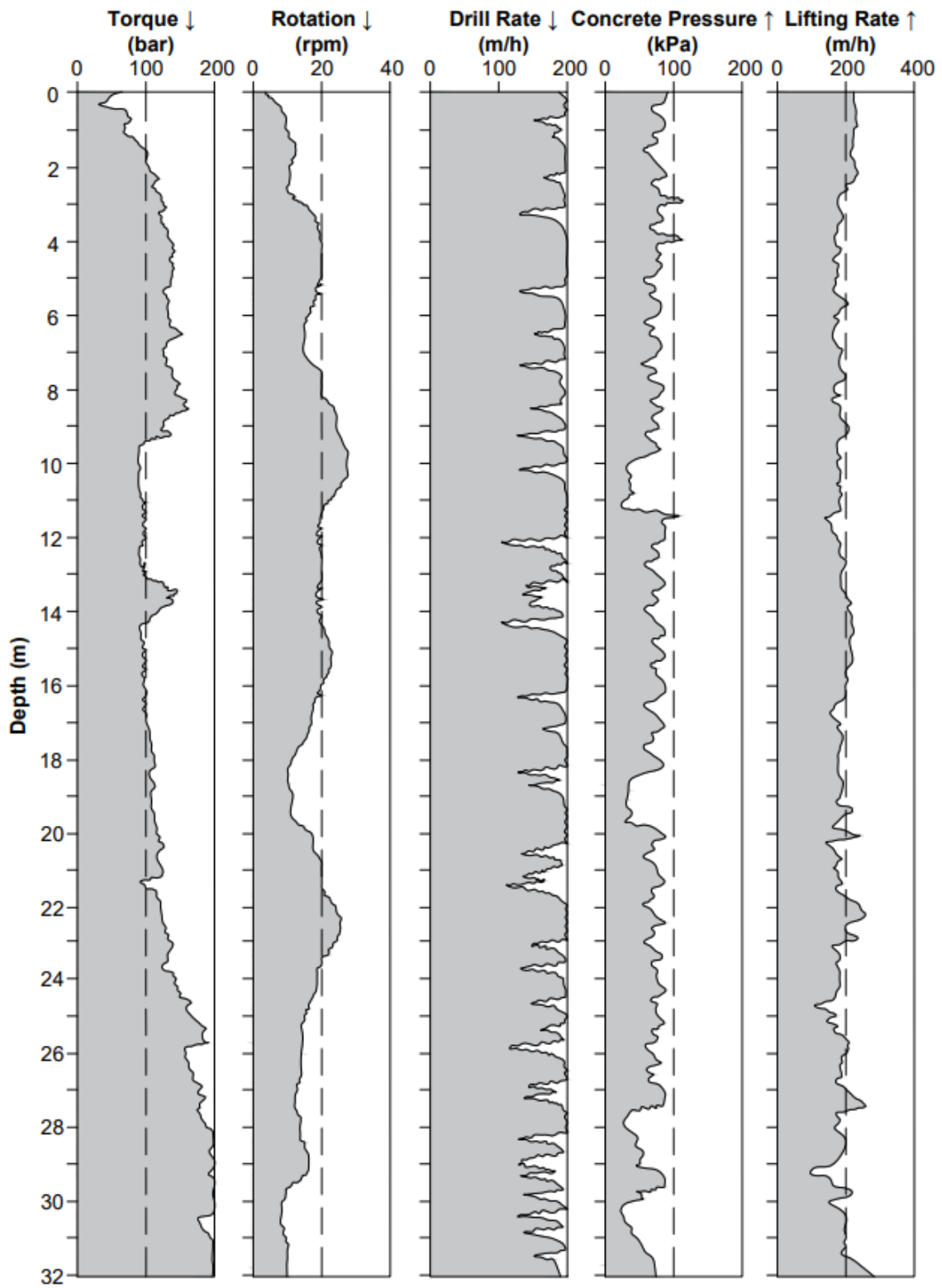


Figure B.0.1: Pile monitoring record for SLT pile – Site A.

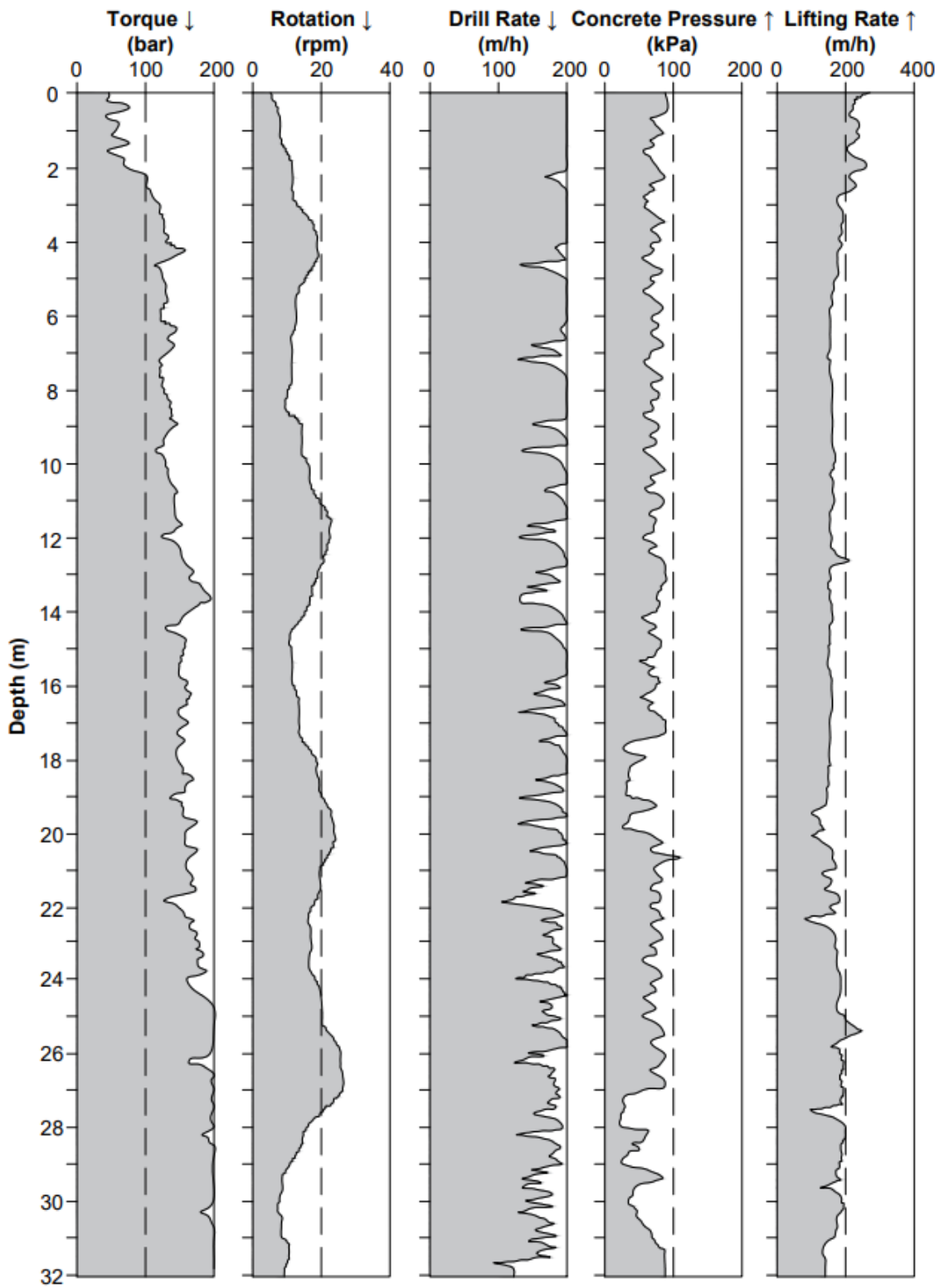


Figure B.0.2: Pile monitoring record for DLT 1A.

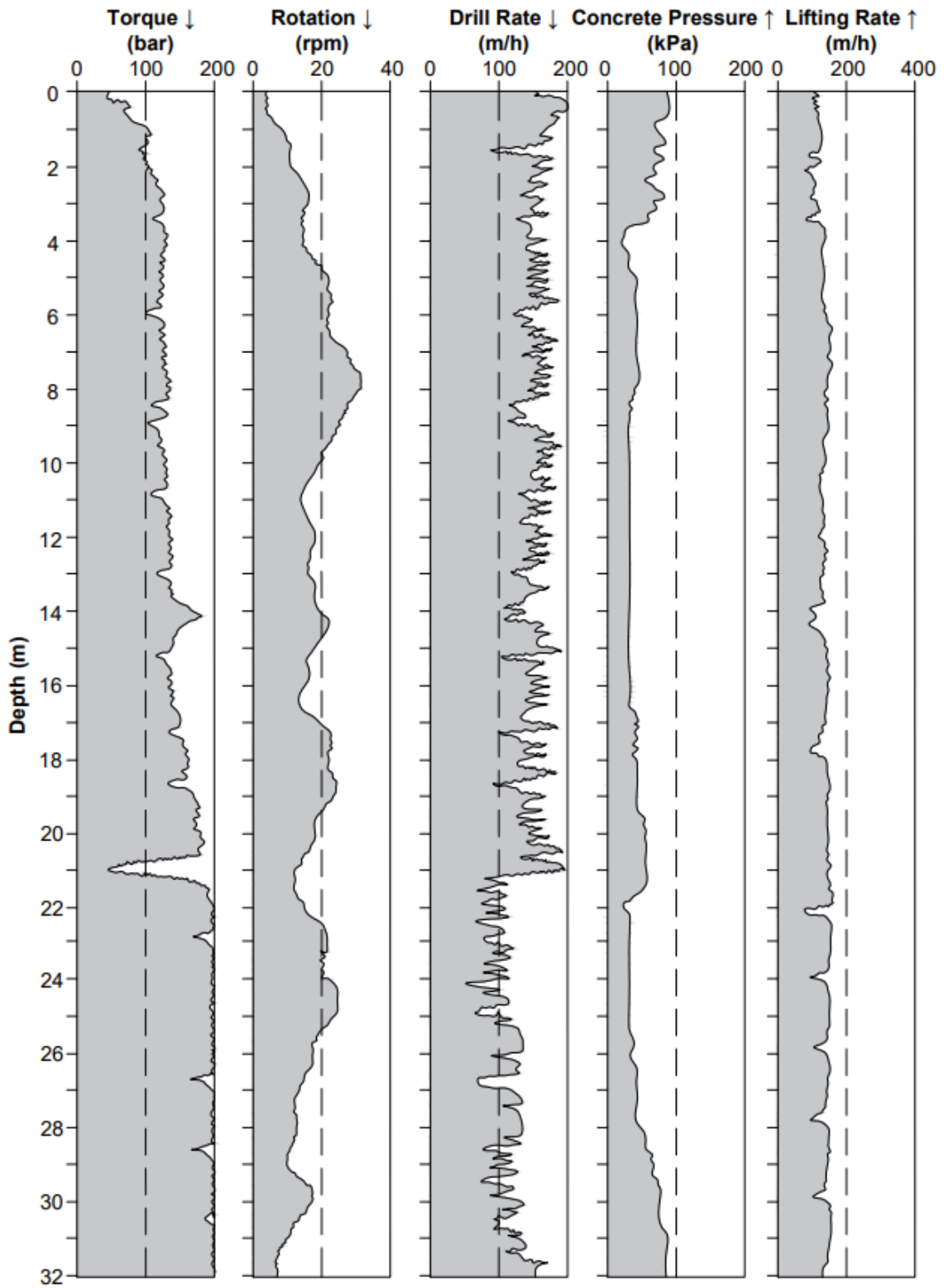


Figure B.0.3: Pile monitoring record for DLT 2A.

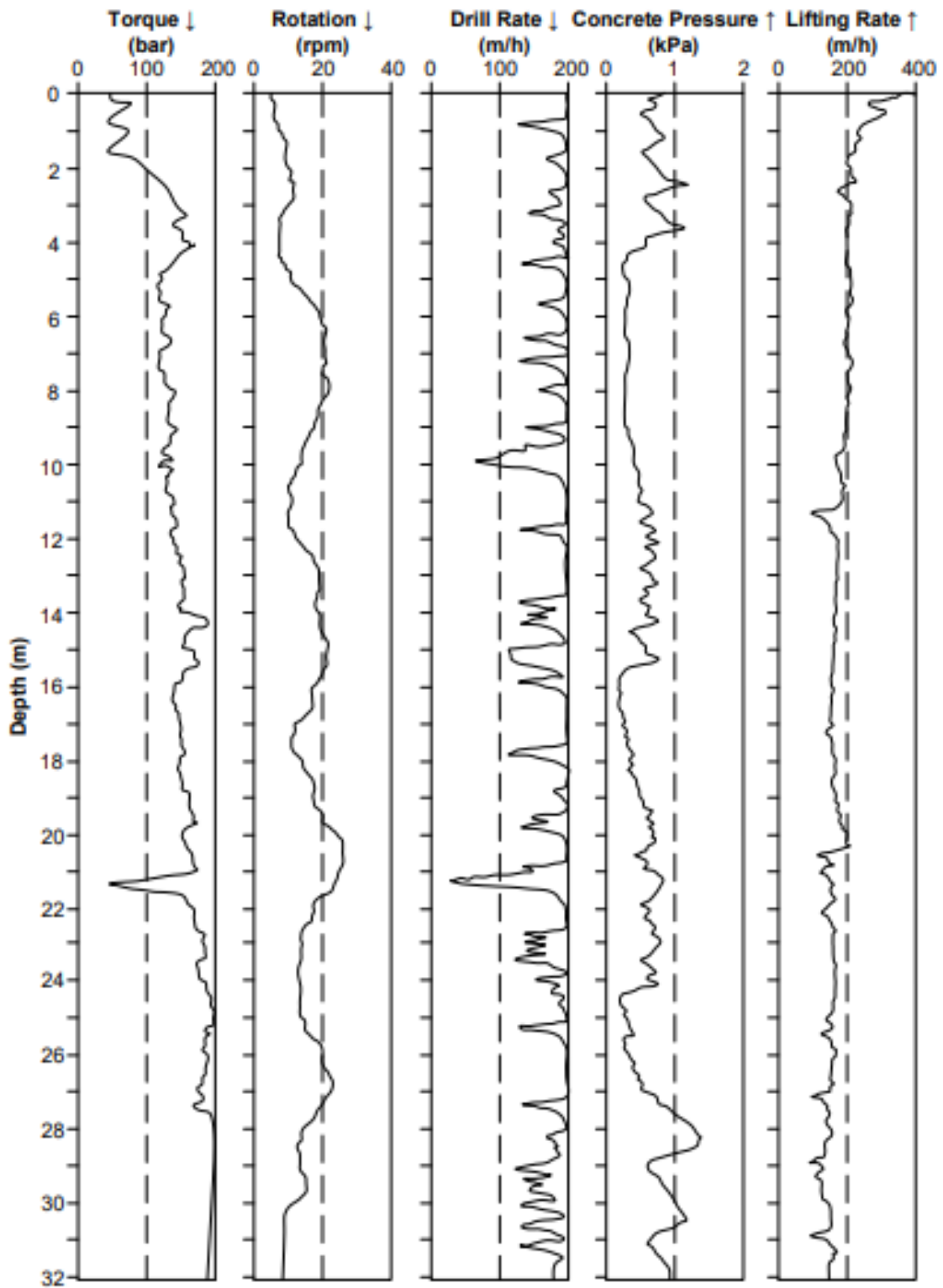


Figure B.0.4: Pile monitoring record for DLT 1B.

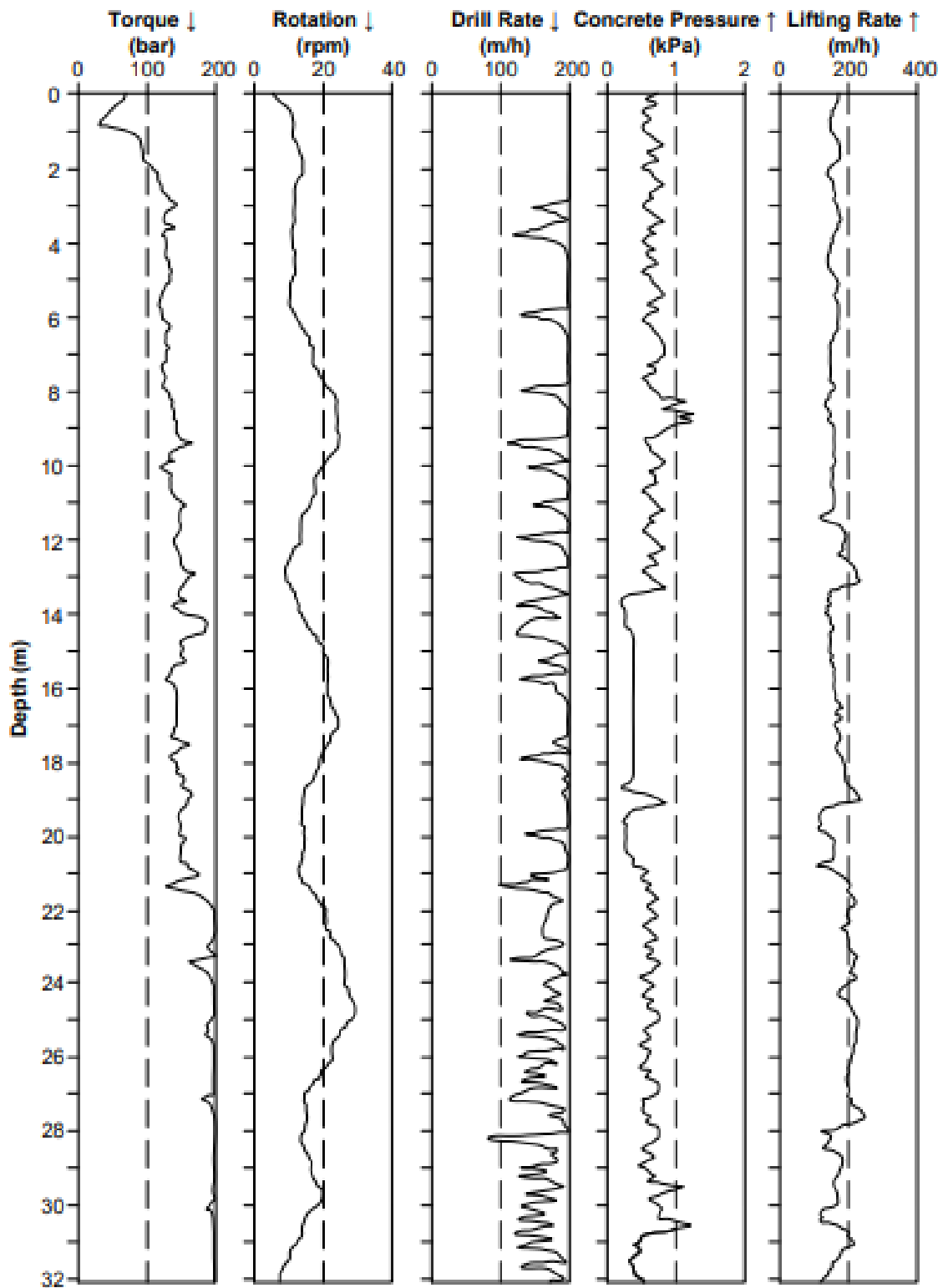


Figure B.0.5: Pile monitoring record for DLT 2B.

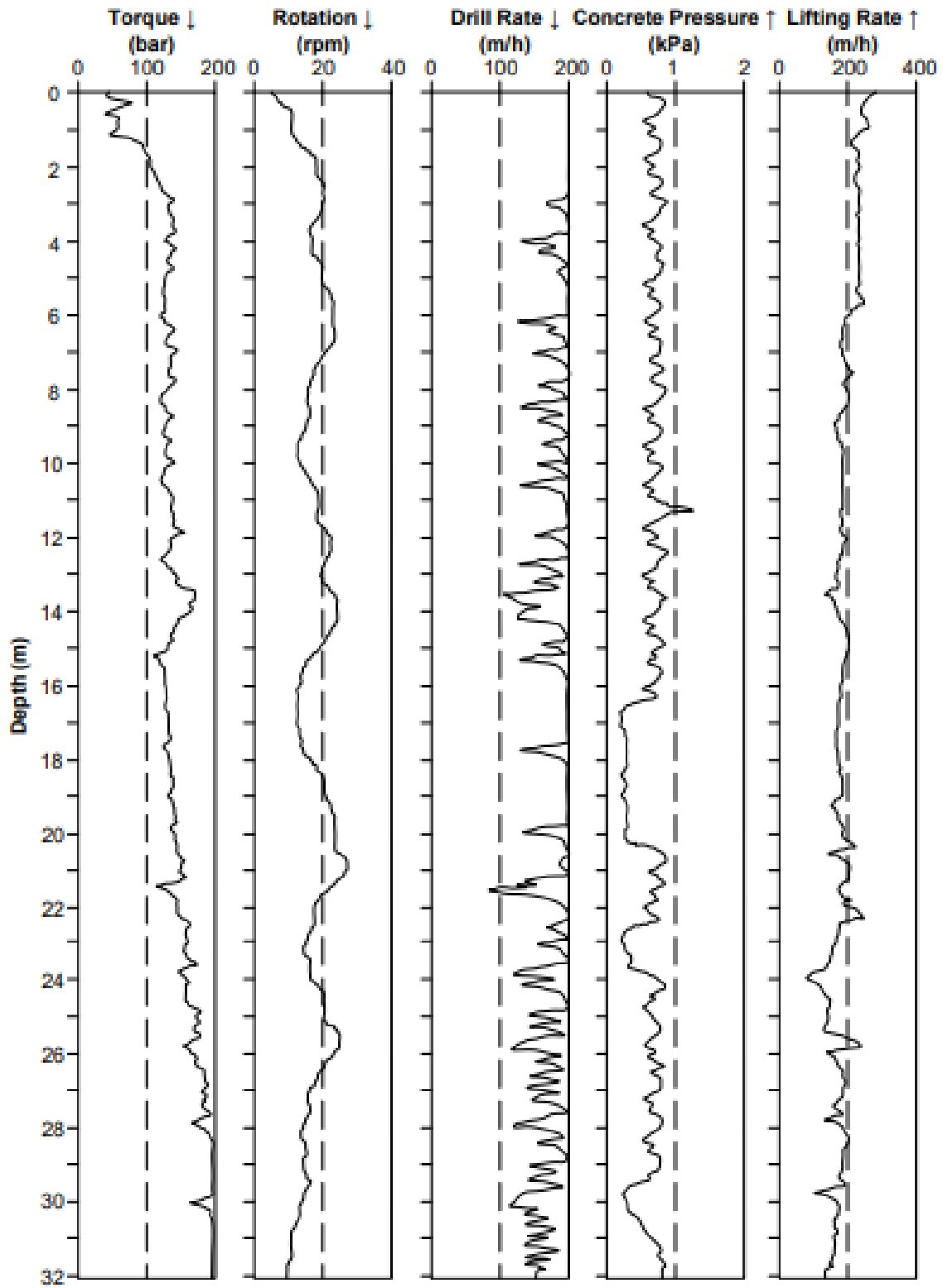


Figure B.0.6: Pile monitoring record for DLT 3B.

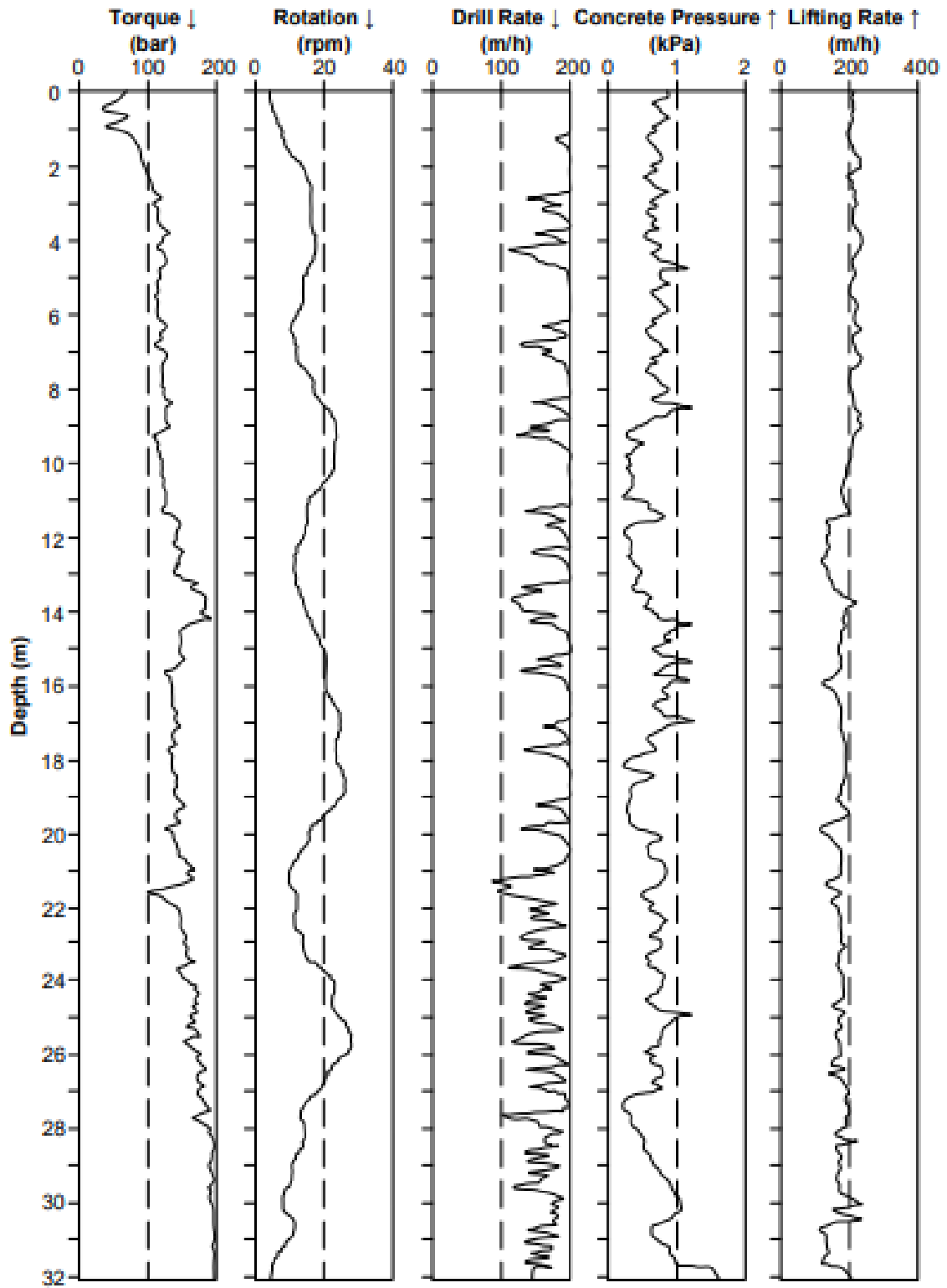


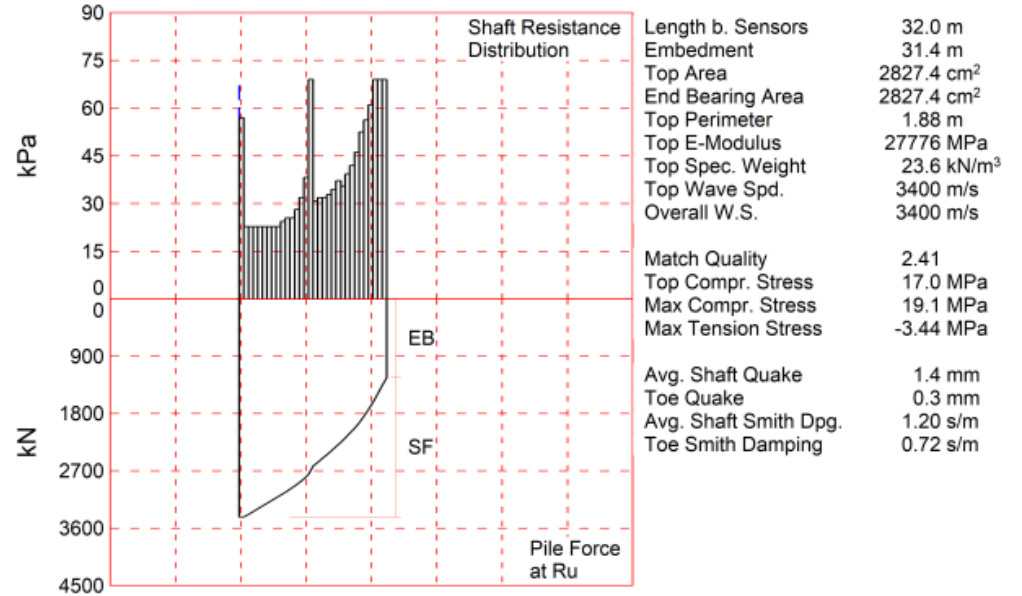
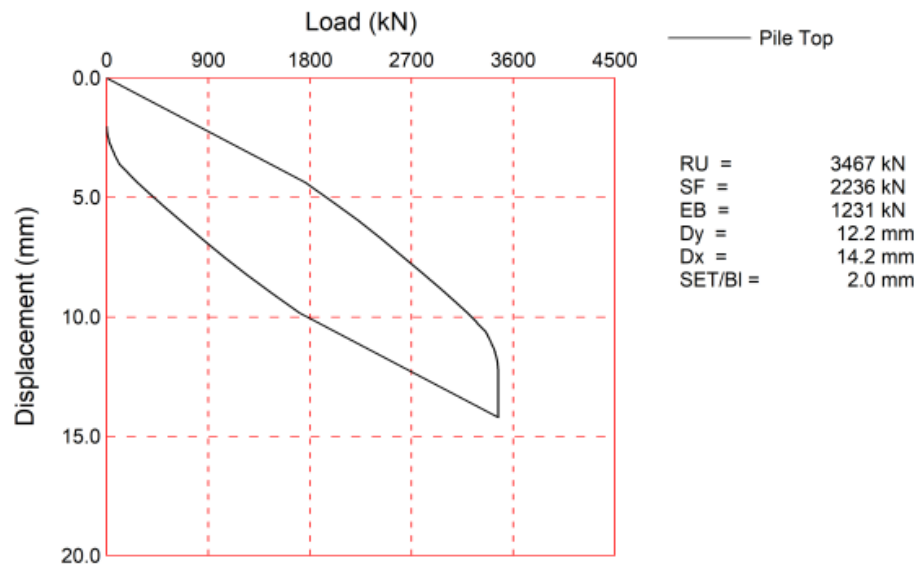
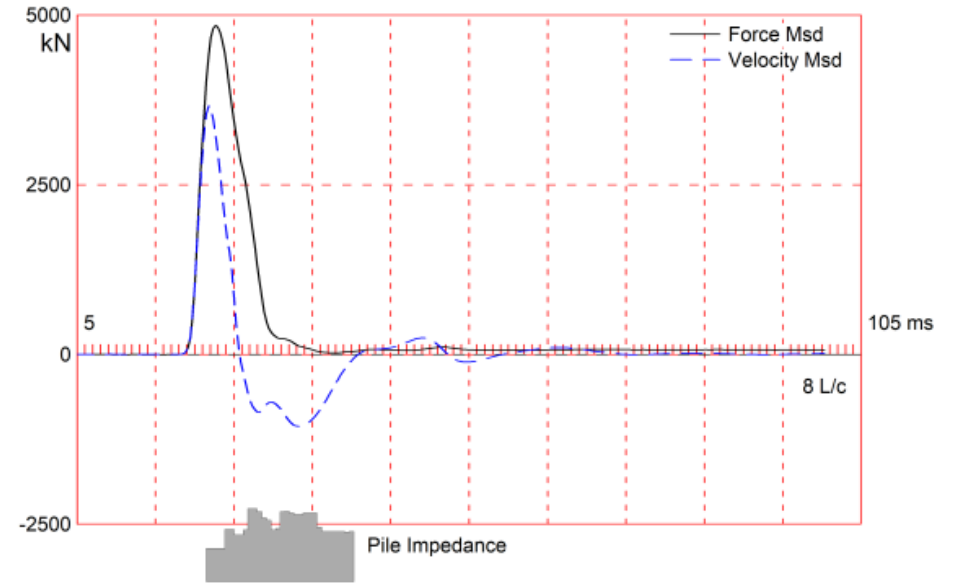
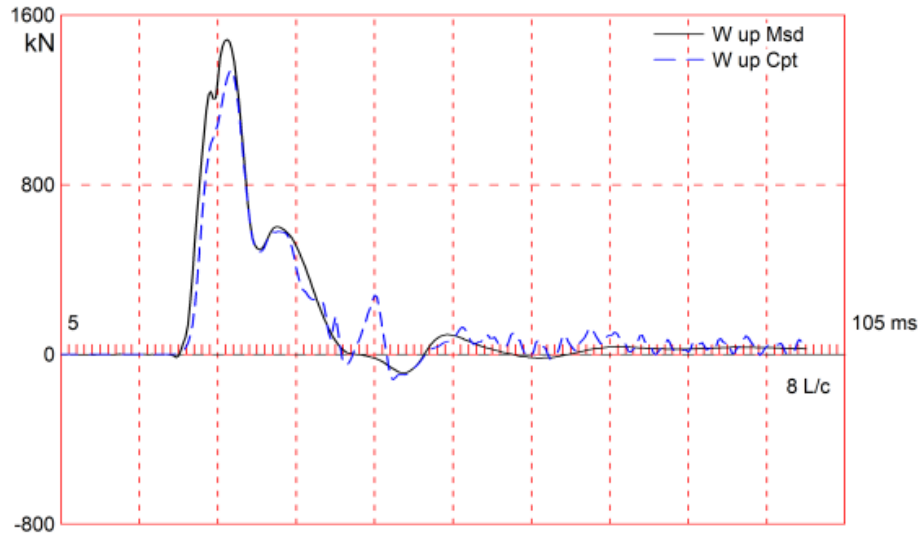
Figure B.0.7: Pile monitoring record for DLT 4B.

Appendix C

FIELD REPORT - STATIC LOAD TEST - NBR 16903 (ABNT, 2020)												
	City		Sinop, Mato Grosso, Brazil							Diameter (cm)		60
	Pile Type		Continuous Flight Auger (CFA)							Service Load (kN)		1470
	Length (m)		32							Maximum Load (kN)		2940
Load (kN)	Deflectometer	Time (minutes)										
		5	10	15	30	45	60	75	90	105	120	720
Displacement (mm)												
294	1	0.32	0.32	0.34	0.34	0.39	0.46	0.51	0.61	0.62		
	2	0.25	0.27	0.30	0.36	0.40	0.46	0.51	0.60	0.60		
	3	0.24	0.25	0.26	0.26	0.27	0.32	0.36	0.44	0.45		
	4	0.21	0.24	0.26	0.31	0.35	0.40	0.45	0.52	0.52		
588	1	1.11	1.13	1.14	1.24	1.31	1.34					
	2	1.00	1.03	1.04	1.11	1.17	1.20					
	3	0.86	0.87	0.88	0.95	1.00	1.02					
	4	0.78	0.80	0.81	0.87	0.93	0.96					
882	1	2.11	2.18	2.22	2.24							
	2	1.86	1.91	1.93	1.96							
	3	1.70	1.76	1.77	1.77							
	4	1.47	1.53	1.54	1.56							
1176	1	3.64	3.73	3.79	3.82							
	2	3.07	3.17	3.20	3.23							
	3	2.89	2.97	3.00	2.99							
	4	2.36	2.44	2.47	2.49							
1470	1	6.09	6.22	6.38	6.53							
	2	5.41	5.51	5.71	5.80							
	3	5.09	5.20	5.36	5.44							
	4	4.42	4.51	4.65	4.72							
1764	1	10.82	10.87	11.33	11.62	11.86	12.01					
	2	9.75	9.78	10.17	10.50	10.63	10.84					
	3	9.39	7.41	9.80	10.05	10.30	10.43					
	4	8.33	8.35	8.75	9.61	9.21	9.31					
2058	1	15.47	16.48	16.67	16.82							
	2	13.98	14.89	15.02	15.18							
	3	13.58	14.56	14.72	14.87							
	4	12.25	13.09	13.25	13.39							
2352	1	22.54	23.07	23.74	23.84							
	2	20.55	20.98	21.51	21.61							
	3	20.22	20.62	21.21	21.24							
	4	19.31	18.67	19.16	19.16							
2646	1	28.90	30.16	30.34	31.17	31.56	31.63					
	2	26.30	27.45	27.62	28.36	28.81	28.65					
	3	26.04	27.10	27.26	28.04	28.31	28.36					
	4	21.45	24.33	24.40	25.08	25.28	28.31					
2940	1	28.90	40.19	41.07	42.52						43.52	
	2	33.50	36.39	37.17	38.36						38.98	
	3	32.33	36.19	36.14	38.23						38.80	
	4	31.40	32.11	32.74	33.72						34.03	
2352	1	42.75	42.74	42.74								
	2	38.55	38.53	38.53								
	3	38.40	38.40	38.40								
	4	33.90	33.90	33.90								
1764	1	42.51	42.50	42.49								
	2	38.48	38.46	38.15								
	3	38.24	38.21	38.21								
	4	33.58	33.57	33.50								
1176	1	41.73	41.72	41.71								
	2	37.62	37.60	37.59								
	3	37.10	37.10	37.10								
	4	32.56	32.55	32.55								
588	1	39.17	39.17	39.16								
	2	35.23	35.22	35.22								
	3	34.31	34.30	34.28								
	4	30.32	30.30	30.30								
0	1				31.86							
	2				29.47							
	3				28.34							
	4				26.05							

Figure C.0.1: SLT field report - Site A.

Appendix D



CAPWAP SUMMARY RESULTS

Total CAPWAP Capacity: 3466.5; along Shaft 2236.0; at Toe 1230.5 kN

Soil Sgmt No.	Dist. Below Gages m	Depth Below Grade m	Ru kN	Force in Pile kN	Sum of Ru kN	Unit Resist. (Depth) kN/m	Unit Resist. (Area) kPa	Smith Damping Factor s/m	Quake mm
				3466.5					
1	1.0	0.4	43.0	3423.5	43.0	107.50	57.03	1.41	5.9
2	2.0	1.4	43.0	3380.5	86.0	43.00	22.81	1.41	5.3
3	3.0	2.4	43.0	3337.5	129.0	43.00	22.81	1.41	3.4
4	4.0	3.4	43.0	3294.5	172.0	43.00	22.81	1.41	2.9
5	5.0	4.4	43.0	3251.5	215.0	43.00	22.81	0.61	2.8
6	6.0	5.4	43.0	3208.5	258.0	43.00	22.81	0.50	3.4
7	7.0	6.4	43.0	3165.5	301.0	43.00	22.81	0.96	0.0
8	8.0	7.4	43.0	3122.5	344.0	43.00	22.81	0.96	0.1
9	9.0	8.4	43.0	3079.5	387.0	43.00	22.81	0.96	1.8
10	10.0	9.4	46.0	3033.5	433.0	46.00	24.40	0.93	2.3
11	11.0	10.4	48.0	2985.5	481.0	48.00	25.46	0.91	3.0
12	12.0	11.4	48.0	2937.5	529.0	48.00	25.46	0.91	2.7
13	13.0	12.4	53.0	2884.5	582.0	53.00	28.12	0.87	4.0
14	14.0	13.4	60.0	2824.5	642.0	60.00	31.83	0.83	3.5
15	15.0	14.4	72.0	2752.5	714.0	72.00	38.20	0.77	2.8
16	16.0	15.4	130.0	2622.5	844.0	130.00	68.97	0.65	3.6
17	17.0	16.4	58.0	2564.5	902.0	58.00	30.77	0.50	1.8
18	18.0	17.4	60.0	2504.5	962.0	60.00	31.83	0.50	1.7
19	19.0	18.4	60.0	2444.5	1022.0	60.00	31.83	2.95	0.1
20	20.0	19.4	62.0	2382.5	1084.0	62.00	32.89	2.98	0.2
21	21.0	20.4	65.0	2317.5	1149.0	65.00	34.48	2.78	0.0
22	22.0	21.4	70.0	2247.5	1219.0	70.00	37.14	2.60	0.1
23	23.0	22.4	67.0	2180.5	1286.0	67.00	35.54	2.84	0.1
24	24.0	23.4	74.0	2106.5	1360.0	74.00	39.26	2.62	0.1
25	25.0	24.4	79.0	2027.5	1439.0	79.00	41.91	2.49	0.0
26	26.0	25.4	87.0	1940.5	1526.0	87.00	46.15	2.21	0.0
27	27.0	26.4	99.0	1841.5	1625.0	99.00	52.52	0.50	0.1
28	28.0	27.4	106.0	1735.5	1731.0	106.00	56.23	0.50	0.0
29	29.0	28.4	115.0	1620.5	1846.0	115.00	61.01	0.50	1.3
30	30.0	29.4	130.0	1490.5	1976.0	130.00	68.97	0.50	0.0
31	31.0	30.4	130.0	1360.5	2106.0	130.00	68.97	0.50	0.4
32	32.0	31.4	130.0	1230.5	2236.0	130.00	68.97	0.50	1.2
Avg. Shaft			69.9			71.21	37.78	1.20	1.4
Toe			1230.5				4352.01	0.72	0.3

Soil Model Parameters/Extensions

	Shaft	Toe
Case Damping Factor	1.17	0.39
Damping Type	Viscous	Sm+Visc
Reloading Level	100	100
Unloading Level	91	

CAPWAP match quality = 2.41 (Wave Up Match) ; RSA = 0
Observed: Final Set = 2.0 mm; Blow Count = 490 b/m
Computed: Final Set = 2.3 mm; Blow Count = 432 b/m

Transducer F1 (Y286) CAL: 91.0; RF: 1.00; F2 (Y293) CAL: 91.4; RF: 1.00
 A3 (K13197) CAL: 365; RF: 1.00; A4 (K13196) CAL: 416; RF: 1.00

max. Top Comp. Stress = 17.0 MPa (T= 22.9 ms, max= 1.126 x Top)
max. Comp. Stress = 19.1 MPa (Z= 8.0 m, T= 24.7 ms)
max. Tens. Stress = -3.44 MPa (Z= 20.0 m, T= 41.2 ms)
max. Energy (EMX) = 23.1 kJ; max. Measured Top Displ. (DMX)= 5.8 mm

EXTREMA TABLE

Pile Sgmnt No.	Dist. Below Gages m	max. Force kN	min. Force kN	max. Comp. Stress MPa	max. Tens. Stress MPa	max. Trnsfd. Energy kJ	max. Veloc. m/s	max. Displ. mm
1	1.0	4806.8	-125.6	17.0	-0.44	23.1	1.60	5.9
2	2.0	4896.2	-152.4	17.3	-0.54	22.1	1.47	5.6
4	4.0	4873.0	-233.4	17.2	-0.83	20.8	1.34	5.2
6	6.0	5234.3	-408.6	18.5	-1.45	20.0	1.24	5.1
8	8.0	5414.3	-486.2	19.1	-1.72	19.2	1.09	4.8
10	10.0	5121.9	-598.3	18.1	-2.12	18.4	1.12	4.6
12	12.0	4806.9	-696.5	17.0	-2.46	17.8	1.14	4.4
14	14.0	5053.2	-786.4	17.9	-2.78	17.3	1.07	4.2
16	16.0	5101.9	-811.3	18.0	-2.87	16.8	0.98	4.0
18	18.0	5111.3	-844.4	18.1	-2.99	16.2	0.95	3.9
20	20.0	4991.8	-973.6	17.7	-3.44	15.1	0.90	3.8
22	22.0	4447.1	-889.8	15.7	-3.15	13.4	0.92	3.7
23	23.0	4207.5	-823.2	14.9	-2.91	12.6	0.92	3.7
24	24.0	4049.3	-774.5	14.3	-2.74	11.8	0.90	3.7
25	25.0	3894.8	-690.7	13.8	-2.44	10.9	0.88	3.7
26	26.0	3719.3	-613.0	13.2	-2.17	10.0	0.85	3.7
27	27.0	3511.5	-523.8	12.4	-1.85	9.1	0.85	3.7
28	28.0	3264.0	-429.9	11.5	-1.52	8.6	0.92	3.6
29	29.0	3064.1	-323.0	10.8	-1.14	8.1	0.93	3.6
30	30.0	3019.3	-338.4	10.7	-1.20	7.6	0.89	3.5
31	31.0	2650.2	-185.0	9.4	-0.65	7.0	0.94	3.4
32	32.0	2276.4	-63.8	8.1	-0.23	6.0	0.96	3.3
Absolute	8.0			19.1			(T = 24.7 ms)	
	20.0				-3.44		(T = 41.2 ms)	

CASE METHOD

J =	0.0	0.1	0.2	0.3	0.4	0.5	0.6	0.7	0.8	0.9
RP	4440	4066	3692	3318	2944	2570	2197	1823	1449	1075
RX	4479	4097	3715	3333	2952	2574	2197	1823	1449	1075
RU	4625	4270	3914	3559	3204	2848	2493	2138	1783	1427

RAU = 0 (kN); RA2 = 2496 (kN)

Current CAPWAP Ru = 3467 (kN); Corresponding J(RP)= 0.26; J(RX) = 0.27

VMX	TVP	VT1*Z	FT1	FMX	DMX	DFN	SET	EMX	QUS	KEB
m/s	ms	kN	kN	kN	mm	mm	mm	kJ	kN	kN/mm
1.59	21.76	3674	4504	4853	5.8	2.2	2.0	22.7	5807	4102

PILE PROFILE AND PILE MODEL

Depth m	Area cm ²	E-Modulus MPa	Spec. Weight kN/m ³	Perim. m
0.0	2827.4	27776.0	23.563	1.88
32.0	2827.4	27776.0	23.563	1.88

Toe Area 2827.4 cm²

Segmnt Number	Dist. B.G. m	Impedance kN/m/s	Imped. Change %	Slack mm	Tension Eff.	Compression Slack mm	Compression Eff.	Perim. m	Wave Speed m/s
1	1.0	2309.8	0.0	0.00	0.000	-0.00	0.000	1.88	3400.0
5	5.0	3633.7	57.3	0.00	0.000	-0.00	0.000	1.88	3400.0
7	7.0	3231.7	39.9	0.00	0.000	-0.00	0.000	1.88	3400.0
9	9.0	3584.7	55.2	0.00	0.000	-0.00	0.000	1.88	3400.0
10	10.0	5055.7	118.9	0.00	0.000	-0.00	0.000	1.88	3400.0
12	12.0	4859.6	110.4	0.00	0.000	-0.00	0.000	1.88	3400.0
13	13.0	4437.9	92.1	0.00	0.000	-0.00	0.000	1.88	3400.0
14	14.0	4271.2	84.9	0.00	0.000	-0.00	0.000	1.88	3400.0
15	15.0	3584.7	55.2	0.00	0.000	-0.00	0.000	1.88	3400.0
16	16.0	3682.8	59.4	0.00	0.000	-0.00	0.000	1.88	3400.0
17	17.0	4859.6	110.4	0.00	0.000	-0.00	0.000	1.88	3400.0

Sinop - MT / Site A; Pile: DLT 1 - A
 CFA Pile 60cm 32m; Blow: 2
 EPF GEOTECNIA LTDA

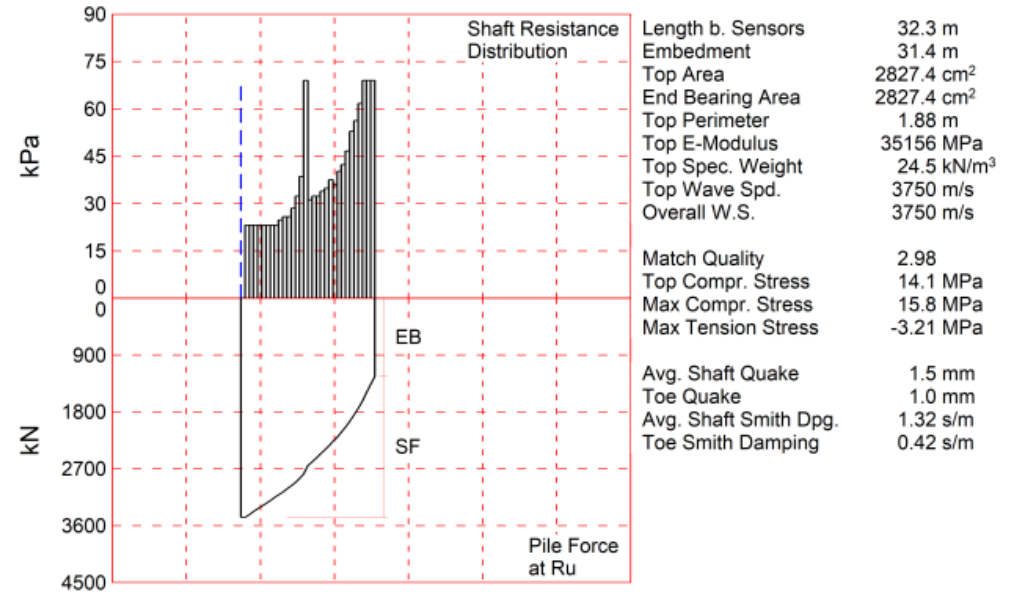
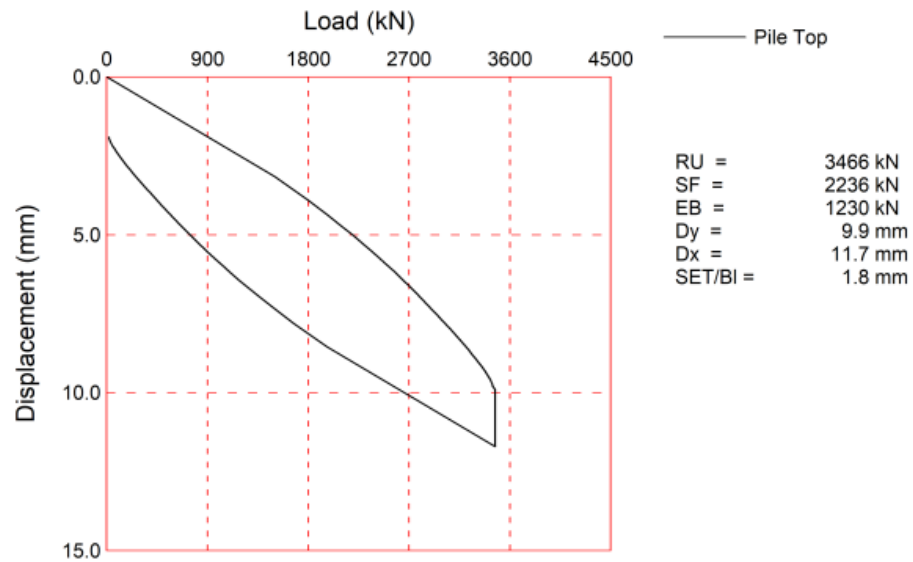
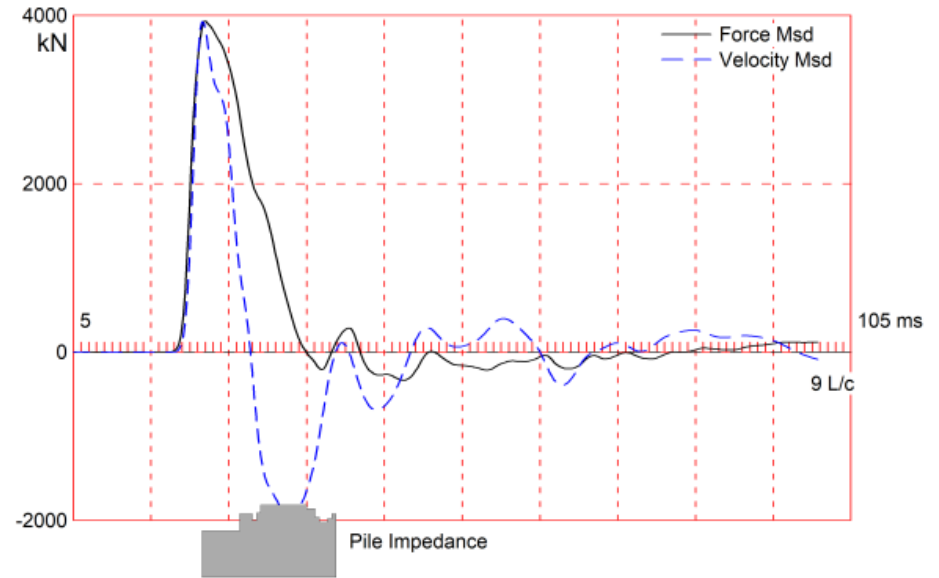
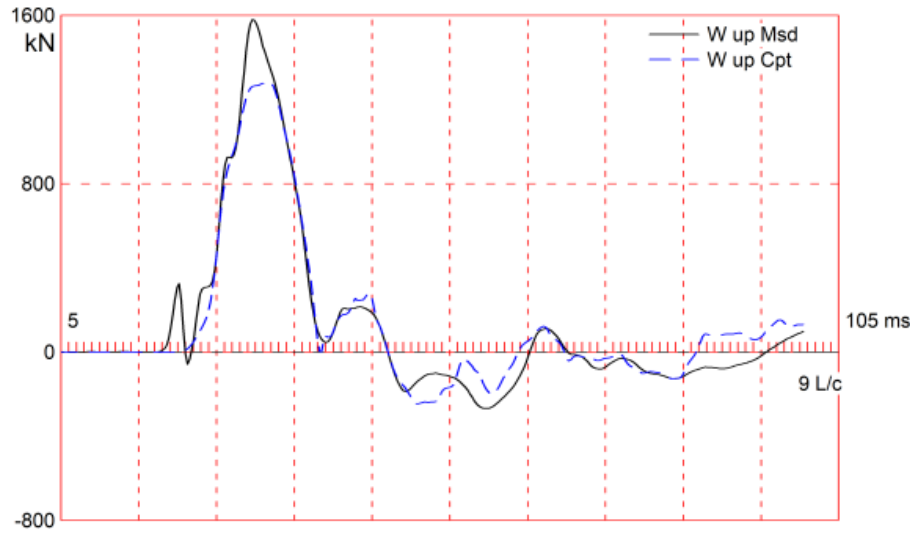
Test: 21-Sep-2023 14:32
 CAPWAP(R) 2014 2
 OP: Clayton Dalla Cort

Segmnt Number	Dist. B.G. m	Impedance kN/m/s	Imped. Change %	Slack mm	Tension Eff.	Compression Slack mm	Compression Eff.	Perim. m	Wave Speed m/s
18	18.0	4869.4	110.8	0.00	0.000	-0.00	0.000	1.88	3400.0
19	19.0	4761.5	106.1	0.00	0.000	-0.00	0.000	1.88	3400.0
20	20.0	4663.4	101.9	0.00	0.000	-0.00	0.000	1.88	3400.0
22	22.0	4761.5	106.1	0.00	0.000	-0.00	0.000	1.88	3400.0
25	25.0	3780.8	63.7	0.00	0.000	-0.00	0.000	1.88	3400.0
26	26.0	3486.6	50.9	0.00	0.000	-0.00	0.000	1.88	3400.0
31	31.0	3437.6	48.8	0.00	0.000	-0.00	0.000	1.88	3400.0
32	32.0	3486.6	50.9	0.00	0.000	-0.00	0.000	1.88	3400.0

Wave Speed: Pile Top 3400.0, Elastic 3400.0, Overall 3400.0 m/s

Pile Damping 2.00 %, Time Incr 0.294 ms, 2L/c 18.8 ms

Total volume: 15.147 m³; Volume ratio considering added impedance: 1.674



CAPWAP SUMMARY RESULTS

Total CAPWAP Capacity: 3466.2; along Shaft 2236.2; at Toe 1230.0 kN

Soil Sgmt No.	Dist. Below Gages m	Depth Below Grade m	Ru kN	Force in Pile kN	Sum of Ru kN	Unit Resist. (Depth) kN/m	Unit Resist. (Area) kPa	Smith Damping Factor s/m	Quake mm
				3466.2					
1	1.0	0.1	0.0	3466.2	0.0	0.00	0.00	0.00	7.3
2	2.0	1.1	44.0	3422.2	44.0	43.59	23.13	0.50	7.1
3	3.0	2.1	44.0	3378.2	88.0	43.59	23.13	0.50	6.8
4	4.0	3.1	44.0	3334.2	132.0	43.59	23.13	1.84	6.5
5	5.0	4.1	44.0	3290.2	176.0	43.59	23.13	0.50	6.1
6	6.1	5.2	44.0	3246.2	220.0	43.59	23.13	0.50	5.7
7	7.1	6.2	44.0	3202.2	264.0	43.59	23.13	0.50	4.8
8	8.1	7.2	44.0	3158.2	308.0	43.59	23.13	0.50	4.2
9	9.1	8.2	44.0	3114.2	352.0	43.59	23.13	1.61	3.7
10	10.1	9.2	47.2	3067.0	399.2	46.76	24.81	1.33	1.1
11	11.1	10.2	49.2	3017.8	448.4	48.74	25.86	1.30	0.9
12	12.1	11.2	49.2	2968.6	497.6	48.74	25.86	1.30	1.5
13	13.1	12.2	54.3	2914.3	551.9	53.80	28.54	1.22	3.1
14	14.1	13.2	61.5	2852.8	613.4	60.93	32.32	1.30	2.6
15	15.1	14.2	73.5	2779.3	686.9	72.82	38.63	1.43	2.0
16	16.1	15.3	131.3	2648.0	818.2	130.08	69.01	1.17	2.1
17	17.2	16.3	59.3	2588.7	877.5	58.75	31.17	1.66	1.0
18	18.2	17.3	61.5	2527.2	939.0	60.93	32.32	3.69	0.8
19	19.2	18.3	61.5	2465.7	1000.5	60.93	32.32	4.17	0.7
20	20.2	19.3	64.5	2401.2	1065.0	63.90	33.90	3.54	0.6
21	21.2	20.3	66.4	2334.8	1131.4	65.78	34.90	4.34	0.5
22	22.2	21.3	71.5	2263.3	1202.9	70.84	37.58	1.46	0.4
23	23.2	22.3	68.4	2194.9	1271.3	67.76	35.95	1.93	0.3
24	24.2	23.3	76.5	2118.4	1347.8	75.79	40.21	0.50	0.3
25	25.2	24.3	80.6	2037.8	1428.4	79.85	42.36	0.50	0.2
26	26.2	25.3	88.8	1949.0	1517.2	87.98	46.67	0.50	0.3
27	27.3	26.4	100.7	1848.3	1617.9	99.76	52.93	0.50	0.2
28	28.3	27.4	107.0	1741.3	1724.9	106.01	56.24	0.50	0.0
29	29.3	28.4	117.4	1623.9	1842.3	116.31	61.70	0.50	0.1
30	30.3	29.4	131.3	1492.6	1973.6	130.08	69.01	0.50	0.7
31	31.3	30.4	131.3	1361.3	2104.9	130.08	69.01	1.84	0.2
32	32.3	31.4	131.3	1230.0	2236.2	130.08	69.01	1.17	0.1
Avg. Shaft			69.9			71.22	37.78	1.32	1.5
Toe			1230.0				4350.24	0.42	1.0

Soil Model Parameters/Extensions

	Shaft	Toe
Case Damping Factor	1.12	0.19
Damping Type	Viscous	Sm+Visc
Reloading Level (% of Ru)	100	100
Unloading Level (% of Ru)	58	

CAPWAP match quality = 2.98 (Wave Up Match) ; RSA = 0
 Observed: Final Set = 1.8 mm; Blow Count = 549 b/m
 Computed: Final Set = 2.2 mm; Blow Count = 461 b/m

Transducer F1 (Y286) CAL: 91.0; RF: 1.00; F2 (Y293) CAL: 91.4; RF: 1.00
 A3 (K13197) CAL: 365; RF: 1.00; A4 (K13196) CAL: 416; RF: 1.00

max. Top Comp. Stress = 14.1 MPa (T= 22.1 ms, max= 1.125 x Top)
 max. Comp. Stress = 15.8 MPa (Z= 15.1 m, T= 26.1 ms)
 max. Tens. Stress = -3.21 MPa (Z= 8.1 m, T= 36.3 ms)
 max. Energy (EMX) = 25.1 kJ; max. Measured Top Displ. (DMX)= 7.3 mm

EXTREMA TABLE

Pile Sgmt No.	Dist. Below Gages m	max. Force kN	min. Force kN	max. Comp. Stress MPa	max. Tens. Stress MPa	max. Trnsfd. Energy kJ	max. Veloc. m/s	max. Displ. mm
1	1.0	3982.9	-393.5	14.1	-1.39	25.1	1.45	7.4
2	2.0	4016.0	-471.6	14.2	-1.67	24.8	1.44	7.1
4	4.0	4067.4	-724.2	14.4	-2.56	23.6	1.40	6.6
6	6.1	4189.1	-855.3	14.8	-3.03	22.0	1.32	6.1
8	8.1	4382.7	-908.9	15.5	-3.21	21.2	1.18	5.6
10	10.1	4402.6	-852.7	15.6	-3.02	20.5	1.12	5.2
12	12.1	4480.3	-714.3	15.8	-2.53	19.4	1.04	4.9
14	14.1	4474.4	-693.6	15.8	-2.45	18.5	0.97	4.6
16	16.1	4467.8	-698.8	15.8	-2.47	17.5	0.92	4.4
18	18.2	4344.5	-635.7	15.4	-2.25	16.1	0.85	4.4
20	20.2	4019.0	-529.7	14.2	-1.87	14.0	0.80	4.3
22	22.2	3594.3	-535.0	12.7	-1.89	11.8	0.77	4.3
23	23.2	3481.6	-545.8	12.3	-1.93	11.1	0.76	4.2
24	24.2	3324.9	-535.4	11.8	-1.89	10.3	0.76	4.2
25	25.2	3190.8	-528.7	11.3	-1.87	9.9	0.77	4.2
26	26.2	3064.2	-527.5	10.8	-1.87	9.3	0.77	4.1
27	27.3	2914.1	-535.8	10.3	-1.90	8.8	0.78	4.0
28	28.3	2696.5	-510.3	9.5	-1.80	8.3	0.80	4.0
29	29.3	2453.3	-459.6	8.7	-1.63	7.7	0.86	3.9
30	30.3	2128.5	-394.6	7.5	-1.40	7.0	0.89	3.8
31	31.3	2144.4	-305.7	7.6	-1.08	6.4	0.88	3.7
32	32.3	1893.9	-181.8	6.7	-0.64	4.8	0.81	3.6
Absolute	15.1			15.8			(T = 26.1 ms)	
	8.1				-3.21		(T = 36.3 ms)	

CASE METHOD

J =	0.0	0.1	0.2	0.3	0.4	0.5	0.6	0.7	0.8	0.9
RP	3945	3560	3175	2790	2406	2021	1636	1252	867	482
RX	3975	3586	3198	2809	2421	2032	1679	1362	1046	732
RU	5258	5005	4752	4499	4245	3992	3739	3485	3232	2979

RAU = 0 (kN); RA2 = 2212 (kN)

Current CAPWAP Ru = 3466 (kN); Corresponding J(RP)= 0.12; J(RX) = 0.13

VMX m/s	TVP ms	VT1*Z kN	FT1 kN	FMX kN	DMX mm	DFN mm	SET mm	EMX kJ	QUS kN	KEB kN/mm
1.49	21.80	3935	3857	3938	7.3	1.8	1.8	25.3	5546	1193

PILE PROFILE AND PILE MODEL

Depth m	Area cm ²	E-Modulus MPa	Spec. Weight kN/m ³	Perim. m
0.0	2827.4	35156.2	24.517	1.88
32.3	2827.4	35156.2	24.517	1.88

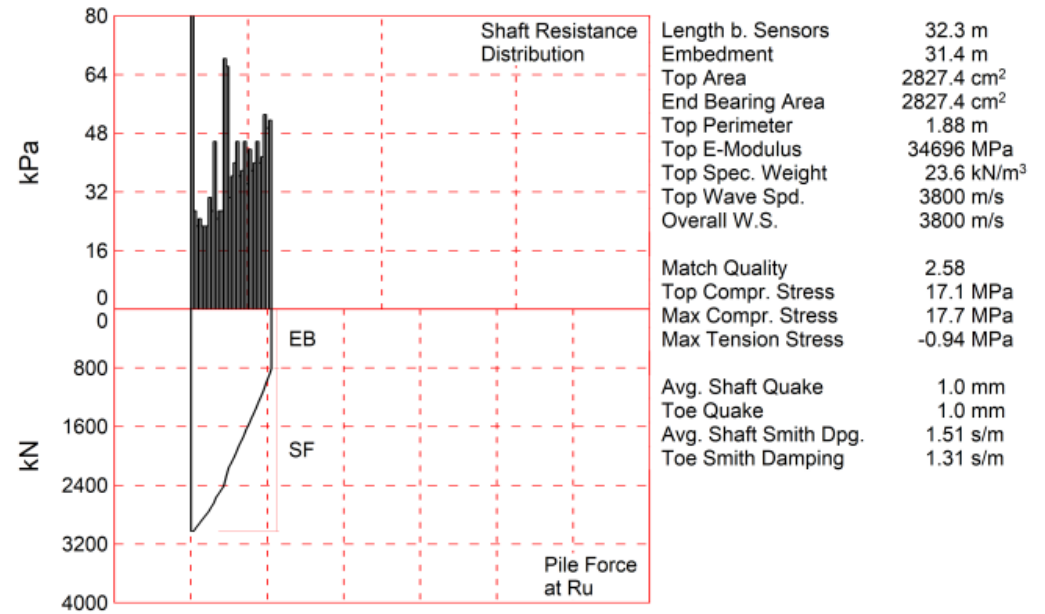
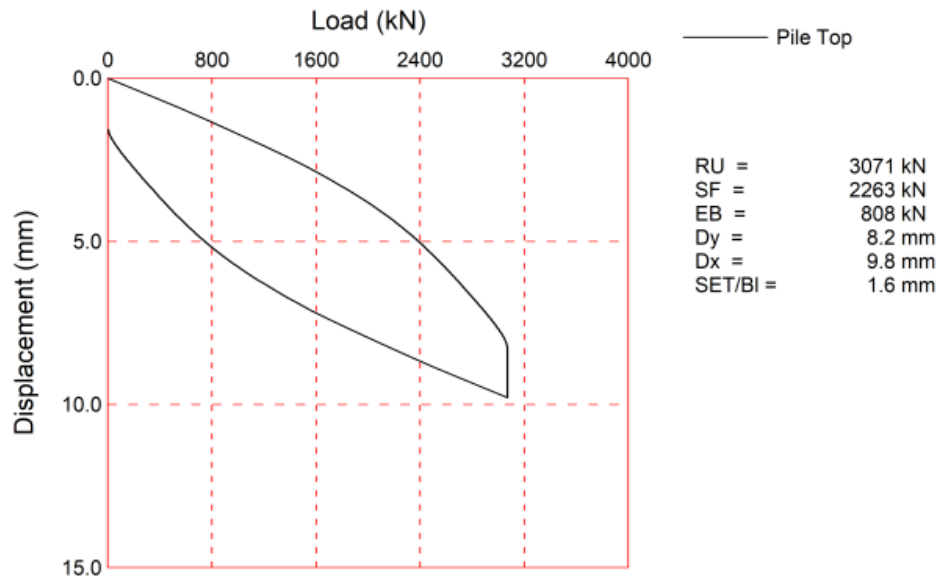
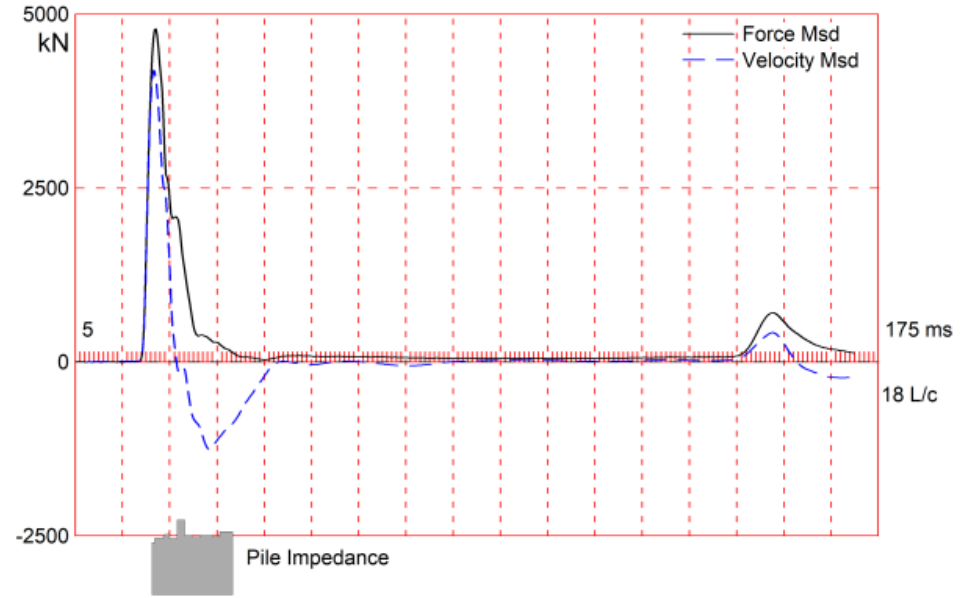
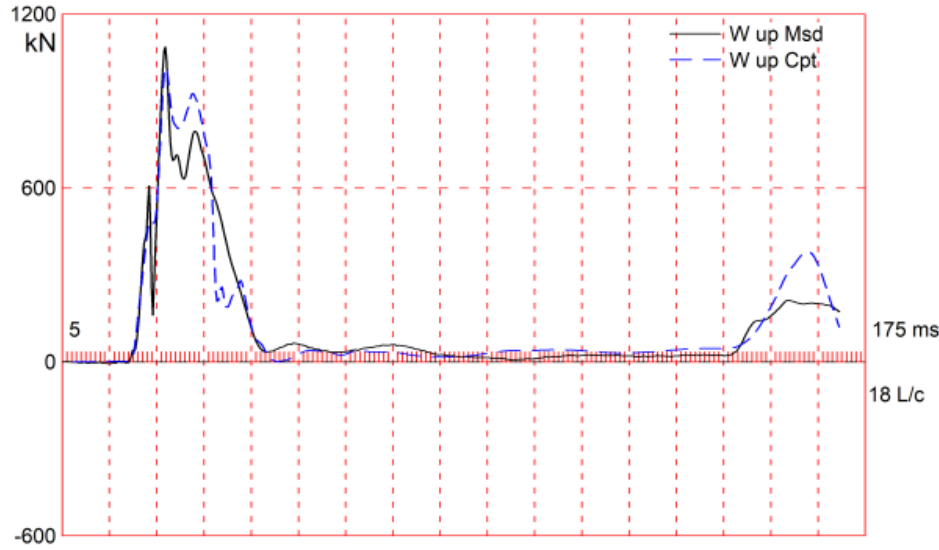
Toe Area 2827.4 cm²

Segmnt Number	Dist. B.G. m	Impedance kN/m/s	Imped. Change %	Slack mm	Tension Eff.	Compression Slack mm	Compression Eff.	Perim. m	Wave Speed m/s
1	1.0	2650.7	0.0	0.00	0.000	-0.00	0.000	1.88	3750.0
10	10.1	3631.4	37.0	0.00	0.000	-0.00	0.000	1.88	3750.0
13	13.1	3248.9	22.6	0.00	0.000	-0.00	0.000	1.88	3750.0
14	14.1	3690.2	39.2	0.00	0.000	-0.00	0.000	1.88	3750.0
15	15.1	4121.7	55.5	0.00	0.000	-0.00	0.000	1.88	3750.0
26	26.2	3925.6	48.1	0.00	0.000	-0.00	0.000	1.88	3750.0
28	28.3	3435.2	29.6	0.00	0.000	-0.00	0.000	1.88	3750.0
29	29.3	3141.0	18.5	0.00	0.000	-0.00	0.000	1.88	3750.0
31	31.3	3356.8	26.6	0.00	0.000	-0.00	0.000	1.88	3750.0
32	32.3	3631.4	37.0	0.00	0.000	-0.00	0.000	1.88	3750.0

Wave Speed: Pile Top 3750.0, Elastic 3750.0, Overall 3750.0 m/s

Pile Damping 2.00 %, Time Incr 0.269 ms, 2L/c 17.2 ms

Total volume: 12.014 m³; Volume ratio considering added impedance: 1.316



CAPWAP SUMMARY RESULTS

Total CAPWAP Capacity: 3071.0; along Shaft 2263.0; at Toe 808.0 kN

Soil Sgmt No.	Dist. Below Gages m	Depth Below Grade m	Ru kN	Force in Pile kN	Sum of Ru kN	Unit Resist. (Depth) kN/m	Unit Resist. (Area) kPa	Smith Damping Factor s/m	Quake mm
				3071.0					
1	1.0	0.1	43.0	3028.0	43.0	393.14	208.57	0.94	4.4
2	2.0	1.1	51.0	2977.0	94.0	50.53	26.81	1.07	3.2
3	3.0	2.1	43.0	2934.0	137.0	42.60	22.60	1.03	3.5
4	4.0	3.1	47.0	2887.0	184.0	46.56	24.70	0.97	2.7
5	5.0	4.1	43.0	2844.0	227.0	42.60	22.60	0.97	2.8
6	6.1	5.2	43.0	2801.0	270.0	42.60	22.60	0.97	2.8
7	7.1	6.2	43.0	2758.0	313.0	42.60	22.60	0.97	2.8
8	8.1	7.2	58.0	2700.0	371.0	57.46	30.48	1.03	2.5
9	9.1	8.2	51.0	2649.0	422.0	50.53	26.81	0.99	2.6
10	10.1	9.2	87.0	2562.0	509.0	86.19	45.73	1.12	2.5
11	11.1	10.2	47.0	2515.0	556.0	46.56	24.70	3.48	0.3
12	12.1	11.2	51.0	2464.0	607.0	50.53	26.81	3.17	0.3
13	13.1	12.2	51.0	2413.0	658.0	50.53	26.81	3.17	0.3
14	14.1	13.2	130.0	2283.0	788.0	128.79	68.33	0.55	0.8
15	15.1	14.2	126.0	2157.0	914.0	124.83	66.22	0.70	0.6
16	16.1	15.2	58.0	2099.0	972.0	57.46	30.48	2.69	0.4
17	17.2	16.3	69.0	2030.0	1041.0	68.36	36.27	2.09	0.4
18	18.2	17.3	76.0	1954.0	1117.0	75.29	39.94	1.79	0.4
19	19.2	18.3	87.0	1867.0	1204.0	86.19	45.73	1.42	0.5
20	20.2	19.3	69.0	1798.0	1273.0	68.36	36.27	2.09	0.4
21	21.2	20.3	72.0	1726.0	1345.0	71.33	37.84	1.94	0.4
22	22.2	21.3	87.0	1639.0	1432.0	86.19	45.73	1.42	0.5
23	23.2	22.3	65.0	1574.0	1497.0	64.40	34.16	2.28	0.4
24	24.2	23.3	83.0	1491.0	1580.0	82.23	43.62	1.54	0.4
25	25.2	24.3	72.0	1419.0	1652.0	71.33	37.84	1.94	0.4
26	26.2	25.3	76.0	1343.0	1728.0	75.29	39.94	1.79	0.4
27	27.3	26.4	87.0	1256.0	1815.0	86.19	45.73	1.42	0.5
28	28.3	27.4	76.0	1180.0	1891.0	75.29	39.94	1.79	0.4
29	29.3	28.4	79.0	1101.0	1970.0	78.27	41.52	1.66	0.4
30	30.3	29.4	101.0	1000.0	2071.0	100.06	53.08	1.06	0.5
31	31.3	30.4	94.0	906.0	2165.0	93.13	49.41	1.22	0.5
32	32.3	31.4	98.0	808.0	2263.0	97.09	51.51	1.14	0.5
Avg. Shaft			70.7			72.07	38.23	1.51	1.0
Toe			808.0				2857.72	1.31	1.0

Soil Model Parameters/Extensions

	Shaft	Toe
Case Damping Factor	1.32	0.41
Damping Type	Viscous	Sm+Visc
Unloading Quake (% of loading quake)	100	98
Reloading Level (% of Ru)	100	100
Unloading Level (% of Ru)	0	

CAPWAP match quality = 2.58 (Wave Up Match) ; RSA = 0
 Observed: Final Set = 1.6 mm; Blow Count = 645 b/m
 Computed: Final Set = 0.9 mm; Blow Count = 1066 b/m

Transducer F1 (Y286) CAL: 91.0; RF: 1.00; F2 (Y293) CAL: 91.4; RF: 1.00
 A3 (K13197) CAL: 365; RF: 1.00; A4 (K13196) CAL: 416; RF: 1.00

max. Top Comp. Stress = 17.1 MPa (T= 22.0 ms, max= 1.036 x Top)
 max. Comp. Stress = 17.7 MPa (Z= 8.1 m, T= 24.2 ms)
 max. Tens. Stress = -0.94 MPa (Z= 8.1 m, T= 35.6 ms)
 max. Energy (EMX) = 23.7 kJ; max. Measured Top Displ. (DMX)= 6.5 mm

EXTREMA TABLE

Pile Sgmnt No.	Dist. Below Gages m	max. Force kN	min. Force kN	max. Comp. Stress MPa	max. Tens. Stress MPa	max. Trnsfd. Energy kJ	max. Veloc. m/s	max. Displ. mm
1	1.0	4826.1	-173.4	17.1	-0.61	23.7	1.60	6.2
2	2.0	4829.1	-189.3	17.1	-0.67	23.0	1.57	6.0
4	4.0	4711.5	-199.7	16.7	-0.71	21.7	1.53	5.7
6	6.1	4685.7	-232.8	16.6	-0.82	20.6	1.49	5.4
8	8.1	5000.2	-266.6	17.7	-0.94	19.6	1.34	5.2
10	10.1	4919.9	-237.4	17.4	-0.84	18.4	1.25	4.8
12	12.1	4463.0	-230.2	15.8	-0.81	16.6	1.25	4.6
14	14.1	4174.2	-187.7	14.8	-0.66	14.6	1.19	4.3
16	16.1	3967.3	-217.6	14.0	-0.77	12.8	1.12	4.0
18	18.2	3740.1	-224.0	13.2	-0.79	11.2	1.04	3.7
20	20.2	3505.3	-220.1	12.4	-0.78	9.7	0.97	3.5
22	22.2	3271.7	-214.7	11.6	-0.76	8.6	0.91	3.4
23	23.2	3176.6	-208.0	11.2	-0.74	8.0	0.88	3.3
24	24.2	3099.9	-197.6	11.0	-0.70	7.5	0.84	3.3
25	25.2	3014.3	-192.8	10.7	-0.68	7.0	0.80	3.2
26	26.2	2924.7	-184.7	10.3	-0.65	6.5	0.76	3.2
27	27.3	2758.9	-173.8	9.8	-0.61	6.1	0.79	3.1
28	28.3	2467.8	-162.1	8.7	-0.57	5.6	0.87	3.1
29	29.3	2022.3	-149.6	7.2	-0.53	5.1	0.91	3.0
30	30.3	1974.3	-136.3	7.0	-0.48	4.6	0.89	3.0
31	31.3	1939.9	-139.3	6.9	-0.49	4.1	0.82	2.9
32	32.3	1794.6	-131.0	6.3	-0.46	3.3	0.76	2.9
Absolute	8.1			17.7			(T = 24.2 ms)	
	8.1				-0.94		(T = 35.6 ms)	

CASE METHOD

J =	0.0	0.1	0.2	0.3	0.4	0.5	0.6	0.7	0.8	0.9
RP	4948	4549	4151	3752	3354	2955	2557	2159	1760	1362
RX	4959	4558	4157	3756	3355	2955	2557	2159	1760	1362
RU	5464	5117	4771	4424	4077	3730	3383	3037	2690	2343

RAU = 69 (kN); RA2 = 1694 (kN)

Current CAPWAP Ru = 3071 (kN); Corresponding J(RP)= 0.47; J(RX) = 0.47

VMX m/s	TVP ms	VT1*Z kN	FT1 kN	FMX kN	DMX mm	DFN mm	SET mm	EMX kJ	QUS kN	KEB kN/mm
1.63	21.52	4212	4720	4807	6.5	1.5	1.6	23.9	5969	808

PILE PROFILE AND PILE MODEL

Depth m	Area cm ²	E-Modulus MPa	Spec. Weight kN/m ³	Perim. m
0.0	2827.4	34696.0	23.563	1.88
32.3	2827.4	34696.0	23.563	1.88
Toe Area		2827.4	cm ²	

Segmnt Number	Dist. B.G. m	Impedance kN/m/s	Imped. Change %	Slack mm	Tension Eff.	Compression Slack mm	Perim. m	Wave Speed m/s
1	1.0	2581.6	0.0	0.00	0.000	-0.00	1.88	3800.0
2	2.0	2791.6	8.1	0.00	0.000	-0.00	1.88	3800.0
4	4.0	2781.6	7.7	0.00	0.000	-0.00	1.88	3800.0
5	5.0	2831.6	9.7	0.00	0.000	-0.00	1.88	3800.0
6	6.1	2981.6	15.5	0.00	0.000	-0.00	1.88	3800.0
8	8.1	2784.6	7.9	0.00	0.000	-0.00	1.88	3800.0
11	11.1	3681.6	42.6	0.00	0.000	-0.00	1.88	3800.0
14	14.1	2936.6	13.8	0.00	0.000	-0.00	1.88	3800.0
17	17.2	2835.6	9.8	0.00	0.000	-0.00	1.88	3800.0
20	20.2	2936.6	13.8	0.00	0.000	-0.00	1.88	3800.0
25	25.2	2860.6	10.8	0.00	0.000	-0.00	1.88	3800.0

SSinop - MT / Site B; Pile: DLT 1 - B
 CFA Pile - 60cm - 32m; Blow: 3
 EPF GEOTECNIA LTDA

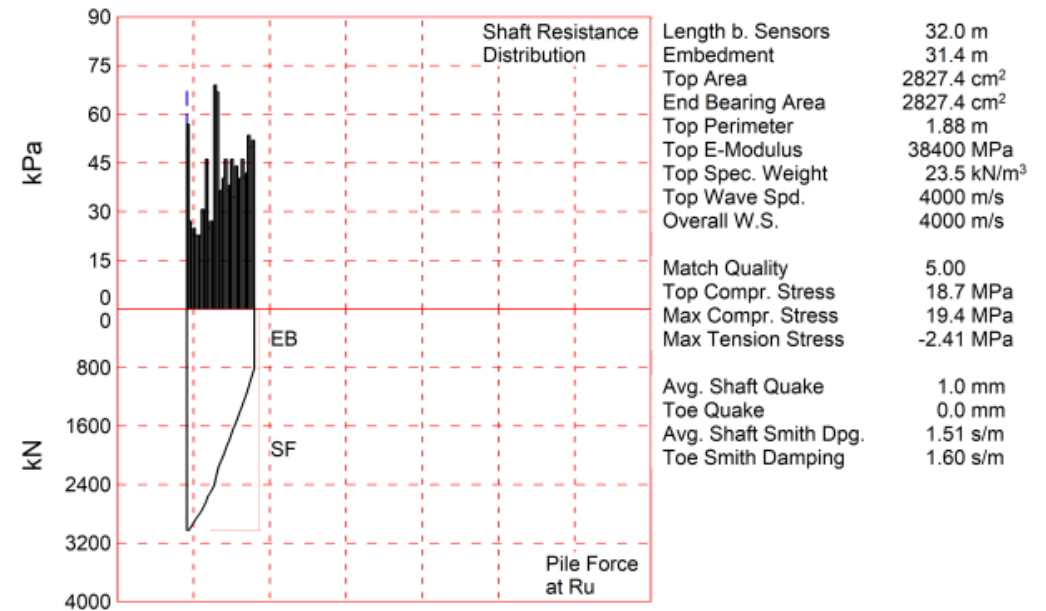
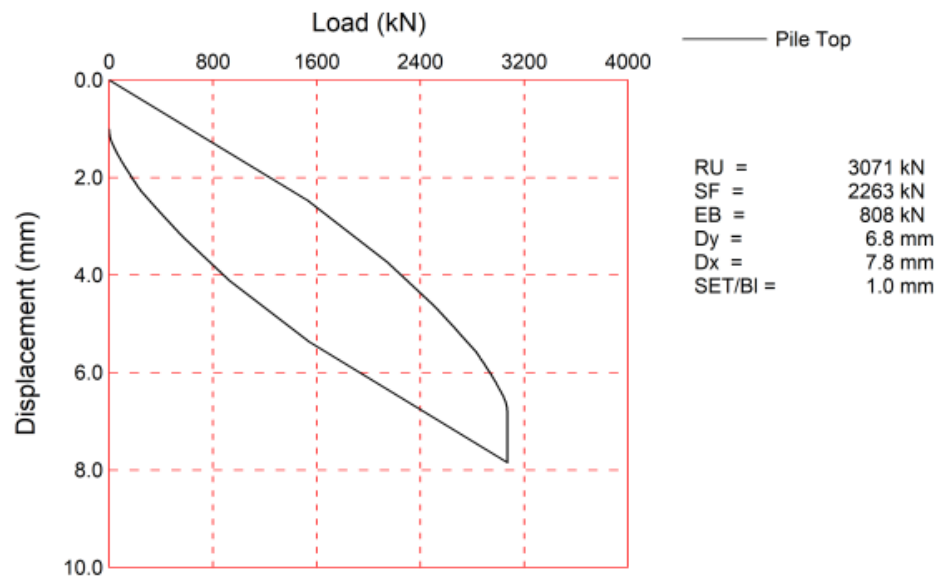
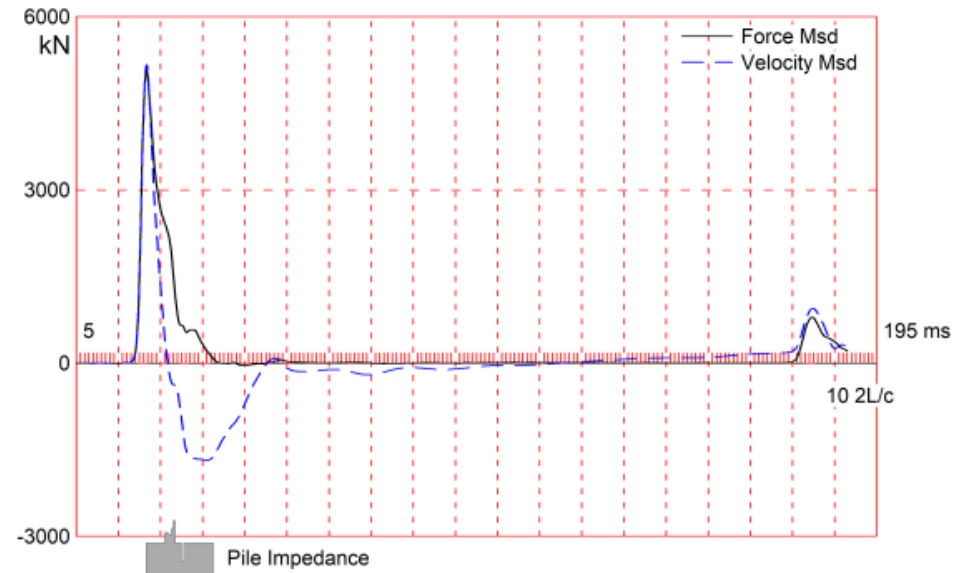
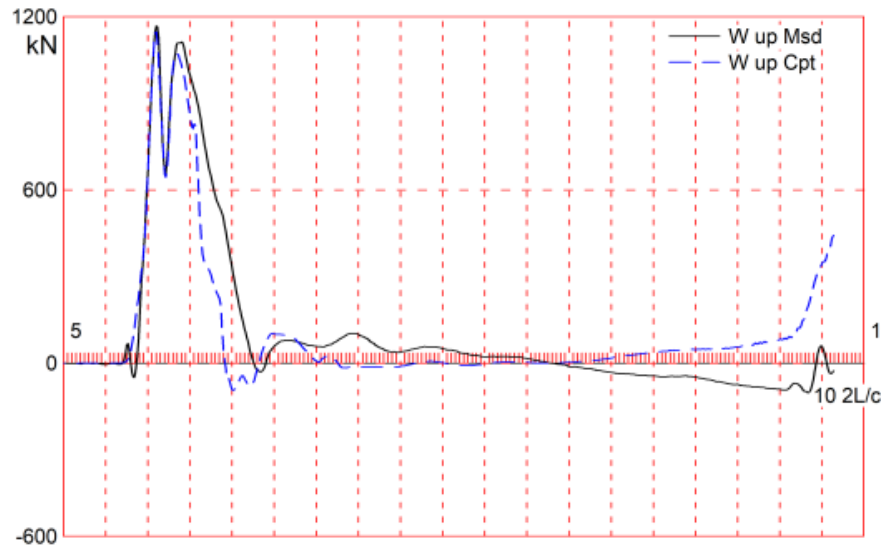
Test: 21-Sep-2023 15:20
 CAPWAP(R) 2014-3
 OP: Clayton Dalla Cort

Segmnt Number	Dist. B.G. m	Impedance kN/m/s	Imped. Change %	Slack mm	Tension Eff.	Compression Slack mm	Compression Eff.	Perim. m	Wave Speed m/s
28	28.3	3114.6	20.6	0.00	0.000	-0.00	0.000	1.88	3800.0
32	32.3	3114.6	20.6	0.00	0.000	-0.00	0.000	1.88	3800.0

Wave Speed: Pile Top 3800.0, Elastic 3800.0, Overall 3800.0 m/s

Pile Damping 2.00 %, Time Incr 0.266 ms, 2L/c 17.0 ms

Total volume: 10.535 m³; Volume ratio considering added impedance: 1.154



CAPWAP SUMMARY RESULTS

Total CAPWAP Capacity: 3071.0; along Shaft 2263.0; at Toe 808.0 kN

Soil Sgmt No.	Dist. Below Gages m	Depth Below Grade m	Ru kN	Force in Pile kN	Sum of Ru kN	Unit Resist. (Depth) kN/m	Unit Resist. (Area) kPa	Smith Damping Factor s/m	Quake mm
				3071.0					
1	1.0	0.4	43.0	3028.0	43.0	107.50	57.03	0.94	4.4
2	2.0	1.4	51.0	2977.0	94.0	51.00	27.06	1.07	3.2
3	3.0	2.4	43.0	2934.0	137.0	43.00	22.81	1.03	3.5
4	4.0	3.4	47.0	2887.0	184.0	47.00	24.93	0.97	2.7
5	5.0	4.4	43.0	2844.0	227.0	43.00	22.81	0.97	2.8
6	6.0	5.4	43.0	2801.0	270.0	43.00	22.81	0.97	2.8
7	7.0	6.4	43.0	2758.0	313.0	43.00	22.81	0.97	2.8
8	8.0	7.4	58.0	2700.0	371.0	58.00	30.77	1.03	2.5
9	9.0	8.4	51.0	2649.0	422.0	51.00	27.06	0.99	2.6
10	10.0	9.4	87.0	2562.0	509.0	87.00	46.15	1.12	2.5
11	11.0	10.4	47.0	2515.0	556.0	47.00	24.93	3.48	0.3
12	12.0	11.4	51.0	2464.0	607.0	51.00	27.06	3.17	0.3
13	13.0	12.4	51.0	2413.0	658.0	51.00	27.06	3.17	0.3
14	14.0	13.4	130.0	2283.0	788.0	130.00	68.97	0.55	0.8
15	15.0	14.4	126.0	2157.0	914.0	126.00	66.85	0.70	0.6
16	16.0	15.4	58.0	2099.0	972.0	58.00	30.77	2.69	0.4
17	17.0	16.4	69.0	2030.0	1041.0	69.00	36.61	2.09	0.4
18	18.0	17.4	76.0	1954.0	1117.0	76.00	40.32	1.79	0.4
19	19.0	18.4	87.0	1867.0	1204.0	87.00	46.15	1.42	0.5
20	20.0	19.4	69.0	1798.0	1273.0	69.00	36.61	2.09	0.4
21	21.0	20.4	72.0	1726.0	1345.0	72.00	38.20	1.94	0.4
22	22.0	21.4	87.0	1639.0	1432.0	87.00	46.15	1.42	0.5
23	23.0	22.4	65.0	1574.0	1497.0	65.00	34.48	2.28	0.4
24	24.0	23.4	83.0	1491.0	1580.0	83.00	44.03	1.54	0.4
25	25.0	24.4	72.0	1419.0	1652.0	72.00	38.20	1.94	0.4
26	26.0	25.4	76.0	1343.0	1728.0	76.00	40.32	1.79	0.4
27	27.0	26.4	87.0	1256.0	1815.0	87.00	46.15	1.42	0.5
28	28.0	27.4	76.0	1180.0	1891.0	76.00	40.32	1.79	0.4
29	29.0	28.4	79.0	1101.0	1970.0	79.00	41.91	1.66	0.4
30	30.0	29.4	101.0	1000.0	2071.0	101.00	53.58	1.06	0.5
31	31.0	30.4	94.0	906.0	2165.0	94.00	49.87	1.22	0.5
32	32.0	31.4	98.0	808.0	2263.0	98.00	51.99	1.14	0.5
Avg. Shaft			70.7			72.07	38.23	1.51	1.0
Toe			808.0				2857.72	1.60	0.0

Soil Model Parameters/Extensions

	Shaft	Toe
Case Damping Factor	1.26	0.48
Damping Type	Viscous	Smith
Reloading Level (% of Ru)	100	100
Unloading Level (% of Ru)	0	

CAPWAP match quality = 5.00 (Wave Up Match) ; RSA = 0
 Observed: Final Set = 1.0 mm; Blow Count = 1000 b/m
 Computed: Final Set = 0.1 mm; Blow Count = 9999 b/m

Transducer F1 (Y286) CAL: 91.0; RF: 1.00; F2 (Y293) CAL: 91.4; RF: 1.00
 A3 (K13197) CAL: 365; RF: 1.00; A4 (K13196) CAL: 416; RF: 1.00

max. Top Comp. Stress = 18.7 MPa (T= 22.0 ms, max= 1.036 x Top)
 max. Comp. Stress = 19.4 MPa (Z= 10.0 m, T= 24.3 ms)
 max. Tens. Stress = -2.41 MPa (Z= 11.0 m, T= 41.0 ms)
 max. Energy (EMX) = 27.1 kJ; max. Measured Top Displ. (DMX)= 7.0 mm

EXTREMA TABLE

Pile Sgmnt No.	Dist. Below Gages m	max. Force kN	min. Force kN	max. Comp. Stress MPa	max. Tens. Stress MPa	max. Trnsfd. Energy kJ	max. Veloc. m/s	max. Displ. mm
1	1.0	5290.9	-539.1	18.7	-1.91	27.1	1.82	6.6
2	2.0	5251.1	-549.9	18.6	-1.94	26.5	1.80	6.5
4	4.0	5139.7	-570.5	18.2	-2.02	25.1	1.75	6.2
6	6.0	5191.7	-605.9	18.4	-2.14	23.9	1.67	6.0
8	8.0	5392.4	-640.5	19.1	-2.27	22.8	1.53	5.6
10	10.0	5483.0	-676.7	19.4	-2.39	21.6	1.40	5.3
12	12.0	4991.7	-664.5	17.7	-2.35	19.3	1.40	5.0
14	14.0	4335.1	-650.7	15.3	-2.30	16.6	1.43	4.8
16	16.0	4085.8	-619.7	14.5	-2.19	14.6	1.36	4.4
18	18.0	3936.9	-538.1	13.9	-1.90	12.5	1.17	4.0
20	20.0	3683.1	-482.8	13.0	-1.71	10.8	1.10	3.7
22	22.0	3443.8	-467.6	12.2	-1.65	9.4	1.02	3.4
23	23.0	3327.7	-454.5	11.8	-1.61	8.7	0.99	3.3
24	24.0	3213.4	-429.0	11.4	-1.52	8.1	0.95	3.2
25	25.0	3107.7	-390.9	11.0	-1.38	7.5	0.92	3.1
26	26.0	3015.0	-349.5	10.7	-1.24	7.0	0.88	3.0
27	27.0	2946.7	-302.0	10.4	-1.07	6.5	0.84	2.9
28	28.0	3000.8	-250.5	10.6	-0.89	6.0	0.78	2.8
29	29.0	2890.2	-197.6	10.2	-0.70	5.5	0.72	2.7
30	30.0	2602.8	-140.6	9.2	-0.50	5.1	0.76	2.7
31	31.0	2308.4	-83.3	8.2	-0.29	4.6	0.80	2.6
32	32.0	2050.1	-29.9	7.3	-0.11	3.8	0.81	2.5
Absolute	10.0			19.4			(T = 24.3 ms)	
	11.0				-2.41		(T = 41.0 ms)	

CASE METHOD

J =	0.0	0.1	0.2	0.3	0.4	0.5	0.6	0.7	0.8	0.9
RP	5790	5339	4889	4439	3989	3539	3088	2638	2188	1738
RX	5790	5339	4889	4439	3989	3539	3088	2638	2188	1738
RU	6839	6493	6148	5803	5457	5112	4767	4421	4076	3731

RAU = 291 (kN); RA2 = 2315 (kN)

Current CAPWAP Ru = 3071 (kN); Corresponding J(RP)= 0.60; J(RX) = 0.60

VMX	TVP	VT1*Z	FT1	FMX	DMX	DFN	SET	EMX	QUS	KEB
m/s	ms	kN	kN	kN	mm	mm	mm	kJ	kN	kN/mm
1.91	21.75	5197	5095	5095	7.0	0.6	1.0	27.0	6776	20200

PILE PROFILE AND PILE MODEL

Depth m	Area cm ²	E-Modulus MPa	Spec. Weight kN/m ³	Perim. m
0.0	2827.4	38400.0	23.536	1.88
32.0	2827.4	38400.0	23.536	1.88

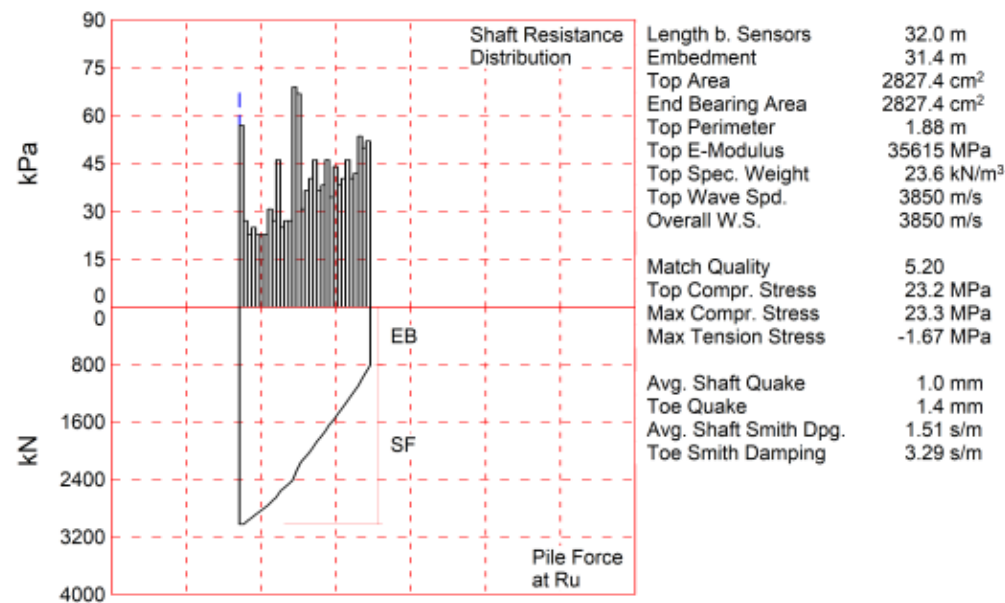
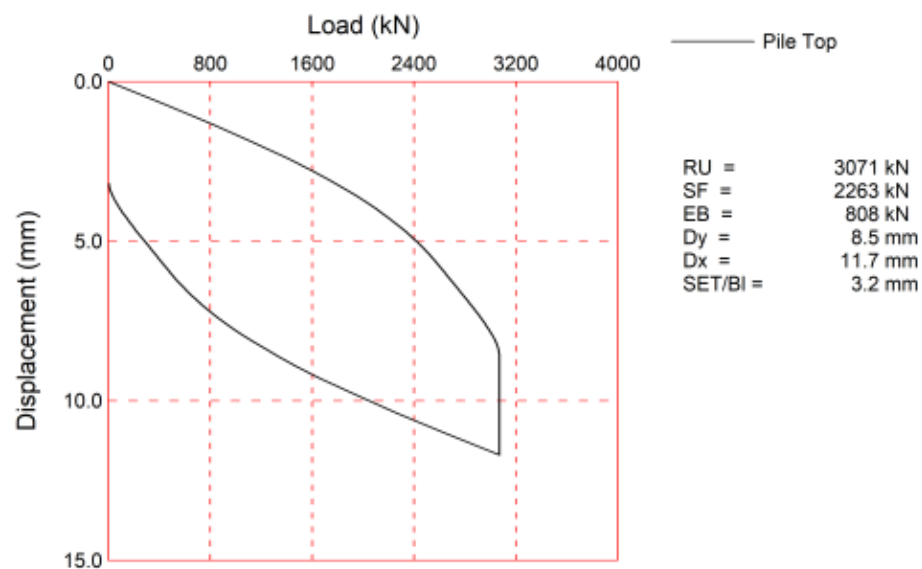
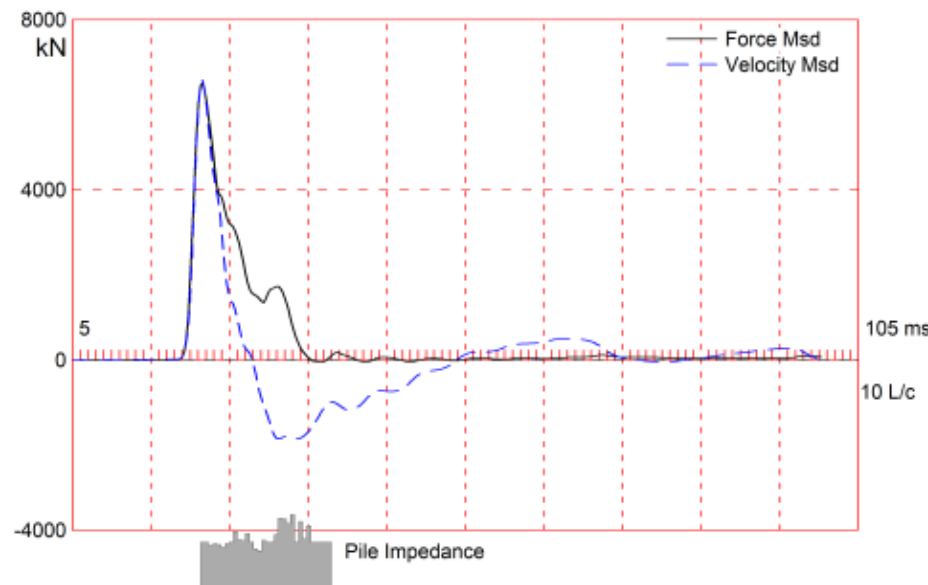
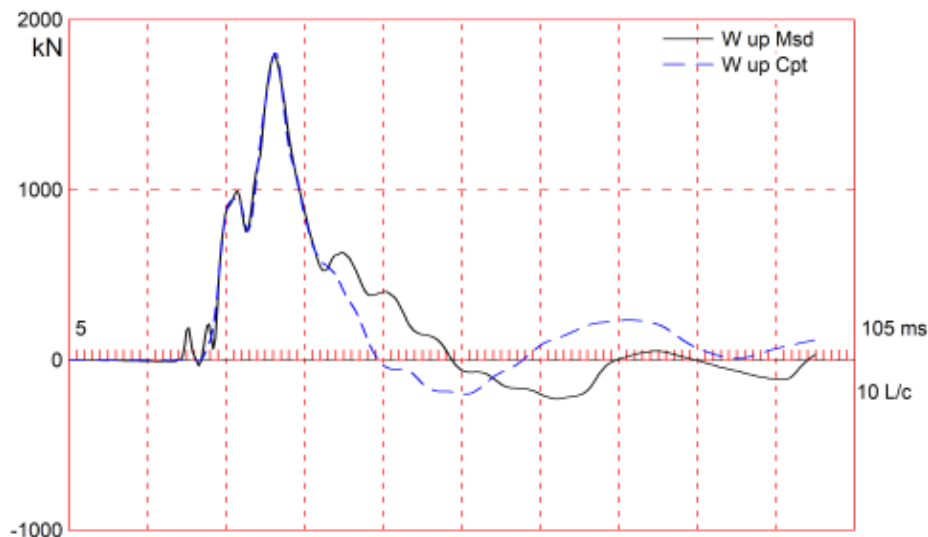
Toe Area 2827.4 cm²

Segmnt Number	Dist. B.G. m	Impedance kN/m/s	Imped. Change %	Slack mm	Tension Eff.	Compression Slack mm	Compression Eff.	Perim. m	Wave Speed m/s
1	1.0	2714.3	0.0	0.00	0.000	-0.00	0.000	1.88	4000.0
10	10.0	3283.1	21.0	0.00	0.000	-0.00	0.000	1.88	4000.0
11	11.0	3224.3	18.8	0.00	0.000	-0.00	0.000	1.88	4000.0
12	12.0	3165.4	16.6	0.00	0.000	-0.00	0.000	1.88	4000.0
13	13.0	3469.4	27.8	0.00	0.000	-0.00	0.000	1.88	4000.0
14	14.0	3891.1	43.4	0.00	0.000	-0.00	0.000	1.88	4000.0
15	15.0	2714.3	0.0	0.00	0.000	-0.00	0.000	1.88	4000.0
18	18.0	1733.7	-36.1	0.00	0.000	-0.00	0.000	1.88	4000.0
19	19.0	2714.3	0.0	0.00	0.000	-0.00	0.000	1.88	4000.0
32	32.0	2714.3	0.0	0.00	0.000	-0.00	0.000	1.88	4000.0

Wave Speed: Pile Top 4000.0, Elastic 4000.0, Overall 4000.0 m/s

Pile Damping 2.00 %, Time Incr 0.250 ms, 2L/c 16.0 ms

Total volume: 9.306 m³; Volume ratio considering added impedance: 1.029



CAPWAP SUMMARY RESULTS

Total CAPWAP Capacity: 3071.0; along Shaft 2263.0; at Toe 808.0 kN

Soil Sgmnt No.	Dist. Below Gages m	Depth Below Grade m	Ru kN	Force in Pile kN	Sum of Ru kN	Unit Resist. (Depth) kN/m	Unit Resist. (Area) kPa	Smith Damping Factor s/m	Quake mm
				3071.0					
1	1.0	0.4	43.0	3028.0	43.0	107.50	57.03	0.94	4.4
2	2.0	1.4	51.0	2977.0	94.0	51.00	27.06	1.07	3.2
3	3.0	2.4	43.0	2934.0	137.0	43.00	22.81	1.03	3.5
4	4.0	3.4	47.0	2887.0	184.0	47.00	24.93	0.97	2.7
5	5.0	4.4	43.0	2844.0	227.0	43.00	22.81	0.97	2.8
6	6.0	5.4	43.0	2801.0	270.0	43.00	22.81	0.97	2.8
7	7.0	6.4	43.0	2758.0	313.0	43.00	22.81	0.97	2.8
8	8.0	7.4	58.0	2700.0	371.0	58.00	30.77	1.03	2.5
9	9.0	8.4	51.0	2649.0	422.0	51.00	27.06	0.99	2.6
10	10.0	9.4	87.0	2562.0	509.0	87.00	46.15	1.12	2.5
11	11.0	10.4	47.0	2515.0	556.0	47.00	24.93	3.48	0.3
12	12.0	11.4	51.0	2464.0	607.0	51.00	27.06	3.17	0.3
13	13.0	12.4	51.0	2413.0	658.0	51.00	27.06	3.17	0.3
14	14.0	13.4	130.0	2283.0	788.0	130.00	68.97	0.55	0.8
15	15.0	14.4	126.0	2157.0	914.0	126.00	66.85	0.70	0.6
16	16.0	15.4	58.0	2099.0	972.0	58.00	30.77	2.69	0.4
17	17.0	16.4	69.0	2030.0	1041.0	69.00	36.61	2.09	0.4
18	18.0	17.4	76.0	1954.0	1117.0	76.00	40.32	1.79	0.4
19	19.0	18.4	87.0	1867.0	1204.0	87.00	46.15	1.42	0.5
20	20.0	19.4	69.0	1798.0	1273.0	69.00	36.61	2.09	0.4
21	21.0	20.4	72.0	1726.0	1345.0	72.00	38.20	1.94	0.4
22	22.0	21.4	87.0	1639.0	1432.0	87.00	46.15	1.42	0.5
23	23.0	22.4	65.0	1574.0	1497.0	65.00	34.48	2.28	0.4
24	24.0	23.4	83.0	1491.0	1580.0	83.00	44.03	1.54	0.4
25	25.0	24.4	72.0	1419.0	1652.0	72.00	38.20	1.94	0.4
26	26.0	25.4	76.0	1343.0	1728.0	76.00	40.32	1.79	0.4
27	27.0	26.4	87.0	1256.0	1815.0	87.00	46.15	1.42	0.5
28	28.0	27.4	76.0	1180.0	1891.0	76.00	40.32	1.79	0.4
29	29.0	28.4	79.0	1101.0	1970.0	79.00	41.91	1.66	0.4
30	30.0	29.4	101.0	1000.0	2071.0	101.00	53.58	1.06	0.5
31	31.0	30.4	94.0	906.0	2165.0	94.00	49.87	1.22	0.5
32	32.0	31.4	98.0	808.0	2263.0	98.00	51.99	1.14	0.5
Avg. Shaft			70.7			72.07	38.23	1.51	1.0
Toe			808.0				2857.72	3.29	1.4

Soil Model Parameters/Extensions

	Shaft	Toe
Case Damping Factor	1.30	1.02
Damping Type	Viscous	Viscous
Unloading Quake	(% of loading quake) 100	62
Reloading Level	(% of Ru) 100	100
Unloading Level	(% of Ru) 17	

CAPWAP match quality = 5.20 (Wave Up Match) ; RSA = 0
 Observed: Final Set = 3.2 mm; Blow Count = 314 b/m
 Computed: Final Set = 2.2 mm; Blow Count = 461 b/m

Transducer F1 (Y286) CAL: 91.0; RF: 1.00; F2 (Y293) CAL: 91.4; RF: 1.00
 A3 (K13197) CAL: 365; RF: 1.00; A4 (K13196) CAL: 416; RF: 1.00

max. Top Comp. Stress = 23.2 MPa (T= 21.8 ms, max= 1.003 x Top)
 max. Comp. Stress = 23.3 MPa (Z= 7.0 m, T= 23.4 ms)
 max. Tens. Stress = -1.67 MPa (Z= 7.0 m, T= 43.4 ms)
 max. Energy (EMX) = 43.8 kJ; max. Measured Top Displ. (DMX)= 9.1 mm

EXTREMA TABLE

Pile Sgmnt No.	Dist. Below Gages m	max. Force kN	min. Force kN	max. Comp. Stress MPa	max. Tens. Stress MPa	max. Trnsfd. Energy kJ	max. Veloc. m/s	max. Displ. mm
1	1.0	6560.0	-401.7	23.2	-1.42	43.8	2.49	9.0
2	2.0	6482.9	-388.7	22.9	-1.37	42.8	2.48	8.8
4	4.0	6355.6	-435.3	22.5	-1.54	40.3	2.40	8.4
6	6.0	6568.4	-465.7	23.2	-1.65	37.9	2.20	7.9
8	8.0	6512.8	-472.3	23.0	-1.67	35.6	2.11	7.3
10	10.0	6415.9	-456.4	22.7	-1.61	32.9	2.04	6.7
12	12.0	5715.1	-413.5	20.2	-1.46	28.7	2.05	6.1
14	14.0	5551.5	-396.9	19.6	-1.40	24.9	1.82	5.6
16	16.0	5633.7	-366.0	19.9	-1.29	22.3	1.60	5.2
18	18.0	5657.8	-357.8	20.0	-1.27	20.1	1.32	5.0
20	20.0	5307.5	-358.0	18.8	-1.27	18.1	1.27	4.8
22	22.0	4760.4	-352.0	16.8	-1.24	16.1	1.27	4.6
23	23.0	4628.5	-345.3	16.4	-1.22	15.2	1.25	4.5
24	24.0	4433.1	-332.9	15.7	-1.18	14.2	1.22	4.3
25	25.0	4187.0	-321.9	14.8	-1.14	13.3	1.22	4.2
26	26.0	3960.2	-307.9	14.0	-1.09	12.4	1.21	4.0
27	27.0	3788.1	-295.4	13.4	-1.04	11.6	1.20	3.9
28	28.0	3661.6	-277.9	13.0	-0.98	10.8	1.16	3.8
29	29.0	3550.7	-258.6	12.6	-0.91	10.0	1.12	3.6
30	30.0	3460.4	-238.2	12.2	-0.84	9.4	1.07	3.5
31	31.0	3390.6	-215.0	12.0	-0.76	8.7	1.01	3.4
32	32.0	3321.2	-192.3	11.7	-0.68	7.8	0.96	3.3
Absolute	7.0			23.3			(T = 23.4 ms)	
	7.0				-1.67		(T = 43.4 ms)	

CASE METHOD

J =	0.0	0.1	0.2	0.3	0.4	0.5	0.6	0.7	0.8	0.9
RP	7105	6499	5893	5288	4682	4077	3471	2865	2260	1654
RX	7105	6499	5893	5288	4682	4077	3471	2865	2260	1654
RU	8929	8506	8083	7659	7236	6813	6390	5967	5544	5121

RAU = 741 (kN); RA2 = 2908 (kN)

Current CAPWAP Ru = 3071 (kN); Corresponding J(RP)= 0.67; J(RX) = 0.67

VMX m/s	TVP ms	VT1*Z kN	FT1 kN	FMX kN	DMX mm	DFN mm	SET mm	EMX kJ	QUS kN	KEB kN/mm
2.53	21.56	6619	6542	6543	9.1	3.1	3.2	44.1	7170	574

PILE PROFILE AND PILE MODEL

Depth m	Area cm ²	E-Modulus MPa	Spec. Weight kN/m ³	Perim. m
0.0	2827.4	35615.0	23.563	1.88
32.0	2827.4	35615.0	23.563	1.88

Toe Area 2827.4 cm²

Segmnt Number	Dist. B.G. m	Impedance kN/m/s	Imped. Change %	Slack mm	Tension Eff.	Compression Slack mm	Compression Eff.	Perim. m	Wave Speed m/s
1	1.0	2615.6	0.0	0.00	0.000	-0.00	0.000	1.88	3850.0
3	3.0	2419.4	-7.5	0.00	0.000	-0.00	0.000	1.88	3850.0
4	4.0	2517.5	-3.7	0.00	0.000	-0.00	0.000	1.88	3850.0
5	5.0	2468.5	-5.6	0.00	0.000	-0.00	0.000	1.88	3850.0
6	6.0	2321.4	-11.2	0.00	0.000	-0.00	0.000	1.88	3850.0
7	7.0	2517.5	-3.7	0.00	0.000	-0.00	0.000	1.88	3850.0
8	8.0	2615.6	0.0	0.00	0.000	-0.00	0.000	1.88	3850.0
9	9.0	3225.5	23.3	0.00	0.000	-0.00	0.000	1.88	3850.0
10	10.0	2762.7	5.6	0.00	0.000	-0.00	0.000	1.88	3850.0
11	11.0	2703.8	3.4	0.00	0.000	-0.00	0.000	1.88	3850.0
12	12.0	3105.9	18.7	0.00	0.000	-0.00	0.000	1.88	3850.0

SSinop - MT / Site B; Pile: DLT - 3 B
 CFA Pile - 60cm - 32m; Blow: 5
 EPF GEOTECNIA LTDA

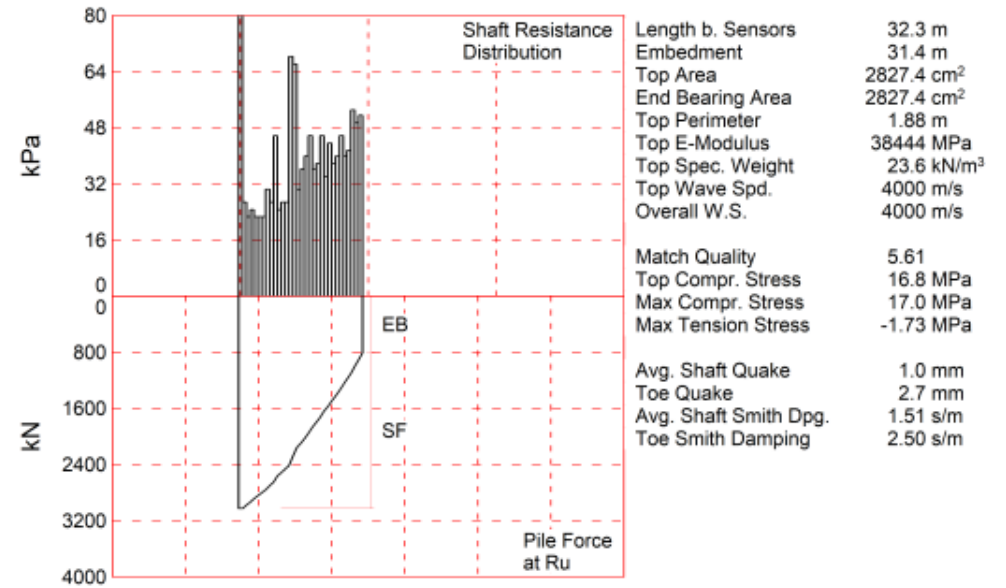
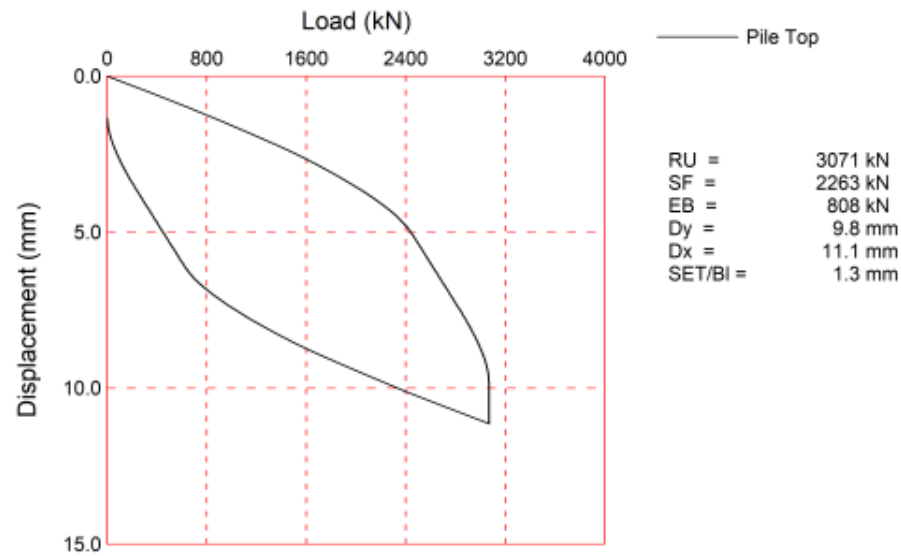
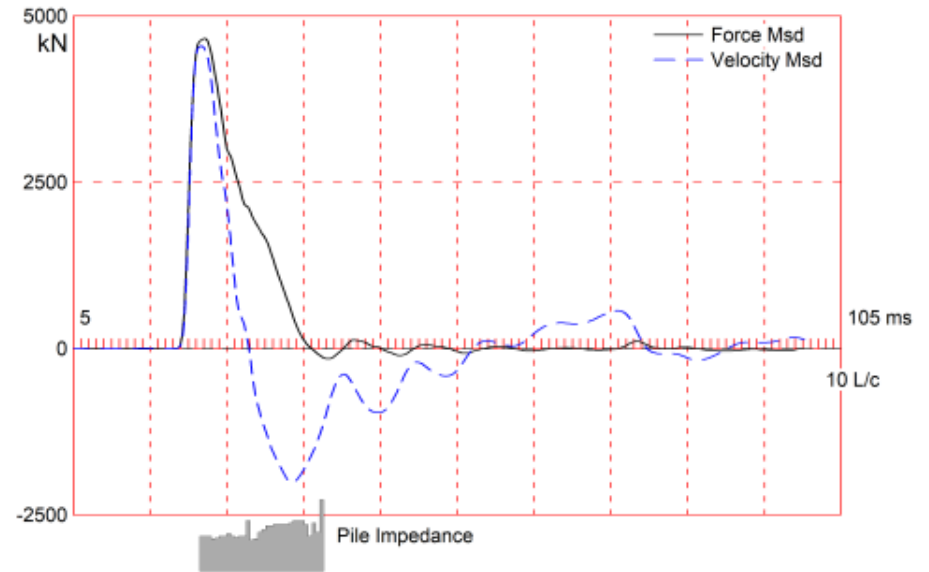
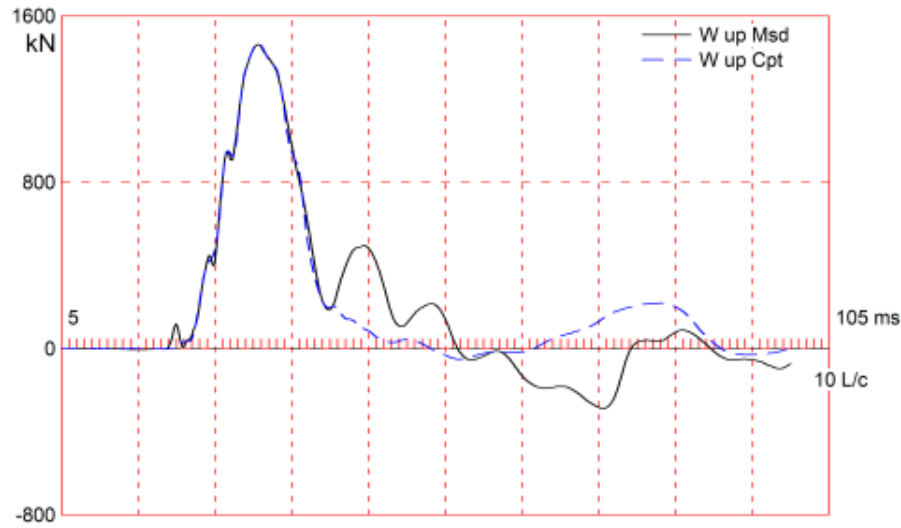
Test: 21-Sep-2023 16:40
 CAPWAP(R) 2014-3
 OP: Clayton Dalla Cort

Segmnt Number	Dist. B.G. m	Impedance kN/m/s	Imped. Change %	Slack mm	Tension Eff.	Compression Slack mm	Compression Eff.	Perim. m	Wave Speed m/s
13	13.0	2615.6	0.0	0.00	0.000	-0.00	0.000	1.88	3850.0
14	14.0	2223.3	-15.0	0.00	0.000	-0.00	0.000	1.88	3850.0
15	15.0	2125.2	-18.7	0.00	0.000	-0.00	0.000	1.88	3850.0
16	16.0	2713.6	3.7	0.00	0.000	-0.00	0.000	1.88	3850.0
17	17.0	2615.6	0.0	0.00	0.000	-0.00	0.000	1.88	3850.0
19	19.0	3056.9	16.9	0.00	0.000	-0.00	0.000	1.88	3850.0
20	20.0	3988.5	52.5	0.00	0.000	-0.00	0.000	1.88	3850.0
21	21.0	3939.5	50.6	0.00	0.000	-0.00	0.000	1.88	3850.0
22	22.0	3694.3	41.2	0.00	0.000	-0.00	0.000	1.88	3850.0
23	23.0	4184.6	60.0	0.00	0.000	-0.00	0.000	1.88	3850.0
24	24.0	2615.6	0.0	0.00	0.000	-0.00	0.000	1.88	3850.0
25	25.0	3792.4	45.0	0.00	0.000	-0.00	0.000	1.88	3850.0
26	26.0	2811.7	7.5	0.00	0.000	-0.00	0.000	1.88	3850.0
27	27.0	3547.2	35.6	0.00	0.000	-0.00	0.000	1.88	3850.0
28	28.0	2615.6	0.0	0.00	0.000	-0.00	0.000	1.88	3850.0
32	32.0	2615.6	0.0	0.00	0.000	-0.00	0.000	1.88	3850.0

Wave Speed: Pile Top 3850.0, Elastic 3850.0, Overall 3850.0 m/s

Pile Damping 2.00 %, Time Incr 0.260 ms, 2L/c 16.6 ms

Total volume: 9.892 m³; Volume ratio considering added impedance: 1.093



CAPWAP SUMMARY RESULTS

Total CAPWAP Capacity: 3071.0; along Shaft 2263.0; at Toe 808.0 kN

Soil Sgmt No.	Dist. Below Gages m	Depth Below Grade m	Ru kN	Force in Pile kN	Sum of Ru kN	Unit Resist. (Depth) kN/m	Unit Resist. (Area) kPa	Smith Damping Factor s/m	Quake mm
				3071.0					
1	1.0	0.1	43.0	3028.0	43.0	393.14	208.57	0.94	4.4
2	2.0	1.1	51.0	2977.0	94.0	50.53	26.81	1.07	3.2
3	3.0	2.1	43.0	2934.0	137.0	42.60	22.60	1.03	3.5
4	4.0	3.1	47.0	2887.0	184.0	46.56	24.70	0.97	2.7
5	5.0	4.1	43.0	2844.0	227.0	42.60	22.60	0.97	2.8
6	6.1	5.2	43.0	2801.0	270.0	42.60	22.60	0.97	2.8
7	7.1	6.2	43.0	2758.0	313.0	42.60	22.60	0.97	2.8
8	8.1	7.2	58.0	2700.0	371.0	57.46	30.48	1.03	2.5
9	9.1	8.2	51.0	2649.0	422.0	50.53	26.81	0.99	2.6
10	10.1	9.2	87.0	2562.0	509.0	86.19	45.73	1.12	2.5
11	11.1	10.2	47.0	2515.0	556.0	46.56	24.70	3.48	0.3
12	12.1	11.2	51.0	2464.0	607.0	50.53	26.81	3.17	0.3
13	13.1	12.2	51.0	2413.0	658.0	50.53	26.81	3.17	0.3
14	14.1	13.2	130.0	2283.0	788.0	128.79	68.33	0.55	0.8
15	15.1	14.2	126.0	2157.0	914.0	124.83	66.22	0.70	0.6
16	16.2	15.3	58.0	2099.0	972.0	57.46	30.48	2.69	0.4
17	17.2	16.3	69.0	2030.0	1041.0	68.36	36.27	2.09	0.4
18	18.2	17.3	76.0	1954.0	1117.0	75.29	39.94	1.79	0.4
19	19.2	18.3	87.0	1867.0	1204.0	86.19	45.73	1.42	0.5
20	20.2	19.3	69.0	1798.0	1273.0	68.36	36.27	2.09	0.4
21	21.2	20.3	72.0	1726.0	1345.0	71.33	37.84	1.94	0.4
22	22.2	21.3	87.0	1639.0	1432.0	86.19	45.73	1.42	0.5
23	23.2	22.3	65.0	1574.0	1497.0	64.40	34.16	2.28	0.4
24	24.2	23.3	83.0	1491.0	1580.0	82.23	43.62	1.54	0.4
25	25.2	24.3	72.0	1419.0	1652.0	71.33	37.84	1.94	0.4
26	26.2	25.3	76.0	1343.0	1728.0	75.29	39.94	1.79	0.4
27	27.3	26.4	87.0	1256.0	1815.0	86.19	45.73	1.42	0.5
28	28.3	27.4	76.0	1180.0	1891.0	75.29	39.94	1.79	0.4
29	29.3	28.4	79.0	1101.0	1970.0	78.27	41.52	1.66	0.4
30	30.3	29.4	101.0	1000.0	2071.0	100.06	53.08	1.06	0.5
31	31.3	30.4	94.0	906.0	2165.0	93.13	49.41	1.22	0.5
32	32.3	31.4	98.0	808.0	2263.0	97.09	51.51	1.14	0.5
Avg. Shaft			70.7			72.07	38.23	1.51	1.0
Toe			808.0				2857.72	2.50	2.7

Soil Model Parameters/Extensions		Shaft	Toe
Case Damping Factor		1.25	0.74
Damping Type		Viscous	Viscous
Reloading Level	(% of Ru)	100	100
Unloading Level	(% of Ru)	5	

CAPWAP match quality	= 5.61	(Wave Up Match)	; RSA = 0
Observed: Final Set	= 1.3 mm;	Blow Count	= 746 b/m
Computed: Final Set	= 0.3 mm;	Blow Count	= 2957 b/m

Transducer F1 (Y286) CAL: 91.0; RF: 1.00; F2 (Y293) CAL: 91.4; RF: 1.00
 A3 (K13197) CAL: 365; RF: 1.00; A4 (K13196) CAL: 418; RF: 1.00

max. Top Comp. Stress	= 16.8 MPa	(T= 22.7 ms, max= 1.016 x Top)
max. Comp. Stress	= 17.0 MPa	(Z= 8.1 m, T= 24.5 ms)
max. Tens. Stress	= -1.73 MPa	(Z= 8.1 m, T= 37.3 ms)
max. Energy (EMX)	= 30.6 kJ;	max. Measured Top Displ. (DMX)= 7.9 mm

EXTREMA TABLE

Pile Sgmnt No.	Dist. Below Gages m	max. Force kN	min. Force kN	max. Comp. Stress MPa	max. Tens. Stress MPa	max. Trnsfd. Energy kJ	max. Veloc. m/s	max. Displ. mm
1	1.0	4740.6	-420.5	16.8	-1.49	30.6	1.67	7.7
2	2.0	4758.9	-419.8	16.8	-1.48	29.7	1.64	7.5
4	4.0	4667.9	-432.4	16.5	-1.53	27.7	1.57	7.0
6	6.1	4602.8	-477.5	16.3	-1.69	25.9	1.53	6.5
8	8.1	4816.2	-490.3	17.0	-1.73	24.2	1.49	6.0
10	10.1	4681.1	-458.9	16.6	-1.62	22.3	1.32	5.5
12	12.1	4605.0	-426.6	16.3	-1.51	19.8	1.31	5.0
14	14.1	4529.6	-354.5	16.0	-1.25	17.5	1.15	4.6
16	16.2	4316.0	-354.1	15.3	-1.25	15.8	1.01	4.3
18	18.2	4106.4	-324.2	14.5	-1.15	14.1	0.94	4.0
20	20.2	3958.8	-313.8	14.0	-1.11	12.7	0.88	3.9
22	22.2	3755.3	-295.6	13.3	-1.05	11.3	0.81	3.8
23	23.2	3605.5	-286.4	12.8	-1.01	10.6	0.78	3.8
24	24.2	3416.4	-272.3	12.1	-0.96	10.1	0.79	3.7
25	25.2	3296.0	-255.1	11.7	-0.90	9.5	0.79	3.7
26	26.2	3265.6	-235.5	11.5	-0.83	8.9	0.77	3.6
27	27.3	3183.0	-215.3	11.3	-0.76	8.4	0.74	3.5
28	28.3	3018.1	-196.4	10.7	-0.69	7.8	0.73	3.5
29	29.3	2802.9	-177.4	9.9	-0.63	7.3	0.76	3.4
30	30.3	2463.9	-166.8	8.7	-0.59	6.7	0.78	3.3
31	31.3	2243.5	-156.2	7.9	-0.55	6.2	0.78	3.3
32	32.3	2141.3	-154.4	7.6	-0.55	5.3	0.78	3.2
Absolute	8.1			17.0			(T = 24.5 ms)	
	8.1				-1.73		(T = 37.3 ms)	

CASE METHOD

J =	0.0	0.1	0.2	0.3	0.4	0.5	0.6	0.7	0.8	0.9
RP	5063	4654	4244	3835	3425	3015	2606	2196	1787	1377
RX	5063	4654	4244	3835	3425	3015	2606	2196	1787	1377
RU	6455	6184	5914	5644	5373	5103	4832	4562	4291	4021

RAU = 942 (kN); RA2 = 2315 (kN)

Current CAPWAP Ru = 3071 (kN); Corresponding J(RP)= 0.49; J(RX) = 0.49

VMX	TVP	VT1*Z	FT1	FMX	DMX	DFN	SET	EMX	QUS	KEB
m/s	ms	kN	kN	kN	mm	mm	mm	kJ	kN	kN/mm
1.68	21.70	4532	4627	4668	7.9	1.2	1.3	30.9	6694	295

PILE PROFILE AND PILE MODEL

Depth m	Area cm ²	E-Modulus MPa	Spec. Weight kN/m ³	Perim. m
0.0	2827.4	38444.3	23.563	1.88
32.3	2827.4	38444.3	23.563	1.88

Toe Area 2827.4 cm²

Segmnt Number	Dist. B.G. m	Impedance kN/m/s	Imped. Change %	Slack mm	Tension Eff.	Compression Slack mm	Perim. m	Wave Speed m/s
1	1.0	2717.5	0.0	0.00	0.000	-0.00	1.88	4000.0
4	4.0	2517.5	-7.4	0.00	0.000	-0.00	1.88	4000.0
5	5.0	2567.5	-5.5	0.00	0.000	-0.00	1.88	4000.0
6	6.1	2717.5	0.0	0.00	0.000	-0.00	1.88	4000.0
8	8.1	2917.5	7.4	0.00	0.000	-0.00	1.88	4000.0
9	9.1	2717.5	0.0	0.00	0.000	-0.00	1.88	4000.0
10	10.1	2617.5	-3.7	0.00	0.000	-0.00	1.88	4000.0
11	11.1	2717.5	0.0	0.00	0.000	-0.00	1.88	4000.0
13	13.1	3917.5	44.2	0.00	0.000	-0.00	1.88	4000.0
14	14.1	2417.5	-11.0	0.00	0.000	-0.00	1.88	4000.0
15	15.1	2517.5	-7.4	0.00	0.000	-0.00	1.88	4000.0

Sinop - MT - Site B; Pile: DLT 4 - B
 CFA Pile - 60cm - 32m; Blow: 4
 EPF GEOTECNIA LTDA

Test: 22-Sep-2023 10:07
 CAPWAP(R) 2014-3
 OP: Clayton Dalla Cort

Segmnt Number	Dist. B.G. m	Impedance kN/m/s	Imped. Change %	Slack mm	Tension Eff.	Compression Slack mm	Compression Eff.	Perim. m	Wave Speed m/s
16	16.2	3017.5	11.0	0.00	0.000	-0.00	0.000	1.88	4000.0
17	17.2	3217.5	18.4	0.00	0.000	-0.00	0.000	1.88	4000.0
18	18.2	3517.5	29.4	0.00	0.000	-0.00	0.000	1.88	4000.0
20	20.2	3617.5	33.1	0.00	0.000	-0.00	0.000	1.88	4000.0
24	24.2	3717.5	36.8	0.00	0.000	-0.00	0.000	1.88	4000.0
25	25.2	3917.5	44.2	0.00	0.000	-0.00	0.000	1.88	4000.0
28	28.3	3609.5	32.8	0.00	0.000	-0.00	0.000	1.88	4000.0
29	29.3	2717.5	0.0	0.00	0.000	-0.00	0.000	1.88	4000.0
30	30.3	3717.5	36.8	0.00	0.000	-0.00	0.000	1.88	4000.0
31	31.3	3017.5	11.0	0.00	0.000	-0.00	0.000	1.88	4000.0
32	32.3	5517.5	103.0	0.00	0.000	-0.00	0.000	1.88	4000.0

Wave Speed: Pile Top 4000.0, Elastic 4000.0, Overall 4000.0 m/s

Pile Damping 2.00 %, Time Incr 0.252 ms, 2L/c 16.1 ms

Total volume: 10.817 m³: Volume ratio considering added impedance: 1.184